ABSTRACT

Title of Dissertation: Improving the performance of solid polymer electrolytes for lithium batteries via plasticization with aqueous salt or ionic liquid

Matthew Widstrom, Doctor of Philosophy 2019

Professor and Chair, Peter Kofinas, Department of Chemical and Biomolecular Engineering

Dissertation directed by:

The goal of this dissertation is to investigate and enable polyethylene oxide (PEO)-based solid polymer electrolytes (SPEs) for lithium batteries. Specifically, two different strategies to plasticize the PEO matrix for improving ion transport are explored. PEO has a propensity to crystallize below 60^{o}C, rendering ion motion too slow to be commercially competitive and constituting one of the main challenges of utilizing PEO SPEs as an alternative to organic liquid electrolytes. ILSPEs incorporating ionic liquids (ILs) were fabricated by blending PEO, IL, and corresponding lithium salt followed by hot-pressing the mixture into a homogenous film. Aqueous SPEs (ASPEs) were fabricated by blending a highly

concentrated solution of lithium salt in water (aqueous salt) with PEO followed by hot-pressing in a similar manner. Thermal analysis and electrochemical characterization were carried out for both classes of SPEs to assess their suitability as electrolytes and to optimize their composition for performance. Additionally, engineering the interface between the SPE and electrodes remains challenging and is critical for achieving good cycling performance. Multiple approaches for quality interface creation are proposed and carried out. Optimized ILSPE compositions show resistance to oxidation and were able to achieve room temperature conductivity of 0.96 mS/cm at room temperature, a value suitable for commercial application, as well as good rate performance at room temperature cycling in Li/ ILSPE/ lithium iron phosphate configuration. ASPE compositions exhibit conductivities between 0.68 and 1.75mS/cm at room temperature, with proof-of-concept cycling in a LTO/ ASPE/ LMO configuration.

IMPROVING THE PERFORMANCE OF SOLID POLYMER ELECTROLYTES FOR LITHIUM BATTERIES VIA PLASTICIZATION WITH AQUEOUS SALT OR IONIC LIQUID

by

Matthew Widstrom

Dissertation submitted to the Faculty of the Graduate School of the
University of Maryland, College Park, in partial fulfillment
of the requirements for the degree of
Doctor of Philosophy
2019

Advisory Committee:
Professor. and Chair Peter Kofinas,
Professor Robert M. Briber
Associate Professor Isabel K. Lloyd
Associate Professor Yifei Mo
Associate Professor Steven Jay, Dean's Representative

Dedication

To my mother,

You taught me what real strength is. Thank you for all you've sacrificed.

To my father,

I wouldn't be who I am without you. You taught me about respect and civic responsibility.

You taught me more than you know.

To my stepmother,

You came into my life at the right time and I'll always be grateful.

Acknowledgements

First, thank you Peter for all that you've done. From mentoring me in undergrad to welcoming me as a graduate student and seeing me through. Your friendship and guidance have kept me on the right path. A big thank you to all of the Kofinas Lab members past and present. Thank you to Aaron Fisher, my first science mentor, for your patience and support. To the other graduate student mentors I had along the way: Adam, Omar, Mert; I thank you. My time in the Kofinas lab has been punctuated with amazing assistant researchers. For this reason, I would like to thank Mian, Dimitri, Mete, Brian, Rahma, Brandon, and Robert.

A big thank you to Kyle Ludwig and Dr. Angelique Jarry for your collaboration on both projects in this dissertation as well as your help preparing me to defend. I couldn't have accomplished all that I have without you.

A special thanks to Jesse Matthews, a special student who has helped me tremendously and put up with me for too long. Another special thanks to Leo Torres, John Daristotle, and Metecan Erdi for their friendship and support.

Thank you to Dr. Briber, Dr. Lloyd, Dr. Cresce, and Dr. Wang for your intellectual guidance.

Thank you Shadden Zaki for your help with figures and your friendship.

Table of Contents

LIST OF TABLES

LIST OF FIGURES

LIST OF ABBREVIATIONS

AC: Alternating current

Al_2O_3: Alumina

ARLB: Aqueous rechargeable lithium-ion battery

ASPE: Aqueous solid polymer electrolyte

BCP: Block copolymer

C_{dl}: Double layer capacitance

CPE: Constant phase element

C-rate: Charge rate

CV: Cyclic voltammetry

DMC: Dimethyl carbonate

DSC: Differential scanning calorimetry

E_a: Activation energy

EC: Ethylene carbonate

EDX: Energy dispersive x-ray spectroscopy

EIS: Electrochemical impedance spectroscopy

EO: Ethylene oxide repeat unit

ESW: Electrochemical stability window

EV: Electric vehicle

GPE: Gel polymer electrolyte

HF: Hydrofluoric acid

IL: Ionic liquid

ILSPE: Ionic liquid solid polymer electrolyte

LSV: Linear sweep voltammetry

Li: Lithium

LATP: Lithium Aluminum Titanium Phosphate

LiBETI: Lithium bis(perfluoroethylsulfonyl)imide

LCO: Lithium cobalt oxide

Li^+: Lithium ion (also called lithium cation)

LFP: Lithium iron phosphate

$LiPF_6$: Lithium hexafluorophosphate

LIB: Lithium-ion battery

LiTFSI: Lithium bis(trifluoromethanesulfonyl) imide

LLTO: Lithium lanthanum titanate

LMO: Lithium manganese oxide

LMB: Lithium metal battery

LIPON: Lithium phosphorous oxynitride

LISICON: Lithium superionic conductor

LTO: Lithium titanate

LiOTf: Lithium trifluoromethane sulfonate

MDSC: Modulated differential scanning calorimetry

MD: Molecular dynamics

Ni-MH: Ni-Metal Hydride

NMP: *N*-Methyl-2-pyrrolidone

NMR: Nuclear magnetic resonance

OCV: Open circuit voltage

POF_3: Phosphorus oxyfluoride

PAN: Polyacrylonitrile

PEG: Polyethylene glycol

PEO: Polyethylene oxide

PFG NMR: Pulsed-field gradient nuclear magnetic resonance

PIL: Polymerized ionic liquid

PiSE: Polymer-in-salt electrolyte

PMMA: Polymethyl methacrylate

PPO: Polypropylene oxide

PS: Polystyrene

PTFE: Polytetrafluoroethylene

PVA: Polyvinyl alcohol

PVDF: Polyvinylidene fluoride

PVDF-HFP: Poly(vinylidene fluoride-*co*-hexafluoropropylene)

PYR13TFSI: N-methyl-N-propylpyrrolidinium bis(trifluoromethanesulfonyl)imide

R_b: Bulk resistance

R_p: Interfacial resistance

RTIL: Room-temperature ionic liquid

SEI: Solid electrolyte interphase

SEM: Scanning electron microscopy

SPE: Solid polymer electrolyte

SS: Stainless steel

S_2TFSI: triethyl sulfonium bis(trifluoromethanesulfonyl) imide

Ti: Titanium

T_g: Glass transition temperature

TGA: Thermogravimetric analysis

TiO_2: Titania

T_{Li^+}: Lithium transference number

t_{sc}: Short circuit time

VTF: Vogel-Fulcher-Tammann empirical relationship

WISE: Water-in-salt electrolyte

XPS: X-ray photoelectron spectroscopy

ZnO: Zinc oxide

Chapter 1: Introduction

1.1 Specific Aims

This goal of this research is to characterize and correlate electrochemical properties with microstructure of thin-film solid polymer electrolytes (SPEs) for lithium-ion batteries (LIBs). SPEs consisting of poly(ethylene oxide) (PEO) blended with aqueous salt or ionic liquid and lithium salt will be prepared by a solvent free hot-pressing process, which will result in free-standing, flexible SPEs with high conductivity.

We hypothesize that with proper understanding of the structure-properties-performance relations, we will be able to optimize a SPE system with an ionic conductivity on the order of 1 mS/cm. These metrics will strike an optimal balance between mechanical and transport properties. The value of 1 mS/cm is a widely accepted threshold required for a battery to power a small consumer device such as a cellphone or laptop. Interfacial studies using lithium stripping/plating and cyclic voltammetry (CV) will help us understand the resistance behavior and passivation capability of the interface as a function of time and SPE composition. This information is crucial when tailoring the SPE for optimal performance, as selecting a SPE composition that creates a passivating interface allows for reversible charge/discharging in a battery.

The goals for this project are to:

1. Develop, characterize, and optimize the ILSPE and ASPE systems
2. Gain an understanding of morphology, electrochemical properties, interface creation, and how these affect cell performance

3. Understand which compositional parameters affect the mechanism of Li^+ conduction in both classes of SPEs

Two specific aims have been designed to address the hypothesis and accomplish these goals:

Aim 1: Determine the effect of the polymer matrix, IL, and lithium salt on the properties of the resulting ILSPEs. Understand Li^+ conduction mechanism and interfacial evolution with time, and how these will affect cell performance.

Aim 2: Determine the effect of the polymer matrix, lithium salt, and water content on the properties of the resulting ASPEs. Understand Li+ conduction mechanism and interfacial evolution with time, and how these will affect cell performance.

Impedance spectroscopy will be used to determine the ionic transport properties of the SPE at various temperatures. Differential scanning calorimetry (DSC) will be used to identify thermal transitions and the effect of changes in SPE microstructure manifested by glass transitions and melting/crystallization different operating temperatures. Potentiodynamic methods such as linear sweep voltammetry (LSV) and cyclic voltammetry (CV) will be used to assess the electrochemical stability window of the SPE. Galvanostatic electrochemical techniques in combination with intermittent impedance spectroscopy, electron microscopy, and x-ray photoelectron spectroscopy (XPS) will be used to study the SPE/electrode interfaces. Charge-discharge curves using a full battery electrochemical couple will be generated to demonstrate the potential of the SPE for use in LIBs.

1.2 Intellectual Merit

Ultimately, what this dissertation aims to achieve is to facilitate the understanding of a new class of SPEs that provide a safe alternative to organic liquid electrolytes without making a big compromise in performance. For SPEs to be considered competitive alternatives to organic liquid electrolytes, their ionic conductivity needs to be improved significantly. Ionic conductivity is the measure of how fast an electrolyte can transport ions, which is the primary function of an electrolyte. SPEs tend to have low conductivity values ($<10^{-4}$S/cm) as compared to their liquid counterparts ($\sim10^{-2}$S/cm) due to their morphology and solid nature. Smart strategies to promote SPE morphologies that facilitate ion transport, an amorphous rather than crystalline polymer matrix, are needed. Incorporating ILs or concentrated aqueous salts into polymer matrices are two approaches to unlock fast ion transport by fully plasticizing the resulting SPE, as well as changing the morphology to fully amorphous. Both methods present an opportunity to tune the mechanical and transport properties of a SPE to make it a safer and environmentally friendly option as compared to organic liquid electrolytes. Gaining insight into the conduction mechanism of these highly ionically conductive SPEs through various characterization techniques and analysis coupled with molecular dynamics (MD) simulations can provide a framework of understanding for the future development of SPEs.

Electrode/ electrolyte interfaces have continued to be a challenging problem from a design perspective for SPEs. Good contact between the electrolyte and both electrodes is crucial for battery performance, and is made difficult with porous electrodes that were designed for liquid electrolytes in the context of SPEs. Porosity is a design parameter for electrodes with the purpose being that liquid electrolyte can seep into electrode pores,

creating good ionic contact through the bulk of the electrode. This ionic contact is necessary for capacity utilization, especially with thick (energy dense) electrodes. Increasing electrode thickness results in a greater volume ratio of active materials relative to inactive components, and is necessary to optimize energy density of a battery cell. Inclusion of SPE components within an electrode are studied extensively as way to provide an ionic and electronic conduction network through the bulk of the electrode, realizing full capacity utilization. Polymer inclusion in a liquid anolyte/catholyte is proposed in this dissertation as an additional way to promote intimate contact between electrolyte components and electrode. This contact issue is usually given a surface-level treatment in most peer-reviewed articles, and while there are some exceptions[1–4], many articles in the SPE field don't state the problem. The investigation and rationalization of these methods in this dissertation gives researchers a deeper understanding of the electrode/ electrolyte contact issue while providing multiple strategies to implement in the design of their own SPE systems.

1.3 Broader Impacts

High-profile failures of LIBs, in devices such as Samsung's Galaxy Note 7[5], highlight safety concerns surrounding devices using state-of-the-art LIBs. At the core of this problem is the ubiquitous use of liquid carbonate-based electrolytes, which are highly combustible and can undergo thermal runaway leading to pressure buildup and the battery cell erupting in fire. To ameliorate this concern, there is great interest in replacing these liquid organic electrolytes with safer alternatives, such as solid electrolytes. Battery power would also benefit greatly from the conformal and safe nature of solid polymer electrolytes.

ILSPEs would be ideal for applications with an elevated operating temperature requiring high energy density such as for a car battery (operating temperature ~100$_{o}$C) as they can be used with a lithium metal anode and high voltage (+4 V) cathode and they work well at higher temperatures. Additionally, battery application where safety is critical would be well suited for ILSPEs. One good example would be implantable medical devices such as a pacemaker. Pacemakers operate at biological temperature (~37$_{o}$C) and require low power density, relieving the concern over slower ion transport in SPEs, however safety cannot be compromised. SPEs also open the possibility for unique applications due to the flexible and conformable nature of SPEs. An ILSPE that demonstrated good cycling stability, high ionic conductivity (~1 mS/cm), and good mechanical properties (+0.1 GPa shear modulus[6]) could replace liquid organic electrolytes for a number of applications. The ultimate goal would be to use ILSPEs for lithium metal batteries (LMBs), which promises high energy density (+300Wh/L, +250Wh/kg) due to the density and potential of lithium metal. ILSPE has demonstrated the ability to create a passivating layer at the interface and stabilize the reversible capacity. For the ASPE system, cycling with a lithium titanate (LTO) anode and lithium manganese oxide (LMO) cathode is demonstrated, boosting the energy density of this aqueous electrolyte by taking advantage of a larger operating voltage. To our knowledge, no SPE system incorporating an aqueous salt has been cycled with these electrodes.

SPEs offer the additional advantages of better safety, lower cost, mechanical integrity and flexibility, and more compact design space due to their conformable nature. An SPE using an aqueous salt to plasticize a polymer matrix could be fabricated without the need for an environment that is kept meticulously dry. Both classes of SPEs would

possess a processing advantage over liquid electrolytes in that they can be formed by a simple hot-pressing procedure that would result in sheets or conformable coatings. Gaining a concrete understanding of these SPE systems and the transport mechanisms involved by correlating properties and structure to performance will greatly benefit the design of future SPEs, leading to unique device applications such as textile or 'wearable' power. Non-flammable SPEs are also ideal candidates for battery applications in which safety is critical such as electric vehicles (EVs) or implantable medical devices.

The dissertation is organized as follows: Chapter 2 gives relevant background information for understanding the field of solid electrolytes and in particular SPEs and gives an overview of materials selection. Chapter 3 will give an overview of research activities including justifications for materials used and general explanation of characterization techniques. Chapter 4 details the investigation of incorporating ILs into a polymer matrix. IL is used to make completely amorphous SPEs, as confirmed directly through DSC and indirectly through impedance spectroscopy. Electrochemical stability and cycling performance are assessed. In Chapter 5, the ASPE project which incorporates aqueous salt into a polymer matrix is described. Many of the same physical and electrochemical characterization methods that were used on the ILSPE system were performed for ASPEs. MD simulations provide an in-depth look at the ion-coordinating environment over a composition range of ASPEs, revealing the conduction mechanism as well as the composition-ion structure-performance relationships that govern this system. Chapter 6 will describe the outlook and future directions of this work as well as my scientific contributions.

Chapter 2: Background

2.1 Significance and Innovation

One of the key technological challenges of the 21st century is meeting our energy supply demands in a sustainable manner, which necessitates improvements in both energy storage and conversion while maintaining safety to the end user. Mobile devices of all types require batteries with high energy densities to fulfill customer expectations and perform increasingly complex and energy-intensive tasks. Electric vehicles (EVs) powered by LIBs that promise to replace fossil fueled vehicles and reduce carbon dioxide emissions suffer from significant barriers to adoption of the technology due to concerns over range, charge times, cost, and safety[7].

Lithium battery technology has a high potential to meet our energy storage demands, however the current liquid organic electrolyte employed in these systems incur a high environmental cost in both recyclability and toxicity. State of the art liquid electrolytes are overwhelmingly a blend of organic carbonates and lithium hexafluorophosphate ($LiPF_6$)[8–10], a heat sensitive salt that decomposes into toxic gases such as phosphorus oxyfluoride (POF_3), hydrofluoric acid (HF), carbon dioxide, and others[4,11]. In addition, the toxic liquid electrolyte can leach out of the battery causing significant environmental concerns. Safety is an important and highly publicized aspect of lithium ion battery integration into EVs, especially in light of battery failures aboard the Boeing 787 next-generation airliners, accidents involving electric cars that resulted in significant battery fires[12,13], and Samsung smart phone recalls[5]. Replacing flammable organic

electrolyte solvents and low boiling point salts such as $LiPF_6$ with more thermally stable materials is critical for improving the safety of LIBs[14].

A solid electrolyte system that could improve upon the safety of the battery and reduce toxic reduction products, eliminate the leakage of environmentally harmful organics to the environment, while meeting the required cycling and conductivity performance, would offer a safer and more sustainable alternative to current liquid organic electrolyte technology. A SPE that incorporates a polymer matrix, lithium salt, water and/or IL could achieve these goals. The polymer matrix provides the mechanical stability and flexibility that current liquid organic electrolytes lack, as well as excellent temperature and stability against reduction, with a tradeoff of poor ionic conductivity[15]. To boost the ionic conductivity of SPEs, lithium salt in water and/or ILs can be added to plasticize the polymer matrix and effectively provide added free volume for lithium conduction[16]. These conductive additives are effectively trapped in the polymer matrix with no leakage, resulting in a truly flexible solid electrolyte.

Volumetric and gravimetric energy densities are key performance metrics as they determine both the size and weight that is needed for a battery to store a certain amount of energy[17]. LIBs provide a performance benchmark in terms of their volumetric and gravimetric densities, as they outperform most other battery chemistries due to the lightweight nature of lithium and the high voltage (+4 V) chemistries possible with these systems. Organic liquid electrolytes for LIBs are limited to the intercalation anode graphite due to dendrite growth when lithium metal is used[6], limiting the energy density of the battery. Ideally Li metal would be used as the anode material instead of graphite which relies on the intercalation of Li^+ and thus has a 10x lower theoretical specific capacity; the

jump from LIB intercalation materials to a lithium metal battery (LMB) would result in a big increase in energy density. However, uneven electrodeposition at the electrode surface invariably leads to pointed structures called dendrites forming at the lithium metal/ organic liquid electrolyte interface. This presents a persistent problem where these dendrites can continue to grow through the interelectrode space until contact is made with the opposite electrode, leading to short circuiting and cell failure[18] often in a catastrophic and safety compromising manner. Additionally, steps have to be taken to ensure that there is no electrolyte leakage and that the internal vapor pressure of the liquid electrolyte is kept in check. This is done by adding multiple packaging layers to the battery casing, which takes up valuable space and hinders the scale down of miniature devices[19,20]. Substituting a solid electrolyte would alleviate many of these problems. Most solid electrolytes have low to nonexistent vapor pressures and are not flammable, decreasing the need for excessive safety-oriented packaging materials. Solid electrolytes can also act as the separator, further increasing the energy density of the battery[8]. A SPE with sufficient mechanical properties to suppress dendrite growth could be used safely with a lithium metal anode, taking advantage of the energy density available to a LMB. Lastly, solid polymer electrolytes can be processed into thin film flexible batteries, avoiding the limitations on shape that is necessary with the use of liquid electrolytes, and resulting in overall smaller devices[20].

2.2 Lithium-Ion Batteries

The potential for Li-ion battery technology was first demonstrated in the 1970s and, with the development of intercalation electrode materials, has largely replaced nickel-cadmium and nickel-metal hydride systems for secondary batteries[20]. Lithium-ion is highly desirable

due to the fact that lithium is the most electropositive (-3.04V vs standard hydrogen electrode) and lightest metal (M = 6.94 g/mol)[20], making it ideally suited for high energy density batteries.

A battery's function is to store chemical energy than can be converted to electrical energy and be used to power mobile devices. Batteries consist of a combination of electrochemical cells designed to achieve a desired voltage and capacity. Within the electrochemical cell there is a positive cathode and negative anode, each of which participate in a redox reaction during charging or discharging of the cell. The anode and cathode are separated by the electrolyte, which is an ionically conductive medium that transports Li^+ between the electrodes, and a polymer or ceramic separator, which isolates the two electrodes from each other physically and electronically[15,21]. The electrolyte should generally have the following properties[10,22]:

- be ionically conductive at its operating temperature (>10^{-4} S/cm)
- have a large electrochemical stability window or have the ability to create a passivating interface (>4V)
- be thermally and mechanically stable in the operating temperature range
- be electronically insulating
- conduct a large fraction of current from Li^+ relative to other ions (high transference number)
- be non-combustible
- maintain a good electrode/ electrolyte interface during cycling
- have low toxicity
- have low cost

Mechanical stability of the electrolyte is crucial to maintain the shape of the battery as well as good contact between the electrode/ electrolyte interface. When liquid electrolytes are used, mechanical stability is achieved through packaging designed to contain the liquid electrolyte, and through the use of a separator. It is important for the electrolyte to be ionically conductive so that ions can migrate to the electrode/ electrolyte interface to participate in charging/ discharging at reasonable rates, but electronically insulating so that the battery won't short. Thermal stability and non-combustibility are important factors that determine the safety level of the battery. The lithium transference number is a measure of the fraction of the total moving charge that is due to Li^+ ions and thus a representation of the useful current for charging and discharging[23]. Besides representing efficient ion transport, a high lithium transference number has a protective effect against lithium dendrite formation by minimizing space-charge formation[24,25].

Although it is unlikely that the electrolyte will be completely stable throughout the voltage window of the battery if lithium metal or graphite is used as an anode, it is expected for the electrolyte to have the ability to create a passivating layer called a solid electrolyte interphase (SEI) when it is irreversibly decomposed to prevent further decomposition of the electrolyte. Lithium should remain conductive across the SEI to maintain the ability to charge and discharge, and solvent molecules/ salt anions should not be able to cross the SEI so that they cannot continue the process of further decomposition. The SEI should be electrically insulating to prevent easy electrolyte decomposition or lithium plating at the SEI surface.

2.3 Solid Polymer Electrolytes

There are many ways to classify polymer electrolytes, but for the purpose of this dissertation two broad classifications will be used. All polymer electrolytes can be placed into two categories; the first category is where the polymer contributes in a significant way to the solvation and transport of ions, and the second is where the polymer does not contribute and instead a second low molecular weight solvent solvates and transports ions contained in an inert polymer matrix. The first category of polymer electrolyte called solid polymer electrolytes (SPE) typically involves high molecular weight polymer and a lithium salt, sometimes with an additional plasticizer such as ceramic fillers or ionic liquid. The second category of polymer electrolyte involves the crosslinking of a polymer matrix and swelling with a solvent and lithium salt; this is called a gel polymer electrolyte (GPE). GPEs are often promoted for their high ionic conductivity as compared to other polymer electrolytes (>10^{-3} S/cm), however the organic solvent/ salt mixtures they contain are typically the very same liquid electrolytes that have safety issues in commercial battery systems[26–28]. The presence of organic liquid electrolytes make GPEs susceptible to the same issues such as poor thermal stability and not-much-improved mechanical properties[27,29]. GPEs can be free-standing films, however they are considered quasi-solid materials[29] and as such won't be the focus of this dissertation.

SPEs offer many advantages that give them an edge over other solid electrolytes for a diverse set of applications. SPEs are easily processible as they can be solution cast[30,31] or fabricated using a solvent-free hot pressing approach[3,32,33]. Depending on the type of SPE, such a system can be flexible and conforming in nature, which leads to some unique device applications such as textile or 'wearable' power. Another benefit of SPEs is that

they are nonflammable and have no vapor pressure; they are ideal candidates for battery applications in which safety is critical such as EVs or implantable medical devices. For SPEs to become commercially viable, they need to have good cycle life and exhibit appreciable conductivity within the operating temperature range that approaches 10^{-4} S/cm[10,22]. Additionally, it is critical that the SPE acts as a separator and maintains good contact with both electrodes while withstanding the internal pressure and temperature variations during operation. An SPE that could meet all of these requirements would be adopted for a diverse set of applications.

There are two big challenges facing SPEs and solid electrolytes in general that prevent their widespread adoption. The first challenge is their poor ionic conductivity, as solid electrolytes are inherently more resistive than their liquid counterparts. The second challenge is the creation of a good interface between electrolyte and electrodes that is stable with long-term cycling. The conductivity issue for SPEs is often addressed with the addition of a plasticizer, although even so the conductivity of SPEs won't approach that of organic liquid electrolytes (~10^{-2} S/cm at room temperature)[4] representing a trade-off. The common approaches used to enhance conductivity through addition of a plasticizer will be covered in the following sections.

The interface challenge for SPEs comes in two broad forms. First, a SPE must be electrochemically stable against both the anode and cathode or have the ability to form a stable SEI for kinetic passivation, the same as any electrolyte. The second form is unique to solid electrolytes and is depicted in Figure 2.1. Intercalation electrodes are fabricated with four main components: active material, carbon black as an electronic additive, polymer binder to hold the electrode together, and a current collector. Typically, there is a

25-40% porosity for intercalation electrodes[34], which allows for the infiltration of liquid electrolyte through the bulk of the electrode represented in the first part of Figure 2.1. This infiltration of the electrolyte into the electrode ensures good ionic contact between the two, facilitating healthy charge and discharging and full capacity utilization. This is crucial for using electrodes with high loading (high mass/area, i.e. thick electrodes) such that ions can be transported to and from active material through the bulk. When using a solid electrolyte, the electrolyte cannot contact the interior of the electrode like a liquid electrolyte can, making the porosity of the electrode into voids which is wasted space as depicted by the white regions in the second part of Figure 2.1. When designing a battery system utilizing a SPE, strategies need to be implemented to address ionic contact through the bulk of the electrode. These strategies will be discussed in Chapters 4 and 6.

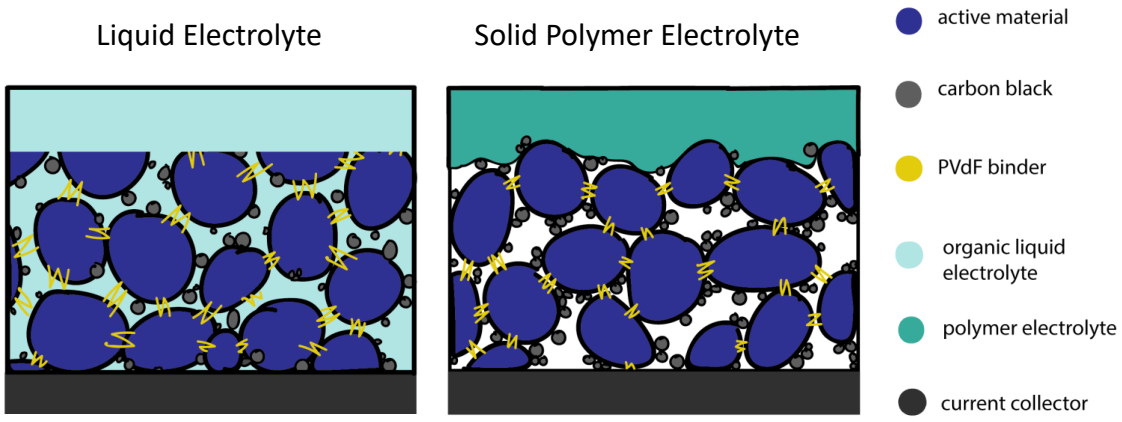

Figure 2.1: Schematic representation of a liquid electrolyte/ electrode interface and a SPE/ electrode interface.

2.4 PEO for Solid Polymer Electrolytes

PEO is the most studied and successful polymer for SPEs mainly for its relatively high ionic conductivity as compared to other polymers. PEO also has a high solvation capability, allowing it to dissolve alkali salts in high concentrations[35–38], and high voltage stability

suitable for use against lithium metal[39–42]. The transport mechanism for Li^+ in PEO is believed to involve the formation and breaking of coordination sites of Li^+ to oxygen atoms along the PEO backbone. PEO has a high chain flexibility[43,44], facilitating the formation and breaking of coordination sites as chains are able to move themselves into place. As these lithium-oxygen bonds are formed/broken, ion transport occurs as Li^+ participates in inter and intra chain hopping, as well as whole chain mobility[16,45]. Polymer electrolytes that rely on segmental chain motion for conduction benefit from low glass transitions (T_g), which is defined as the temperature below which polymer chains 'freeze out' and cease movement[46]. Assuming that operational temperature is above T_g, the further distance between the two will result in greater segmental motion and thus conduction. PEO has a low T_g (-60°C)[43], which increases segmental chain motion and greatly facilitates ionic transport. For the same reason, it is advantageous from a conductivity standpoint to have a large volume fraction of amorphous rather than crystalline PEO, so that PEO chains aren't locked in place[16,22,47–49]. The melting temperature of PEO is above room temperature(~65°C)[50], meaning that a significant fraction of the polymer can be crystalline at room temperature, typically 70-85%[43]. Crystallinity will impair ion conduction, rendering these electrolytes more suitable for elevated temperature operation. This propensity for high amount of crystallinity is a direct manifestation of the ionic conductivity problem discussed in section 2.3. To mitigate this, there are a number of strategies that have been employed to plasticize PEO to reduce crystallinity and favor ion conduction. These strategies will be covered in the rest of this chapter.

2.5 Composite Solid Polymer Electrolytes

One of the most common ways PEO is plasticized is through the addition of micro or nanosized ceramic fillers of either inactive (TiO_2, Al_2O_3, silica, ZnO)[50–54] or active (Li Nasicompound, LLTO, LATP)[55–57] materials. Dispersed ceramic particles are thought to influence the recrystallization kinetics of the PEO polymer chains, effectively depressing crystallization and thereby increasing Li^+ conduction[50,53,58] through an increased amorphous phase volume. In addition to disrupting crystallinity, ceramic fillers have been shown to improve Li^+ transport through increased ion pair dissociation and at the interfacial region between polymer and particle[59,60]. Inactive ceramic nanofillers can provide the advantages listed above, however they do contribute to dead volume where Li^+ conduction does not occur given that the fillers don't themselves contribute to Li^+ transport[61]. On the other hand, active nanofillers consist of materials that have an appreciable Li^+ conductivity, providing an alternative Li^+ conduction pathway often through low energy barrier defect or interstitial hopping[55–57,62]. Ceramic fillers also provide a reinforcing network effect, improving the mechanical properties of the SPE[63]. The surface modification of the ceramic filler provides an interesting avenue to affect and improve the lithium transference of the SPE, as well as improve electrochemical stability[53]. As promising as ceramic fillers are for their ability to improve mechanical and electrochemical stability, their improvement in ionic conductivity to ~10^{-4} S/cm at elevated temperatures alone is not satisfactory for most commercial applications. Therefore, further innovation is needed to achieve a useful SPE of which ceramic filler may be an important component.

2.6 Block Copolymer Solid Polymer Electrolytes

Another well studied strategy to approach the PEO crystallization problem is to incorporate PEO into a block copolymer (BCP) system where PEO crystallization is disrupted. The selection of blocks is often done strategically such that ion conduction occurs mostly within one block while the other provides mechanical stability and rigidity, as is seen in many polystyrene (PS)- PEO BCPs[16,47,64]. This can occur if the BCP is tuned towards block phase segregation, leading to an intimately interdigitated structure with solid-like mechanical properties while segregating ion conduction to one phase[65–67]. Different morphologies are possible in a BCP electrolyte such as lamellae, gyroid networks, disordered, sphere, and hexagonal cylindrical phases. These morphologies are tunable by changing the relative block length[68], changing salt concentration[69], or through functional group selection[70] and all affect the mechanical and transport properties of the electrolyte leading to a rich experimental design space to be explored. Other work involves tailoring the copolymer to have a high lithium transference number by incorporating the anion of the salt covalently to one of the blocks[71]. This effectively "fixes" the anion of the lithium salt in place, ensuring that all ionic current occurs through the movement of Li^+ resulting in a lithium transference number near unity. Although the idea of decoupling the ion transport and mechanical properties through the use of two distinct blocks is promising, in practice these BCPs can be difficult to synthesize and the ionic conductivity accessible by changing BCP morphology is insufficient at ambient temperatures ($<10^{-4}$ S/cm).

2.7 Ionic Liquid Electrolytes

Ionic liquids (ILs) are molten salts that are defined as having a melting point below 100 °C, and are often liquids at room temperature in which case they can be called room temperature ionic liquids (RTILs). ILs have a number of properties that make them attractive for use as electrolytes, including high conductivity, low volatility, and excellent electrochemical and thermal stability[72]. Retrieval and recycling of ILs is easily achieved through distillation or biphasic chemical processes, making them somewhat more environmentally friendly than their organic liquid counterparts[73]. Another benefit of ILs is that they are highly tunable, as the cation and anion can be selected to control the properties of the electrolyte. The most common cationic architectures are the quaternary nitrogen ring structures imidazolium, pyrrolidinium, piperidinium, and pyridinium[72]. Typical anion structures for electrolyte applications are halogens, fluorinated compounds such as BF_4^-, or sulfonated imides. The lesser studied sulfonium based cations have also shown to be promising as they exhibit good conductivity and electrochemical stability windows[31,74,75].

Despite their impressive electrochemical properties, there are a number of factors holding ILs back from widespread use as electrolytes. In most ILs there are no native Li^+, requiring a lithium salt to be introduced to the IL for LIB applications. This increases the viscosity of the electrolyte mixture, making it difficult to handle and limiting the conductivity[45,72]. Additionally, many ILs are air and moisture sensitive and their cost is quite high, limiting their practicality. One common way to take advantage of IL properties while pivoting from the model of IL as electrolyte is to incorporate them into a polymer matrix such that they act as a plasticizing agent to boost the conductivity of the resulting SPE[3,30–32,45,73,76–90]. Multiple approaches on this front have been taken including creating a

polymer gel that is swelled with IL[3,16,28,45,73,91], polymerized ionic liquids (PILs) where either the anion or cation is incorporated covalently into the polymer backbone[92–94], or having a ternary SPE with a polymer matrix, lithium salt, and IL[16,30–32,49,83,85,95,96]. Shin et al. conducted the first study of ternary electrolytes by blending PEO, the IL N-methyl-N-propylpyrrolidinium bis(trifluoromethanesulfonyl)imide ($PYR_{13}TFSI$), and lithium bis(trifluoromethanesulfonyl) imide (LiTFSI) together to make a SPE[83]. They studied different samples with varying amounts of IL and showed that the addition of IL dramatically improved the ionic conductivity over "dry" SPEs, and even demonstrated the viability of this system for battery cycling. The boost in conductivity with the addition of an IL and lithium salt to PEO comes from an effective increase in the free volume of the system, allowing for greater chain mobility and a localized liquid-like environment for Li^+ to move[43]. Ternary SPE systems are a rich field of study given the multiplicity of options with the selection of IL, salt, and polymer. This remains a promising avenue towards the development of a safe, flexible, and commercially viable SPE.

PILs are an interesting option given that they can be made such that the only free ion is Li^+, allow for a lithium transference number ~1[71]. The main drawbacks of this approach are that PILs can be difficult to synthesize, and the conductivity at room temperature remains poor, on the order of ~10^{-7}-10^{-6} S/cm[45,97–100]. Creating a gel where the polymer chains are crosslinked to form a network strikes a reasonable compromise between the mechanical and transport properties of the resulting GPE. Crosslinked chains allow for higher IL loading content to boost ionic conductivity while also maintaining some mechanical integrity. The superior properties of the IL are largely transferred to the gel, namely excellent thermal and electrochemical stability. This is in contrast with gel

electrolytes that are loaded with organic liquids; these SPEs still suffer from many of the same drawbacks of conventional electrolytes such as high volatility with the potential for pressure buildup. As promising as these gel SPEs are, they still suffer from poor interfacial resistance and moderate conductivity values[3].

2.8 PEO Alternatives

Besides PEO, other polymers have been researched for SPE application such as polyacrylonitrile (PAN), polymethyl methacrylate (PMMA), and poly(vinylidene fluoride-*co*-hexafluoropropylene) (PVDF-HFP). Typically, polymer electrolytes with appreciable conductivity that don't incorporate ethylene oxide unit in some fashion are GPEs that rely on a conduction mechanism that is largely independent of Li^+ coordinating to and moving along polymer chains. For instance, PAN-based GPEs can have high ionic conductivity values on the order of 1 mS/cm at room temperature, but they have other drawbacks such as poor reductive stability[101], ruling out anodic materials like lithium metal or graphite and severely limiting its utility as an electrolyte. These systems also have many of the drawbacks of organic liquid electrolytes as mentioned previously.

2.9 Ceramic Electrolytes

A type of solid electrolyte that is fundamentally different than SPEs are those based on ceramics and glasses. Ceramic electrolytes are attractive for their high elastic modulus, high thermal stability, and low flammability[102,103]. The solid nature of ceramic conductors also eliminates the potential for electrolyte leakage, eliminating excess packaging and improving the safety of the battery. Perhaps the biggest advantage to ceramic electrolytes

is their ability for stable Li electrodeposition due to their high shear modulus[104], effectively preventing Li dendrite formation. One of the most common glassy electrolytes of this type is lithium phosphorous oxynitrides (LIPON)[103,105]. Other common ceramic electrolytes include lithium lanthanum titanate (LLTO)[102,106] and lithium superionic conductor (LISICON)[107]. These systems are single-ion conductors with conductivities ranging from 10^{-6} – 10^{-3} S/cm with sustained cycling (+1000 cycles). However, they have trouble forming stable interfaces that don't change volume during cycling[105]. This often leads to poor contact between the electrolyte and electrodes, resulting in high interfacial resistances. Ceramic electrolytes also tend to have a high sensitivity to moisture[108] and to be comprised of expensive elements such as germanium[109], raising the cost of commercial implementation.

2.10 Aqueous Electrolytes

The first secondary (rechargeable) battery was a Pb-acid battery developed in 1859 by G. Planté[110]. With the invention of the generator shortly after secondary batteries became industrially relevant and were used on a wide scale[111]. The aqueous electrolyte chemistries that have been traditionally used as secondary batteries including for grid-level energy storage are lead-acid, Ni-Cd and Ni-MH (Ni-Metal Hydride) aqueous electrolytes[112]. The main advantages of aqueous electrolytes over traditional organic liquid electrolytes is that they are inexpensive, possess high conductivity, and are inherently environmentally friendly[111]. However, the electrochemical stability window of water is only ~1.23V, which is raised to ~2.0V with additives[10,113]. This severely limits the energy density of the resulting battery which is dependent on the operating voltage, as well as the choice of

electrode materials. Aqueous electrolytes also lack the ability to form a passivating SEI as the reduction and oxidation products of water are hydrogen and oxygen gas. Compare this with Li^+ organic liquid electrolyte technology (+4V) which is paired with a number of industrial and experimental high voltage anode/ cathode pairs and it is easy to understand why organic liquid electrolytes have come to prominence in recent years.

One alternative to traditional aqueous batteries is use an aqueous rechargeable lithium-ion battery (ARLB). ARLBs use an aqueous solution with intercalation anodes and cathodes. These batteries benefit from many of the same aspects of other aqueous-based batteries namely high conductivity, sustainability and low toxicity, and lower cost[114]. However, the fact remains that the aqueous nature of the electrolyte leads to serious compromises in the electrode selection and thus energy density of the battery[113].

2.11 Polymer-in-Salt Electrolytes

Angell et al[115] first demonstrated in 1993 the concept of polymer-in-salt electrolytes (PiSE), as opposed to the commonly studied salt-in-polymer electrolytes. With the understanding that polymers such as PEO or polypropylene oxide (PPO) show complete miscibility with many lithium salts, the relative concentration of salt and polymer could be inverted such that salt was the majority component. Angel observed that in some salt-polymer systems the T_g temperature displayed a maximum as salt content was increased, indicating that transport properties of the salt-polymer electrolyte could be improved by increasing the salt content past this maximum. This new insight deviated from the conventional wisdom that as salt concentration increases, T_g increases[46,116]. With the ability to lower T_g and thus improve transport properties of salt-polymer systems a new field of

inquiry was born. Angell called the compositional range past the T_g the salt-in-polymer domain, and showed that with as little as 10-20% of high molecular weight polyether ($+10^5$Da) is needed to impart the mechanical properties of an elastomeric solid. Conductivity values of greater than 10^{-4}S/cm at 25°C were measured for 90% lithium salts and either 10% PEO or 10% PPO[115]. Bushkova et al[117] described the surprising transport properties in terms of percolation theory, when a critical threshold of ions clusters occurs all clusters are in contact making one big cluster. This allows for fast cationic transport of Li^+ through this cluster network. The attractive features of the PiSE approach is to combine fast cationic transport with the mechanical properties of a flexible polymer. Ferry et al showed that the role of the polymer besides forming a solid is to help plasticize the salt, imparting the ability to form an ion cluster network[118]. The PiSE approach is promising field of research with more to be explored. The inclusion of a second small solvent molecule could help further improve the transport properties of these systems.

2.12 Aqueous Salt Electrolytes

Building on this concept of salt-rich systems, a unique approach was taken by Suo et al.[113] where a highly concentrated 21m (molal) solution of LiTFSI in water or "water-in-salt" electrolyte (WISE) was demonstrated to be an effective alternative to other aqueous electrolytes. This approach is different from the PiSE approach in that instead of using small amounts of high molecular weight polymer to solubilize the high salt content of the electrolyte and impart the mechanical properties of a solid, a small amount of water is used which leads to a liquid electrolyte solution with faster ion transport than the PiSE systems. Their research showed an expanded electrochemical stability window (ESW) to ~3V, with

the proof of concept battery pair of a Mo_6S_8 anode and a $LiMn_2O_4$ (LMO) cathode, significantly higher than the ESW of water at 1.23V[113]. This WISE system demonstrated the ability to cycle in a 2.3 V electrochemical cell with minimal capacity fade over 100 cycles and nearly a 100% coulombic efficiency, showing considerable improvement for an aqueous electrolyte. Typically for liquid electrolytes, solvent molecules are the majority component within the first solvation sheath of Li^+. This leads to a selective reduction of solvent molecules at the anode/ electrolyte interface, and for liquid organic electrolytes the resulting decomposition products can form a quality passivating SEI. For aqueous electrolytes where water is the solvent molecule it's a different story, as water is a poor chemical substrate for SEI formation given that water reduction leads to H_2 gas generation. The origin of the increased stability of the aqueous WISE is the drastic alteration of the solvation shell around Li^+, with only 2.6 water molecules for each Li^+[113], allowing $TFSI^-$ to enter the solvation sheath. $TFSI^-$ anions entering the solvation sheath of Li^+ assisted with formation of a solid passivating layer comprised of mostly LiF on the anode surface as $TFSI^-$ and not water becomes the reduced species[119–122].

Since the initial breakthrough of anion-derived SEI in highly concentrated aqueous salts in 2015, multiple efforts have been successful at increasing the salt concentration through the careful selection of two-salt systems. Water-in-bisalt electrolyte added a second lithium salt lithium trifluoromethane sulfonate (LiOTf) to WISE for a mixed aqueous salt with 28m effective concentration[123]. The molar ratio of cation/water is approximately 1:2, an increase in cation content from a 1:2.6 ratio for just WISE[113,123]. Similarly, Yamada *et al* reported two bisalt systems, first an aqueous salt comprised of LiTFSI and lithium bis(perfluoroethylsulfonyl)imide (LiBETI) for an effective

concentration of 28m[124]. Second, an aqueous salt using LiTFSI and $LiN(SO_2CF_3)(SO_2C_2F_5)$ (LiPTFSI) for an impressive effective concentration of 55.5m, or a cation:water ratio of ~1:1[125]. These efforts to reduce the number of water molecules in the first solvation sheath of Li^+ have yielded impressive results, with LTO[124,125] anode and even Li metal/ Al alloying reaction[125] being enabled in these systems.

Another effort to innovate on the anion-passivation mechanism in concentrated aqueous electrolytes involves incorporating WISE into a gel using polyvinyl alcohol (PVA)[126]. The total concentration of salt in water in this system is 25m, greater than the solubility limit of just WISE (~22m) suggesting that PVA chains play some role in solvation of LITFSI. While the prospect of combining an aqueous salt with a polymer matrix to make an aqueous SPE is a promising area for research, there is a lack of peer-reviewed publications on this topic.

Chapter 3: Overview of Research Activities

3.1 Electrolyte Component Selection

In the following section, information on the materials used to synthesize the two different SPEs are given. Figure 3.1 gives an overview of the chemical structures of materials used.

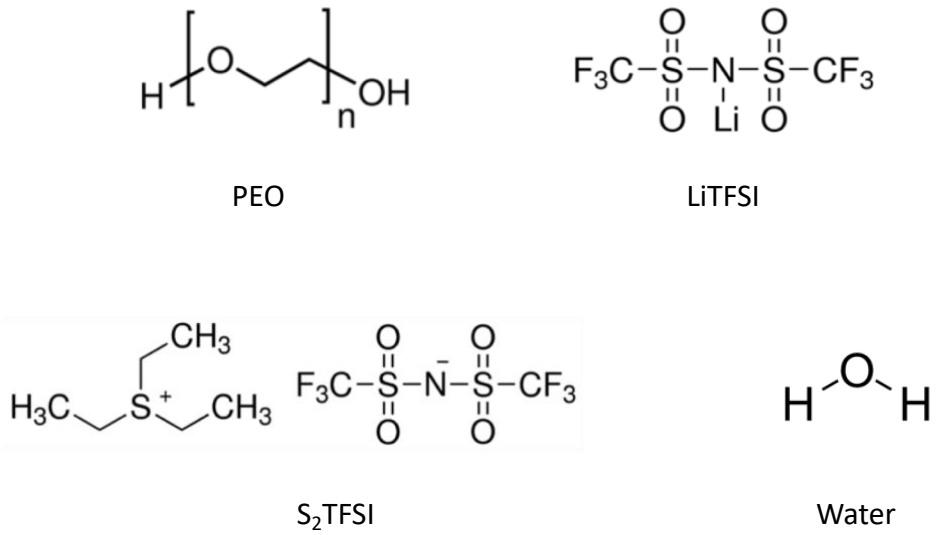

Figure 3.1: Chemical structures of materials used to synthesize SPEs.

Polymer

The polymer matrices that were investigated are various molecular weights of poly(ethylene oxide) (PEO). The polymer matrix will entrap the aqueous salt and the ionic liquid, all the while providing the mechanical stability that will make these electrolytes true solids with no leakage. For this reason, higher molecular weight of $1x10^6$ Da and $4x10^6$ Da was tested. PEO is a popular choice as a polymer host for SPEs[16,31,45,47,49,85,127] due to its electrochemical stability, reasonable conductivity at ambient or elevated temperatures

between 40-80 °C, easy processability and safety. The conductivity of PEO has a strong temperature dependence that is linked to its crystallinity, which disrupts ion conduction. The mechanism of ion conduction in PEO is a combination of inter and intrachain hopping of Li^+ along coordination sites to ether oxygens along the PEO backbone. This hopping mechanism is dependent on the PEO chains being mobile, thus raising the concern over crystallinity. There are many methods to plasticize PEO and increase the amount of amorphous phase present, which will increase the conductivity. These methods include the inclusion of ceramic nanoparticles[33], using a block copolymer with a PEO component[87,128], using low molecular polymers[129], or adding ILs[30,31,45,47,85].

Lithium Salt

LiTFSI was chosen and is easily dissolved in solution or polymer given its bulky anion which can easily disassociate from the Li+ cation, allowing for good ion conduction. One major concern with the use of LiTFSI is that it can corrode aluminum, a popular cathode current collector material, at high potentials (>4.0V)[48,130]. However, it has been previously shown that SPEs incorporating LiTFSI salt can be stable against aluminum[31]. LiTFSI will be the salt of choice for the investigation of the ILSPEs.

Ionic Liquid

The IL that will be most extensively studied is triethyl sulfonium bis(trifluoromethanesulfonyl) imide (S_2TFSI). The TFSI anion was chosen to match that of the lithium salt, as well as the favorable properties previously mentioned. The S_2 structure is an underutilized cation for ILs in SPE applications that has demonstrated

exceptional electrochemical stability and conductivity[30,31]. The structural similarities between the S_2 cation and PEO are thought to lead to better compatibility with regards to electrical properties. Other cations that are more popular in research literature such as the imidazolium or pyrrolidinium structures are also viable options with their own set of drawbacks. The imidazolium architecture suffers from poor stability at low voltages[91], while the pyrrolidinium architecture has shown low conductivities when incorporated into a PEO matrix[83].

Aqueous Salt

The aqueous salt of interest is LiTFSI in water, which has been investigated previously as a "water-in-salt-electrolyte"[113] with a concentration up to 22m. This aqueous salt used to make ASPEs will be varied up to and past their salt concentration limit in water, taking advantage of the additional solvation of LiTFSI from PEO. Ratios of polymer: salt: water were varied to sample a wide range of transport and mechanical properties.

3.2 Electrode Materials Selection

The SPEs will be cycled in a full electrochemical cell to determine battery performance. Lithium metal and lithium titanate (LTO) will be used as anode materials. Lithium iron phosphate (LFP), lithium manganese oxide (LMO), and lithium cobalt oxide (LCO) will be used as cathode materials. For the ILSPE the cathode will be a composite of active material, PVDF (polyvinylidene fluoride) binder, carbon black, IL, and lithium salt. A

composite cathode has often been reported in literature as needed to facilitate a good interface between the cathode and SPE[2,3,33,85].

3.3 Polymer Electrolyte Synthesis

The SPEs will be fabricated in a dry room using a solvent-free hot-pressing process. All components will be thoroughly dried for 24-48 hours in a vacuum oven before use. The SPE components will be mixed with a mortar and pestle, and then vacuum-sealed in a pouch cell and annealed overnight at 60 °C to homogenize the mixture. After annealing, the pouch will be hot-pressed with one metric ton of pressure at 85 °C for one minute to form a homogenous thin film SPE. All SPEs will be stored in their vacuum pouches until they are required for testing, at which point they will be opened in either a dry-room in the case of ILSPE, or normal lab atmosphere in the case of ASPE and be used immediately to limit any possible contamination. Solvent-free hot-pressing produces thin, homogenous SPEs but has the added benefit of eliminating the possibility of trapped solvent molecules, which can produce artificially high conductivity measurements[131].

3.4 Cell Construction

The test cells will be constructed as shown in Figure 3.2, and are crimped to hermetically seal them from the environment. All test cells involving ILSPE will be done in a dry room to prevent any moisture contamination. Prior to testing the cells will be annealed at 60$_o$C for 24-48h to ensure good contact between the electrolyte and the electrodes. The electrode type will depend on what test is being performed.

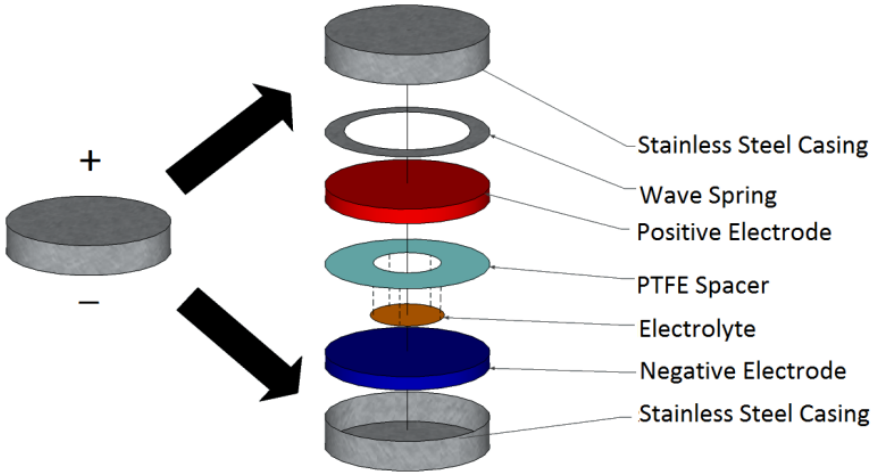

Figure 3.2: Exploded view of test cell construction, image adapted from Aaron Fisher's PhD dissertation.

3.5 Characterization Techniques

Impedance Spectroscopy

The general principle behind AC impedance spectroscopy is that the application of a small amplitude AC current (10 mV) results in an impedance response that can be measured. This response can be understood by modeling this system as a combination of resistances and capacitances. To model this system, an equivalent circuit similar to that shown in Figure 3.3, will be fit to the data. R_b, bulk resistance, models the diffusion of charged species through the electrolyte, while R_p, interfacial resistance, and C_{dl}, double layer capacitance jointly models the interface's electrical properties. If additional components

are needed to better model the system, they will be added. This modeling will be performed on the SPEs to isolate the largest contribution to the overall resistance and how these resistances evolve with time during the overpotential studies. Additionally, experiments will be designed to test the veracity of the proposed model. One such experiment could be adjusting the lithium salt content in the SPE and observing how components in the equivalent circuit respond, and comparing this change with what is expected in literature.

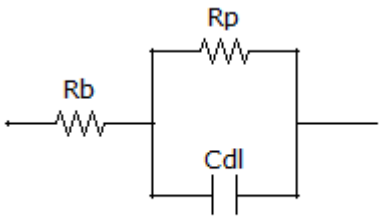

Figure 3.3: Equivalent electrical circuit.

To measure the AC impedance of the SPEs, a two-probe system will be used where an AC amplitude of 10 mV in the frequency range of 1 MHz to 1 Hz will be applied. The cells are to be constructed with two blocking stainless steel electrodes (total electrode thickness 1.0 mm to ensure good physical contact in the cell) such that the cell is symmetric. It is then possible to discern the bulk and interfacial resistance by fitting a semicircle to the Nyquist plot and assigning the low frequency intercept to the interfacial resistance and the high frequency intercept to the bulk resistance. The bulk resistance value is plugged into (1) to give the conductivity in mS/cm, where t is the thickness of the SPE, A is the area, and R is the bulk resistance. Each SPE that is measured will be done with three samples to provide statistical significance. The cells will be measured in a wide range of operating temperatures, from 0-80^{o}C. The target range of ionic conductivity for SPE is between10^{-3}-10^{-4} S/cm at room temperature, a value necessary to be competitive for commercial applications.

$$\sigma = \frac{t}{R*A} \quad (1)$$

DSC

Differential scanning calorimetry (DSC) will be conducted on a TA Instruments Q100 DSC. DSC allows for the detection of thermal transitions that occur in the SPE, which will be informative when coupled with the observed properties. Ion conduction in polymers with high amounts of crystallinity is poor, so the melting temperature needs to be identified and taken into account when designing a SPE system. Additionally, the glass transition temperature T_g is important to identify because the further a SPE is away from its T_g the more conductive it will be due to the polymer chains having a 'rubber-like' quality. Polymers tend to have a hysteresis in melting and crystallization temperature, with the ability to "supercool" down below the melting temperature. Determining melting and recrystallization temperatures is critical to understanding the transport properties of the SPE, as increasing amounts of crystallinity in the SPE will have an adverse effect on the ionic conductivity. Additionally, knowledge of the glass transition temperature is important for comparison to the observed electrical properties and to understanding the mechanical properties of the electrolyte. DSC experiments will consist of placing a SPE sample in a hermetically sealed aluminum pan. The sample will go through a heat/ cool/ heat cycle to erase any thermal history and the relevant transition temperatures will be identified from the thermogram using TA Universal Analysis software. Comparison between samples will determine the relationship between composition (varying polymer content, IL content, etc) and thermal transitions of the SPE.

Modulated DSC

MDSC will be conducted on a TA Instruments Q100, and will be used to determine the homogeneity of the ILSPE and if there is any microphase separation present. IlSPE samples will be placed in hermetically sealed pans and assembled in a dry room to avoid moisture contamination. A heat/cool/heat cycle above the SPE melting point will eliminate any thermal history before recording a thermogram. Varying the relative concentrations of polymer, salt, and IL while measuring phase separation will help determine the Li^+ conduction mechanism by comparing this data with previously proposed conduction mechanisms in Figure 2. The two main mechanisms for consideration are the two panes on the right side of Figure 2. The first mechanism describes an environment where Li^+ coordinates to both the ether oxygens on the polymer chain and to free anions, and moves through a combination of inter and intra chain hopping. The second mechanism proposes that there is some microphase separation with polymer-rich and polymer-poor regions and that polymer chains are largely not participatory. The Li^+ is surrounded by a liquid-like sea of ions in the polymer-poor phase and conducts as though it were in a liquid. The detection of phase separation at various concentrations of ionic additives with MDSC will help determine the Li^+ conduction mechanism for the ILSPEs.

Linear Sweep Voltammetry

The electrochemical stability window (ESW) is the range of potentials at which the electrolyte is thermodynamically stable. Outside of this range, the electrolyte will start to undergo irreversible redox reactions, resulting in capacity fade and a resistive interface. Ideally the electrolyte would have an ESW that is wider than the theoretical potentials of the electrodes. However, current organic liquid electrolyte technology is not stable below 1V and is reliant on forming a passivating SEI. Similarly, electrolytes with aqueous components are notorious for being incompatible with even modestly low potential anodes like LTO. Figure 4 shows the ESW for different generations of aqueous-based electrolytes, none of which are close to the LTO anode (1.5V vs Li/Li^+). Fortunately, polymers electrolytes have been shown to have excellent ESWs as they have demonstrated stabilities that exceed 5V against Li/Li^+[10]. Linear sweep voltammetry (LSV) will be conducted to determine the ESW of the electrolyte. To accomplish this a coin cell will be constructed with a reference electrode (lithium metal) and the other is a blocking electrode. For the cathodic sweep the blocking electrode is aluminum and for the anodic sweep the blocking electrode is stainless steel. For the LSV test the voltage will be set to 3.0V vs Li/Li^+ and then stepped at a rate of 1mV/s to either 0 or 6.5V against the lithium reference. 6.5V was chosen as an arbitrarily large potential to ensure that some breakdown of the electrolyte occurs. At the point where the current density becomes nonlinear and increases sharply, the electrolyte has broken down. With both the anodic and cathodic sweeps the ESW is determined. Electrode materials with potentials within the ESW will be stable with the SPE, while electrode materials outside of the ESW will need to make a passivating layer (SEI) at the interface to be used effectively in a LIB.

Cyclic Voltammetry

Cyclic voltammetry (CV) will also be conducted to elucidate any time dependent changes. This experiment will be run in a similar manner as LSV, but the voltage will be cycled from 3V to the voltage of the desired working electrode and back to 3V, which will count as one cycle. This will be done for +100 cycles in both the cathodic and anodic directions. If the shape of the CV curve is flat with no spikes in current density across many cycles, then the SPE is stable at the given potential with cycling time. If current density increases with cycle time, then the SPE has begun to breakdown under the stress of continued cycling. Intermittent impedance spectroscopy will be conducted to quantify the growing interfacial resistance at the electrode/ electrolyte interface with time as the electrolyte is cycled.

Lithium Stripping and Plating

AC impedance gives a good picture of the bulk properties of an electrolyte, but overpotential studies lead to an understanding of how the interface between the electrode and electrolyte evolves with time. The overpotential is the difference between the thermodynamic reduction potential of a given redox reaction and the actual potential at which the reaction takes place, in this case it will be the reduction of Li^+ and the plating of lithium metal at the electrode surface. This gives a direct measure of the excess energy (wasted as heat) needed to drive a reaction above what is thermodynamically predicted, and is a mode of inefficiency in the cell. For symmetrical Li/ SPE/ Li coin cells, the increase of the overpotential value measured with cycle time can be attributed to the passivating

quality of a growing SEI as the SPE isn't stable at the potential of lithium and will be reduced. If the SEI is passivating, the overpotential value will increase slowly with cycle time. If the quality of the SEI is poor and fails to prevent further electrolyte degradation, the overpotential will increase more rapidly as electrolyte reduction contributes to the SEI becoming thicker and more resistive. Intermittent impedance spectroscopy is coupled with this technique at set cycle intervals to measure the resistance of the cell, directly observing the growing resistance of the cell with cycle time which is also attributed to the growth of the SEI. Stability of this interface is critical to long cycle life, capacity retention, and high coulombic efficiency, all of which are important metrics when considering the validity of an electrolyte for application. Symmetrical coin cells with Li/ SPE/ Li will be constructed and lithium plating/ stripping tests will be conducted galvanostatically by reversing the polarity of a constant current density of 0.1 mA/cm_2 each hour. It is ideal to have a low value for the overpotential that increases very slowly with time, indicating that the interfacial resistance and SEI is stable and not increasing much with time. Impedance scans will be taken intermittently every 20 cycles while the overpotential is being measured. The equivalent circuit in Figure 6 will be used to model the resistances in the cell, and to determine which resistances are growing with time and having the largest contribution. This modeling will be used to confirm that the growth of a SEI is the main contributor to increased resistance in the cell.

Cycling performance

The ultimate goal of developing a SPE is to successfully use it in a LIB, therefore the SPEs performance must be tested in an electrochemical cell. Ideally the electrolyte would cycle

and deliver capacity without interfering with the normal capacity fade of the cathode. Capacity fade is an inevitable result of electrolyte degradation and the physical and chemical changes that occur in the structure of the cathode during the intercalation/deintercalation of Li^+ ions. The lifetime of a battery is considered as the number of charge cycles it can undergo before it is only able to deliver 80% of its initial capacity, which is typically in the range of +500 cycles for LIBs. Coulombic efficiency is another metric that is measured during cycling and is the ratio of electrons that participated in charging the battery to the number of electrons that completed the discharging of the battery. Any percentage less than 100% represents a loss in the system in the form of heat and/ or unwanted chemical reactions (continual electrolyte degradation and SEI formation). Accelerated capacity fade (over dozens of cycles rather than hundreds) coupled with less than stellar coulombic efficiency (>95%) is indicative of a poorly passivating and growing SEI layer. Comparison of the rate of capacity fade between samples will help determine the relationship between different component concentrations and the passivation ability of the SEI. Another variable that will be looked at is operating temperature, with cells cycling at ambient temperature as well as elevated temperatures (60^oC) to measure differences in cell performance at different operating temperatures.

Rate Performance

Rate capability, or the ability to cycle at different C rates (C is charge rate, where 1C is full discharge in one hour, C/2 would be full discharge in two hours), is an important aspect of battery performance and will be investigated here. It is typical for a battery system to delivery less capacity at higher C-rates which place a greater demand on the ability of the

battery to transport Li^+. However, to demonstrate healthy cycling and good rate capability a battery should be able to demonstrate reversible capacity at any given rate. Li/ ILSPE/ LFP cells will be made and cycled at rates from C/20 to C/2. Li/ ILSPE/ LFP cells were cycled on an Arbin BT2000 between 2.8-4.0V vs. Li/Li^+. The variable rate routine involves cells completing 5 cycles at the following rates in succession: C/20, C/10, C/5, C/2, and C/20 at 22°C. All cells were annealed at 60°C for 24hr prior to cycling.

Transference number

The lithium transference number is a measure of the fraction of the total moving charge that is due to Li^+ ions. The lithium transference number is determined by the Bruce-Vincent method which involves potentiostatic measurements in a Li/ SPE/ Li cell and dividing the steady state current I_{ss} by the initial current I_o while accounting for the change in resistance between the steady and initial states (Equation 2)[132,133]. ΔV is the polarization potential, R_i is the interfacial resistance, R_b is the bulk resistance, o represents the initial condition, and *ss* represents the steady state. T_{Li^+} corresponds to the ability of each ion present to diffuse through the electrolyte and depends on the relative concentration of each ionic species. T_{Li^+} is a good measure of the concentration gradient that develops in the electrolyte system, and as the gradient becomes steeper it will be more difficult for the battery to deliver capacity. A value of 1 is the ideal case because it means that all moving charge is due to Li^+, but given the complex nature of the solid electrolytes this is expected to be between 0.2 and 0.5. The presence of other ions such as the TFSI anion or IL cation will affect T_{Li^+} and make it lower, given that the movement of these ions contributes to the overall current. This being the case, the design of the SPE must take the ionic additives adversely affecting

T_{Li^+} into account and stay above a reasonable threshold of ~0.3. The potentiostatic measurements will be run at 10 mV for 2hrs where the system is assumed to be at equilibrium by observing a linear response in I over time. The relevant values will be measured using a solartron and by using (2) T_{Li^+} will be determined.

$$T_{Li^+} = \frac{I_{ss} * R_{b,ss}(\Delta V - I_0 * R_{i,0})}{I_0 * R_{b,0}(\Delta V - I_{ss} * R_{i,ss})} \quad (2)$$

Scanning Electron Microscopy and Energy Dispersive X-ray Spectroscopy

Scanning electron microscopy (SEM) in combination with energy dispersive x-ray spectroscopy will be used to directly image and characterize the composite cathode surface. Imaging of the interface along with specific point chemical mapping via EDX will be a useful tool to visualize if the cathode is well mixed. Imaging will be done with a Tescan GAIA SEM system and accompanying EDX attachment.

Pulsed-Field Gradient Nuclear Magnetic Resonance

Pulsed-field gradient nuclear magnetic resonance (PFG NMR) will be used to determine the diffusion coefficients for different ionic species in ASPE electrolytes. All NMR samples are packed into 5 mm tubes in ambient atmosphere, and the tubes are then sealed to preserve the same relative humidity value in which they were prepared. Sample preparation time will be minimized to five minutes or less in an effort to lessen the air exposure of the electrolyte. PFG NMR experiments will be performed at 25 °C with a 300 MHz Varian-S Direct Drive Wide Bore spectrometer equipped with a DOTY Scientific PFG probe (DS-1034, 1400 G/cm maximum gradient). Single peaks are observed for $_{1}H$, $_{19}F$, and $_{7}Li$ resonances centered at 302.7, 280.5 and 117.3 MHz, respectively,

corresponding to all hydrogen-, lithium-, and fluorine-containing species. A PFG-stimulated echo pulse sequence will be used. Gradient pulse durations δ of 2 to 4 ms and diffusion delays Δ of 100 ms will be used. The gradient strength g will be linearly increased with 32 values steps from 1.7 up to 700 G/cm as needed. From each experiment, the integrated intensities S as a function of applied gradient g (in T/cm) will be obtained. Subsequently, diffusion coefficients D can then be computed using least-squares fitting of the Stejskal-Tanner Equation[134] (3):

$$S = S_0 e^{-D(g\delta\gamma)^2\left(\delta-\frac{\Delta}{3}\right)} \quad (3)$$

Data will be collected at multiple temperatures such that diffusion coefficients of different species as a function of temperature are elucidated. Using the diffusion coefficients calculated from PFG NMR, transport number is determined using (4):

$$t^+ = \frac{D_+}{D_+ + D_-} \quad (4)$$

Transport number is analogous to transference number, with the only change being that transport number does not take into account the mobility of any charged or neutral ion pairs/aggregates that may be in the system. ASPE instability against lithium metal precludes it from transference number determination by the Bruce-Vincent method, thus the PFG NMR method was used for this system. Additionally, ionic conductivity can be calculated from the diffusion coefficients measured by PFG NMR using the Nernst-Einstein Equation:

$$\sigma_{\mathrm{NMR}} = \frac{F^2[C]}{RT}(D_+ + D_-) \quad (5)$$

Ionic conductivities calculated by Nernst-Einstein will be compared to those measured by EIS. A significant deviation from EIS measurements could indicate significant ion pairing in the ASPE system.

CHAPTER 4: Ionic Liquid-Based Solid Polymer Electrolytes[1]

4.1 ILSPE Justification

ILSPEs have shown great promise as safer and more green alternatives to liquid organic electrolytes, with the sulfonium cation architecture in particular warranting further investigation for its superior electrochemical stability[30,135]. ILSPEs would be ideal for applications with an elevated operating temperature requiring high energy density such as for a car battery (operating temperature ~100^{o}C) as they can be used with a lithium metal anode and high voltage (+4 V) cathode and they work well at higher temperatures. Additionally, battery application where safety is critical would be well suited for ILSPEs. One example would be implantable medical devices such as a pacemaker. Pacemakers operate at physiological temperature (~37^{o}C) and require low power density, relieving the concern over slower ion transport in SPEs, however safety cannot be compromised. SPEs also open the possibility for unique applications due to their flexible and conformable nature. An ILSPE that demonstrated good cycling stability and high ionic conductivity (~1 mS/cm) could replace liquid organic electrolytes for a number of applications.

[1] This work resulting in a manuscript that is in preparation for submission to a peer-review journal: **Matthew D. Widstrom**, Kyle B. Ludwig, Jesse Matthews, Metecan Erdi, Arthur V. Cresce, Gary Rubloff, Angelique Jarry, Peter Kofinas, "Enabling High Performance All-Solid-State Lithium Metal Batteries using Solid Polymer Electrolytes Plasticized with Ionic Liquid," (*In Prep)*.

4.2 Introduction

Lithium-ion batteries (LIBs) are an important energy storage technology due to their high energy densities and long cycle life[136], however there are concerns over the safety of these devices[137]. At the core of this problem is the ubiquitous use of flammable organic liquid electrolytes such as ethylene carbonate (EC) and dimethyl carbonate (DMC), which are electrochemically unstable in an operating battery and rely on a passivating layer consisting of electrolyte degradation products called the solid electrolyte interphase (SEI) to operate. Because of this instability, harsh conditions or flawed manufacturing process and design leave open the possibility for catastrophic failure in the form of thermal runaway leading to battery fire[138]. There is growing research interest in replacing these liquid organic electrolytes with solid alternatives that are intrinsically safer[4,20,48,139,140]. Ideally, an alternative to liquid organic electrolytes shall simultaneously address the safety concerns while maintaining suitable performance metrics for conductivity and electrochemical stability.

Due to its unique characteristics, solid polymer electrolytes (SPEs) is a very promising alternatives to organic liquid electrolytes[20,89,139,141,142]. SPEs are nonflammable and have little to no vapor pressure, making them ideal candidates for battery applications in which safety is critical[143]. They are easily processible as they can be solution cast[87] or fabricated into thin films using a solvent-free hot pressing approach[2], they are flexible and conforming in nature, and they can eliminate the need for inactive cell components such as spacers and packaging which are currently required in the manufacturing process in order to prevent liquid electrolyte from escaping. However, the biggest challenge facing SPEs is their inferior ionic conductivity, as solid electrolytes are inherently less conductive towards

Li^+ than their liquid counterparts. For poly(ethylene oxide) (PEO), whose ether-containing architecture is commonly employed in SPEs due to its ability to dissolve lithium metal salts[142], this challenge is embodied in its propensity to crystallize below 60 °C for even moderately high molecular weights[31]. EO-containing SPEs exhibit ionic conductivity values several orders of magnitude lower compared to conventional liquid electrolytes below their melting point. Appreciable transport of ions in PEO relies on segmental chain motion which is only possible in the amorphous state, making it advantageous to have a fully plasticized PEO matrix and avoid any crystallization[47].

There are a number of strategies researchers have used to create a more favorable morphology for ion conduction at lower temperatures in EO-containing SPEs. One approach is to introduce micro or nanosized ceramic fillers such as TiO_2, Al_2O_3, and silica[51,53,140] as plasticizers that form composites with better mechanical properties and enhanced conductivity due to the disruption of crystal formation. Conductivity values on the order of ~10^{-4} S/cm have been obtained at elevated temperatures using ceramic fillers, which alone isn't satisfactory for most commercial applications. A second approach is to incorporate PEO into a block copolymer (BCP) to disrupt crystallization while simultaneously imparting robust mechanical properties from the second block[68,69]. The inclusion of a second rigid block drastically improves the mechanical properties of the SPE which can help stabilize Li metal anode for long-term cycling. The drawbacks of this approach are that the rigid block is not conductive, leading to a low overall conductivity making these BCP SPEs only suitable for high (>80 °C) temperatures[70,144].

A third approach is to plasticize PEO with an ionic liquid (IL) to form an amorphous SPE[30,31,83,87]. ILs are molten salts that have melting points below 100 °C, and are often in

the liquid state at room temperature. ILs have high ionic conductivity coupled with high thermal and electrochemical stability, and when incorporated into a polymer matrix can lead to significant increases in conductivity of the resulting SPE[32].

Here we investigate Polymer: IL: lithium salt ratios that have not previously studied and their effect on the physical and electrochemical properties of the resulting ILSPE system. We demonstrate a conductivity of ~1 mS/cm at room temperature, a value suitable for commercial application. Optimized ILSPE compositions are resistant to oxidation and show ideal Li stripping/plating behavior. ILSPEs with excellent transport properties were able to achieve room temperature cycling in Li/ ILSPE/ lithium iron phosphate configuration with high coulombic efficiency and capacity utilization. This work has the potential to enable the commercialization of ILSPEs for room temperature applications.

4.3 Materials and Experimental Methods

PEO with molecular weights of 300,00Da (300k), 1×10^6 Da (1M), and 4×10^6 Da (4M) was obtained from Sigma Aldrich. Triethylsulfonium bis(trifluoromethylsulfonyl)imide (S_2TFSI) was obtained from Sigma Aldrich. Lithium bis(trifluoromethylsulfonyl)imide (LiTFSI) was obtained from Solvay. Lithium iron phosphate (LFP) was obtained from Saft America Inc, Cockeysville Maryland. Kynar 1800 (polyvinylidene fluoride, PVDF) was obtained from Arkema. Anhydrous *N*-Methyl-2-pyrrolidone (NMP) was obtained from Sigma Aldrich. CR2032 stainless steel coin cells were obtained from Pred Materials International. All materials were opened, handled, and stored in a humidity-controlled dry room (dew point <-30°C) or glove box.

Electrolyte Preparation

Electrolytes were prepared by a simple three step process (see Figure 4.1). First the specific ratios of PEO, S2TFSI, and LiTFSI were mixed in a mortar and pestle until roughly homogeneous by inspection. The resulting sphere of electrolyte was placed in a sealable aluminum pouch and vacuum sealed (30s, -30psig). The pouch was then pressed at 85°C, above the melting point of PEO, with a force of 1 metric ton for one minute, resulting in a homogeneous film with a thickness of 100-200µm. All materials including the pressed film were handled in a dry room.

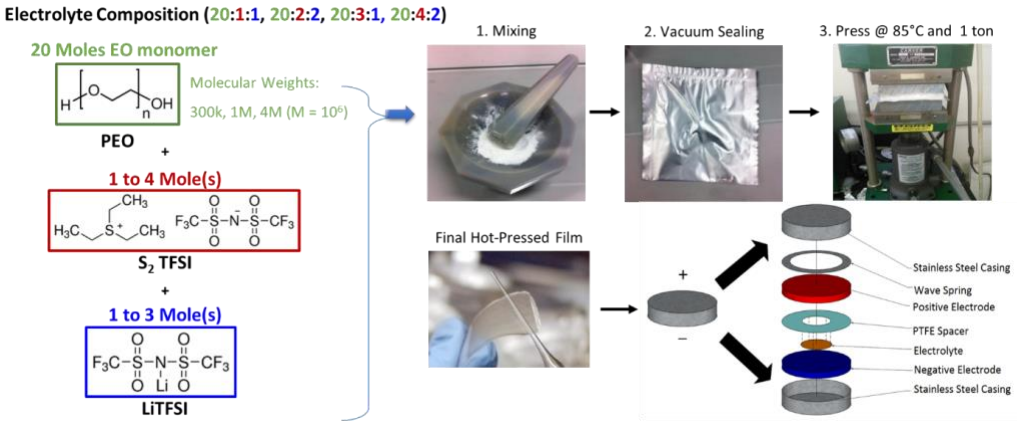

Figure 4.1: High molecular weight poly(ethylene oxide) (300k, 1M, or 4M Da; M = 106), ionic liquid S2TFSI, and lithium salt LiTFSI are combined in varying molar ratios. The components are mixed by mortar and pestle, vacuum sealed in a pouch, and then pressed with heat to produce an ILSPE (100-200µm).

Electrode Preparation

LFP cathodes were prepared by ball mixing 60wt% LFP, 10wt% Kynar 1800, 10wt% Super-P, 5wt% PEO, 10wt% S2TFSI, and 5wt% LiTFSI in NMP for 20 minutes. The electrode was casted on an aluminum current collector using a doctor blade and then vacuum dried for at least 24hr prior to use. The morphology of the cathodes was imaged by scanning electron microscopy (SEM) using a Tescan GAIA SEM system in Figure 4.2.

Figure 2A and 2B show a broad and zoomed-in view, respectively, of the electrode's surface morphology. EDX analysis was performed contemporaneously on the cathode imaged in Figure 2B. The analysis in Figure 2C shows the traces that were taken and the respective components at three of those traces. Trace 1 was taken on one of the numerous small, high contrast nanoparticles and was found to be carbon, as expected. Traces 5, 6, and 7 were taken on the larger, low contrast particles scattered in the image. These traces produced characteristic signals for oxygen, phosphorous, and carbon, with minor iron signals, leading to the confirmation that these larger particles are LFP. Traces 2, 3, and 4 show the "grey matter" connecting the larger LFP particles, which is coated with carbon nanoparticles. EDX analysis on these traces showed characteristic signals for carbon and oxygen with minor signals for sulfur and fluorine, suggesting that it contains the ILSPE components (PEO, S_2TFSI, and LiTFSI) and traditional PVDF binder.

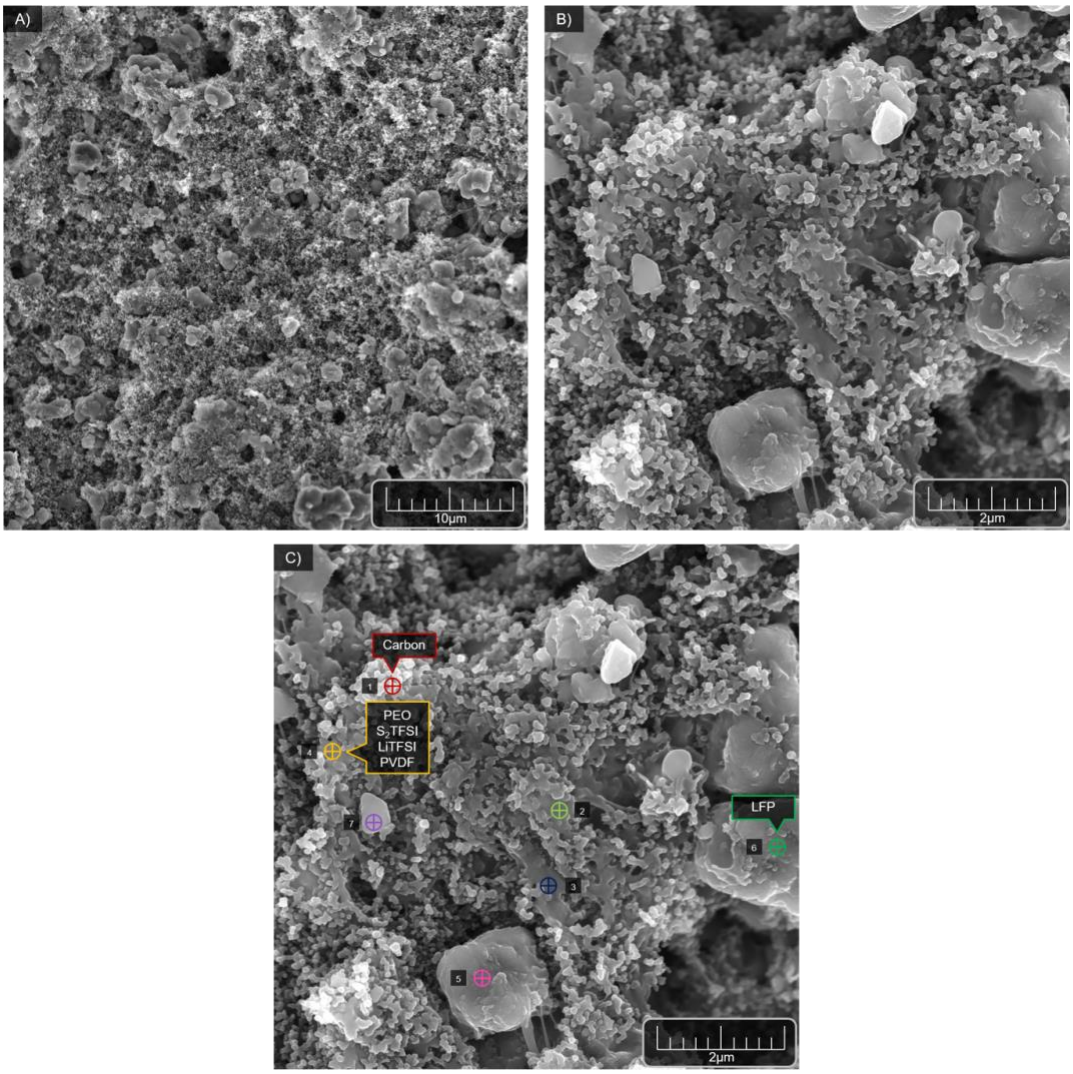

*Figure 4.2: Micrographs of the composite cathode incorporating the ILSPE taken using scanning electron microscopy at **A)** 10kx magnification and **B)** 50kx magnification. **C)** EDX spectroscopy traces overlaid on image **B**, highlighting the compositions of different regions. The small, high contrast spheres ("1") are carbon nanoparticles and the larger, low contrast particles ("5/6/7") are lithium iron phosphate, connected by the grey matter ("2/3/4") containing the ILSPE and PVDF.*

Differential Scanning Calorimetry

Modulated differential scanning calorimetry (DSC) was performed on a TA Instruments Q100 differential scanning calorimeter. Samples were prepared by hermetically sealing 10-15mg of electrolyte in an aluminum pan in a dry atmosphere. Samples were heated from

room temperature to 100°C, allowed to equilibrate, then cooled to -50°C and heated back to 100°C at a rate of 3°C/min with a ±0.20°C/min modulation.

Electrochemical Impedance Spectroscopy

Impedance measurements were performed using a Solartron 1287A/ 1255B platform. ILSPE was placed in a symmetrical coin cell using stainless steel blocking electrodes and annealed for 24hr to create a good contact before measurement. Impedance spectroscopy was measured over the frequency range of 1MHz to 1Hz with a 10mV amplitude. Temperatures ranging from 0°C to 80°C were measured, with a one-hour dwell time between each temperature to allow the electrolyte to equilibrate before measurement. A 0.25mm thick PTFE spacer with a 4mm inner diameter was used to create a clean, well-defined volume for ion diffusion. The samples were made using an empirically-determined amount of electrolyte that would best fill the volume defined by the PTFE spacer.

Transference Number

Transference number was measured on Li/ ILSPE/ Li cells using the Bruce-Vincent polarization method[133,145]. The cells were annealed for 24hr and conditioned by running 5 galvanostatic cycles with a 4hr charge, 45min rest, 4hr discharge, and 45 min rest constituting one cycle with a current density of 0.02mA/cm$_2$ being applied. This was done to create a stable interface before the transference measurement. The transference measurement involves applying a 10mV potential to the cell and measuring the current until a steady-state current is reached at 60°C. Impedance spectroscopy was run before and after the polarization to take into account any change in the resistance of the electrolyte.

Cyclic Voltammetry

Cyclic voltammetry was performed on an Arbin BT2000 to determine the oxidative stability of the electrolyte. Li metal/ ILSPE/ titanium-coated SS coin cells were prepared and cycled at 60°C. The voltage was swept from 2.5V to 4.5V vs. Li/Li^+ and back for a single cycle at a rate of 5mV/sec, for a total of 100 cycles.

Galvanostatic Cycling

Li/ ILSPE/ LFP cells were cycled on an Arbin BT2000 between 2.8-4.0V vs. Li/Li^+. Cells were cycled at 60°C for constant rate cycling, with a charge/ discharge rate of 1 hour (1C). Some cells in the same configuration were cycled at 22°C with a C/20 rate, while others cycled using a variable rate routine. These cells completed 5 cycles at the following rates in succession: C/20, C/10, C/5, C/2, and C/20. All cells were annealed for 24hr prior to cycling.

4.4 Results and Discussion

The ILSPE molar composition follows the nomenclature 20 PEO: x S_2TFSI: y LiTFSI (PEO molecular weight) where x and y are varied between 1 and 4 and the PEO molecular weight is 1 or 4 million Da. The molar ratios and molecular weight of SPE (from 20:4:2 (4M) with the highest salt/ionic liquid loading to 20:1:1 (1M) with the least loading) are varied to sample a wide spectrum of electrochemical properties while maintaining the ability to form homogenous, coherent thin films with a hot-pressing method. Increasing the molecular weight of PEO for higher salt/ionic liquid content is necessary for the

mechanical integrity of the resulting SPE film and has been shown to have a negligible effect on conductivity for molecular weights higher 1,000g/mol[146]. PEO was selected for its ability to dissolve alkali salts in high concentrations[36,147] as well as its reductive stability against lithium metal[39,41]. $TFSI^-$ was chosen as an anion for both the lithium salt and IL component for its ease of dissociation due to its highly delocalized charge, as well as its chemical and thermal stability[148,149]. $TFSI^-$ is also known to be a good plasticizer[150], which will help aid in amorphization of the electrolyte.

DSC

DSC was used to characterize the thermal properties of the ILSPE electrolytes, specifically to measure if there are any thermal transitions that could influence its conductivity behavior with temperature, such as melting phase transitions which would indicate the presence of PEO crystals. PEO crystallinity effectively shuts down the segmental motion of polymer chains, stunting the main conduction mechanism in PEO electrolytes and leading to poor ionic conductivity values[31,46,148]. Therefore, it is imperative to find ILSPE compositions with sufficient salt and IL content to fully plasticize PEO into an amorphous electrolyte. On the other hand, high content of salt will create aggregates that result in a significant decrease of conductivity and high content of IL will begin solvating PEO and result in a significant decrease of mechanical integrity. A compromise then has to be found to ensure the best performance of the ILSPE. DSC is the perfect tool to understand what effect that PEO, IL, and LiTFSI have on the morphology of the electrolyte. From a design perspective, we seek to determine what is the minimum IL + salt content that will ensure an amorphization of the electrolyte in the desired temperature range.

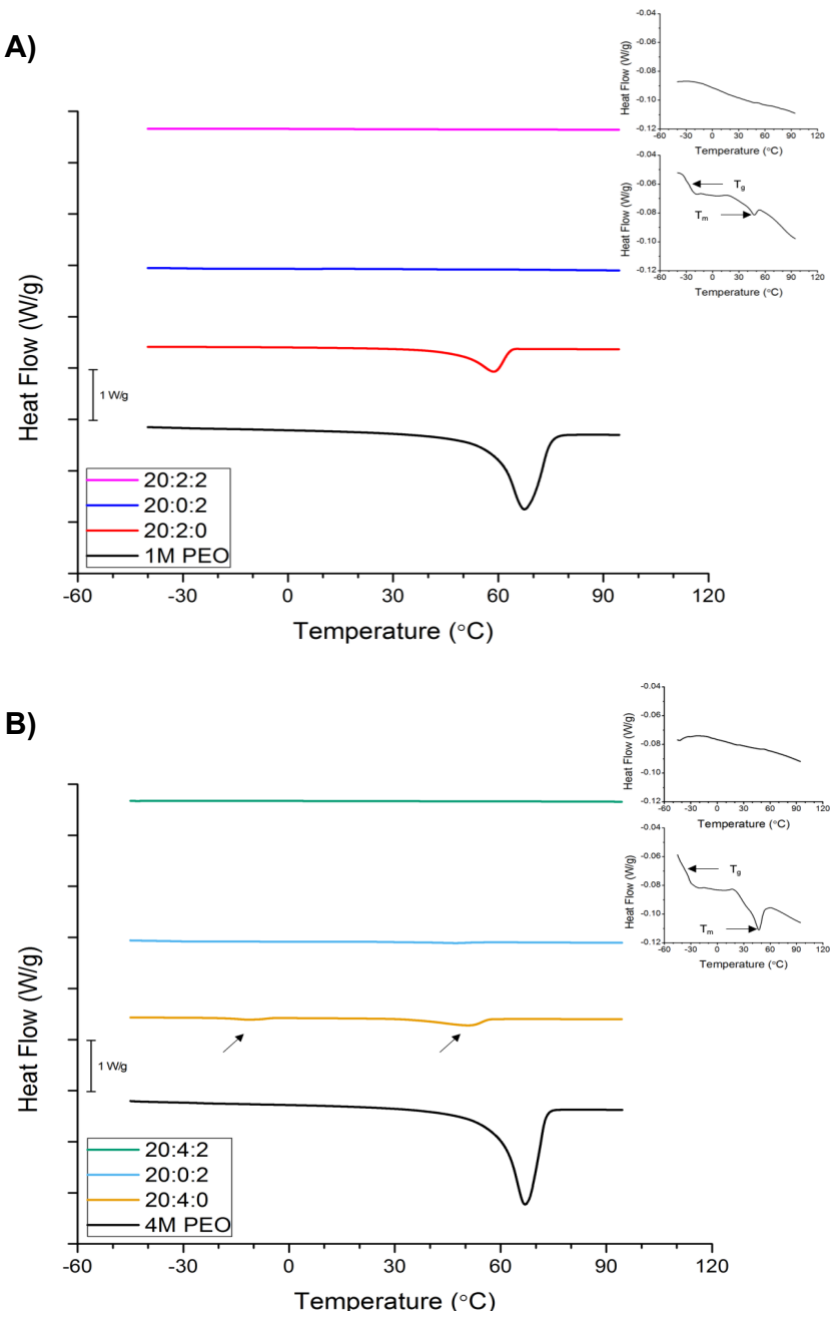

Figure 4.3: : Offset modulated DSC scans in the heating direction over the range of -50°C to 100°C for ***A)*** *1M PEO based electrolytes and* ***B)*** *4M PEO based electrolytes. Inset plots are zoomed in from the scans immediately to the left of the plot for better clarity. Arrows are used to point to thermal transitions, e.g.* T_g *and* T_m*. The thermograms show the impact each component has on the plasticization of the ILSPE individually and cooperatively. Individually each component (*S_2*TFSI, LiTFSI) fails to fully create an amorphous ILSPE with observable glass transitions and melting points. The composition designations represent molar ratios in the form of x PEO: y IL: z LiTFSI.*

To assess the impact of each component, reference DSC thermograms of the PEO matrix, PEO and S_2TFSI, and PEO and LiTFSI were collected and compared to thermograms of the full ILSPE (Figure 4.3) for two compositions. The PEO matrix (1M and 4M MW) shows a sharp melting peak above 65°C that is consistent with the melting temperature of high molecular weight PEO[151]. Adding IL into the PEO matrix has a strong effect on the PEO crystallinity. For 20:2:0 (1M), the PEO and IL thermogram (Figure 4.3A, red curve) shows a suppressed melting peak at ~59°C with an enthalpy of melting, ΔH_m, of 92J/g that is smaller compared to the 130J/g for PEO, indicating a lesser degree of crystallinity (45.3%). For 20:4:0 (4M) (Figure 4.3B, orange curve), the thermogram shows two melting peaks, indicating that this composition is phase separated. The first peak is at ~ -12°C and can be assigned to the melting temperature of pure IL[30]. The second peak at ~51°C corresponds to PEO melting, but is smaller in size (32J/g) and at a lower temperature than the melting peak for 20:2:0. These results demonstrate that while presence of IL into the PEO matrix has a beneficial impact on suppressing crystallinity, the salt is however necessary to fully plasticize and make the electrolyte amorphous.

As expected, adding Li salt into the PEO matrix changes drastically its thermal behavior. The thermograms for the PEO and LiTFSI salt in Figure 1 (20:0:2 (1M) and 20:0:2 (4M)) lack large features but the insets highlight the glass transition and melting temperature for both compositions. The glass transitions for 20:0:2 (1M) and 20:0:2 (4M) are at ~ -26°C and ~ -40°C respectively, while the melting transitions occurs at ~47°C for both compositions. While the salt alone plasticizes the polymer to a significant degree as evidenced by the 20:0:2 (1M and 4M) scans, it also increases the glass transition of the polymer from -67°C[151] to -26°C and -40°C respectively. The full ILSPE scans show no

features for both 20:2:2 (1M) and 20:4:2 (4M), indicating full plasticization and ideal morphology for ion conduction in this system. Both IL and salt have some plasticization effect as they either suppress the magnitude or the temperature for the melting transition of PEO. Increasing salt content can aid transport through plasticization of the polymer matrix and by increasing the number of charge carriers, but there is a tradeoff with a commensurate increase in T_g which decreases the segmental motion of the polymer making it less ionically conductive[69,152]. This is evidenced by the thermograms for 20:1:1(1M), and 20:1:3 (1M) in Figure 4.4 where 20:1:3 (1M) has a suppressed melting peak in both location (37.6°C) and size (2.63J/g) as compared to 20:1:1 (1M) (47.5°C, 38.6J/g), however a T_g becomes detectable at -44.0°C for 20:1:3 (1M) where none is detectable for 20:1:1 (1M).

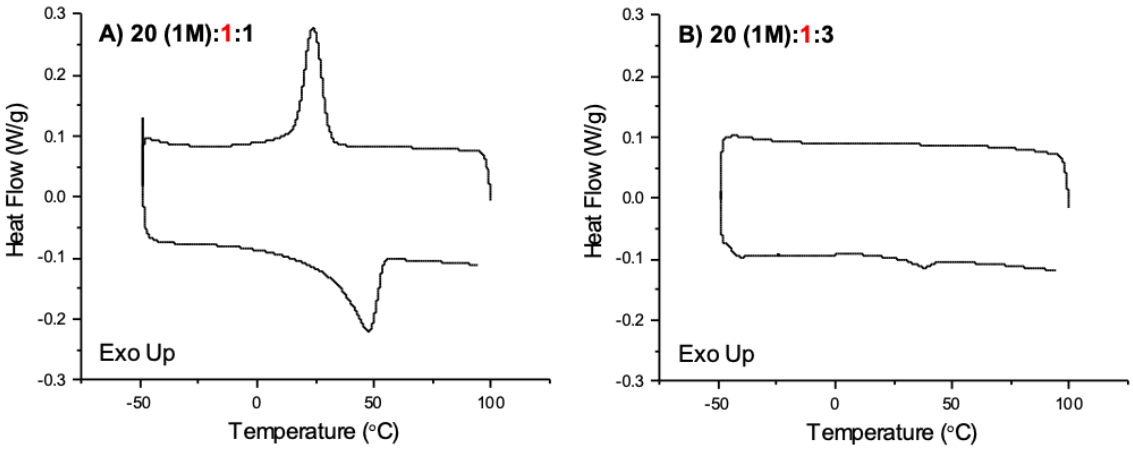

*Figure 4.4: Full modulated DSC scans in the range of -50°C to 100°C for **A)** 20:1:1 (1M) and **B)** 20:1:3 (1M). Note, M = 10_6 Da. An increase in the salt (LiTFSI) content of **A** leads to significant suppression of the PEO melting peak and complete suppression of the PEO recrystallization peak in **B**, but increases the T_g to an observable temperature of -44°C and shifts the melting peak down to ~38°C.*

An increase in T_g with increasing salt content was not observed when the IL content was increased to the same degree or more as is evidenced by the 20:2:2 and 20:4:2 thermograms

where no T_g was measured in the range of the scan down to -50°C. Figure 4.5 shows the individual full thermograms that were plotted together in Figure 4.3.

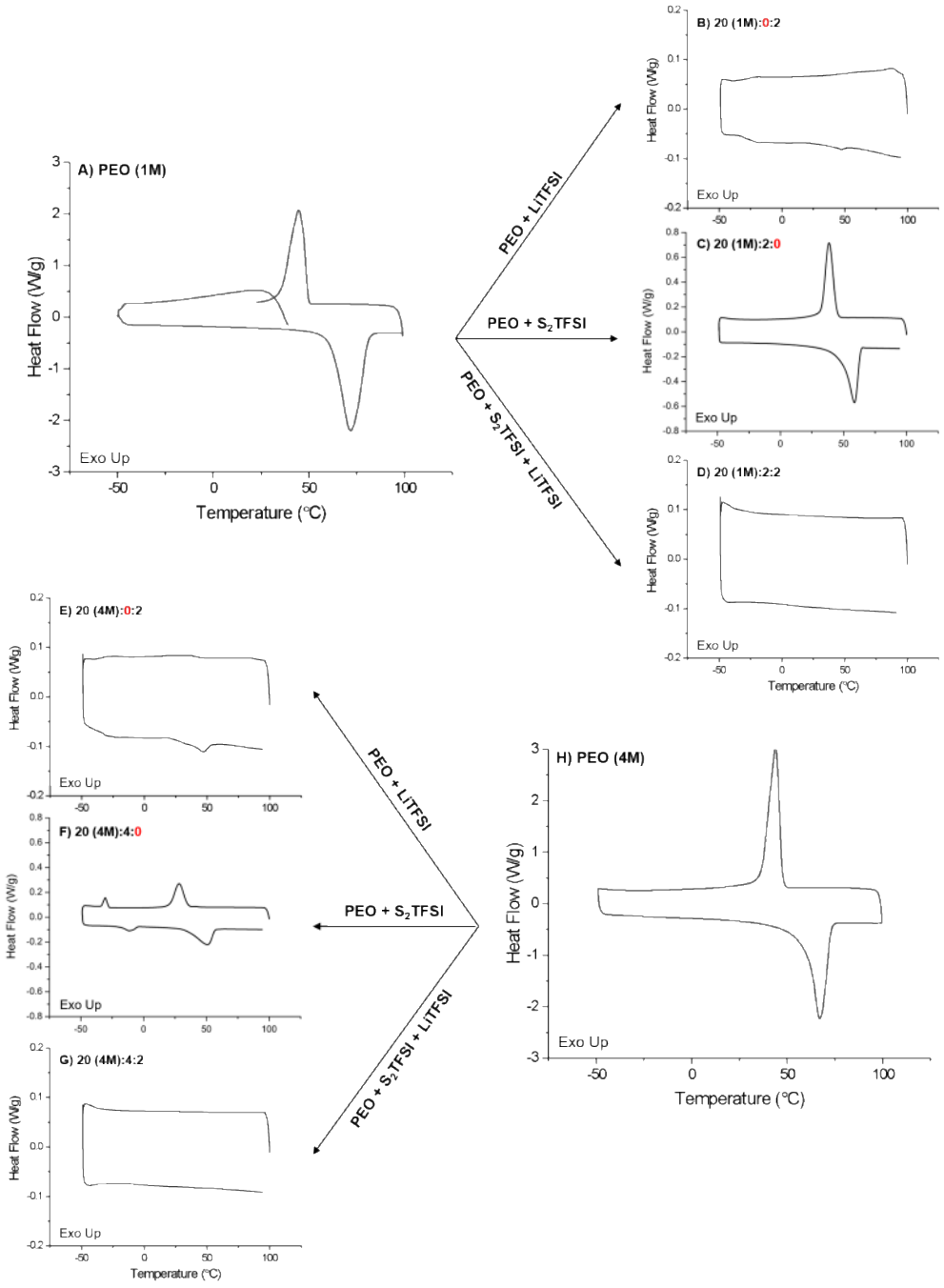

Figure 4.5: Full modulated DSC scans in the range of -50°C to 100°C for ***A)*** *PEO (1M)* ***B)*** *20 (1M):0:2* ***C)*** *20 (1M):2:0* ***D)*** *20 (1M):2:2* ***E)*** *20 (4M):0:2* ***F)*** *20 (4M):4:0* ***G)*** *20 (4M):4:2* ***H)*** *PEO (4M). Note, M = 10₆ Da. Arrows indicate the different combinations of components that were mixed and tested. The thermograms show the impact each component has on the plasticization of the ILSPE individually and cooperatively. Individually, both components fail to fully create an amorphous ILSPE with observable glass transitions and melting points.*

Table 4.1 shows a summary of the transition temperatures measured by DSC as well as enthalpy of melting and crystallization. Degree of crystallization is defined as:

$$\Delta x_c = \frac{\Delta H_m}{\Delta H_{PEO}} \times 100 \quad (6)$$

Where ΔH_m is the enthalpy of melting and ΔH_{PEO} is the 100% crystalline enthalpy of melting for PEO which is taken as 203J/g[59].

Table 4.1: A summary of the thermal transitions observed, using modulated DSC in the range of -50°C to 100°C, of the ILSPE compositions studied and their individual components. The enthalpy of melting and crystallization are provided, long with the degree of crystallization. Degree of crystallization was calculated using a reference enthalpy of melting of 203J/g for 100% crystalline PEO[59].

	T_g (°C)	T_m (°C)	ΔH_m (J/g)	T_c (°C)	ΔH_c (J/g)	Δx_c (%)
PEO (1M)	-67[36]	66.3	128.2	44.4	100.9	63.2%
PEO (4M)	-67[36]	66.9	119.8	43.8	107.4	59.0%
S_2TFSI	NA	-7.8	17.4	-31.3	17.8	NA
LiTFSI	NA	236		ND		NA
20 (1M):0:2	-25.6	47.2	0.4	ND	NA	0.2%
20 (1M):2:0	ND	58.7	92.0	38.5	78.0	45.3%
20 (1M):2:2	ND	ND	NA	ND	NA	NA
20 (4M):0:2	-39.7	47.0	5.5	ND	NA	2.7%
20 (4M):4:0	ND	-11.5 50.7	5.8 32.2	-30.5 28.2	4.5 31.6	2.9% 15.9%
20 (4M):4:2	ND	ND	NA	ND	NA	NA
20 (1M):1:1	ND	47.5	38.6	23.9	35.3	19.0%
20 (1M):1:3	-44.0	37.6	2.6	ND	NA	1.3%

ND = not detected; NA = not applicable

EIS

Electrochemical impedance spectroscopy was performed to measure the resistance of the electrolyte, R, in order to calculate the ionic conductivity from

$$\sigma = \frac{l}{R*A} \quad (1)$$

where l and A are the thickness and area, respectively, of the electrolyte. Resistance was extracted from equivalent circuit models based on the associated Nyquist plots. The area and thickness in Equation 1 were held constant by using a PTFE spacer. We validated our equivalent circuit model and technique for defining the area of the electrolyte by varying the inner diameter of the PTFE spacer, measuring and extracting resistance through EIS, and calculating the associated conductivity values (see Figure 4.6). For low temperatures, an equivalent circuit containing a resistor (R1) in series with a second resistor (R2) and capacitor that are in parallel with each other, was found to be appropriate. A constant phase element (CPE) was used in place of a traditional capacitor because the Nyquist plots showed nonideal capacitive behavior. R1 represents the resistance to ionic motion in the bulk electrolyte while R2 represents resistance to charge transfer at the interface due to the build-up of charge known as the double layer. For high temperatures (>40°C), the Nyquist plots show behavior of a pure ionic conductor (see Figure S7) and a simple equivalent circuit of one resistor in series with a capacitor was used. Linear regression shows that the calculated conductivity values are independent of the dimensions of the sample (see Figure 4.6B).

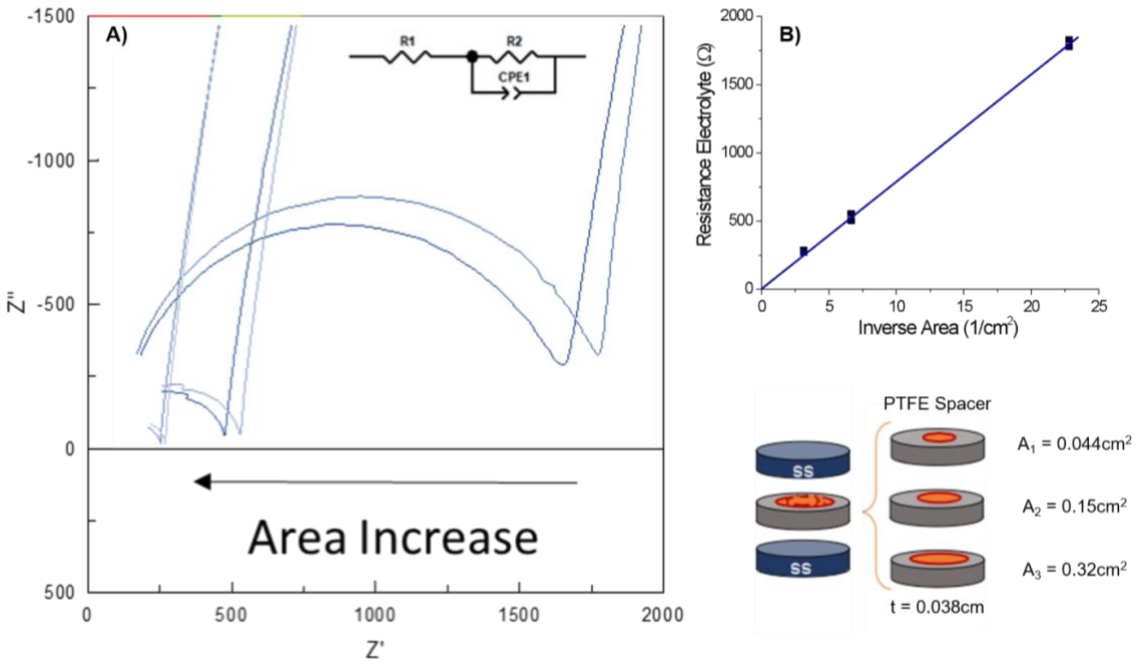

Figure 4.6: ***A)*** *Nyquist plots produced by electrical impedance spectroscopy of the ILSPE with different electrolyte volumes, as defined by the area of the opening in the PTFE spacers (below* ***B****). Two samples for each area were ran and show agreement. The spacer with the smallest opening area shows much higher resistance and produces a semicircle.* ***B)*** *Linear regression model for the fit between the reciprocal of spacer area and electrolyte bulk resistance, verifying that our conductivity measurements are independent of spacer area.*

Logarithmic scale conductivity as a function of inverse temperature is plotted in Figure 4.7 and shows a trend of higher ionic liquid loading leading to higher ionic conductivity. 20:4:2 (4M) and 20:2:2 (1M) have the highest conductivities at room temperature (25°C) with values of 0.96 mS/cm and 0.45 mS/cm respectively. 20:1:1 (1M) is the next most conductive at room temperature with a value of 0.24 mS/cm and 20:1:3 (1M) is the least conductive with a value of 0.01 mS/cm. These results show a clear connection between increasing conductivity and increasing ionic liquid content, while an increase of lithium salt in the absence of higher ionic liquid content decreases system conductivity. Increasing the salt content increases the amount of Li^+ charge carriers present, but this increase in Li^+

content appears to increase the likelihood of ion-ion and ion-cluster interactions, decreasing the mobility of Li^+ in the system[58].

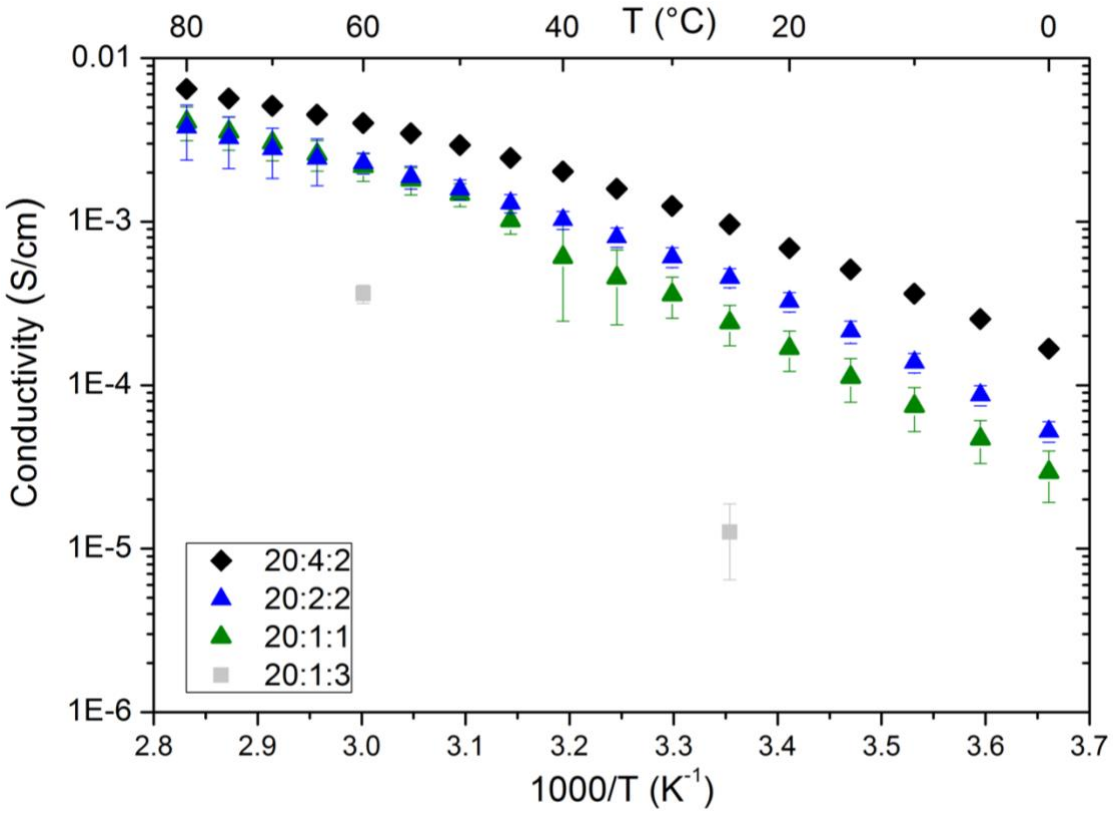

Figure 4.7: Ionic conductivity of the various compositions of ILSPE measured by EIS in the temperature range of 0°C to 80°C. The composition designations represent molar ratios in the form of x PEO: y IL: z LiTFSI.

High ionic liquid content leading to better conductivity values is corroborated with the DSC results in Figure 4.3 where 20:2:2 (1M) and 20:4:2 (4M) have no melting transitions while having the highest conductivities, with 20:4:2 (4M) having a room temperature conductivity value twice as high as 20:2:2 (1M). 20:1:1 (1M) also shows a rapid increase in conductivity comparable to 20:2:2 (1M) around 50°C corresponding to a melting phase

transition (Figure 4.8) that leads to increased segmental motion and thus ionic conductivity in the electrolyte.

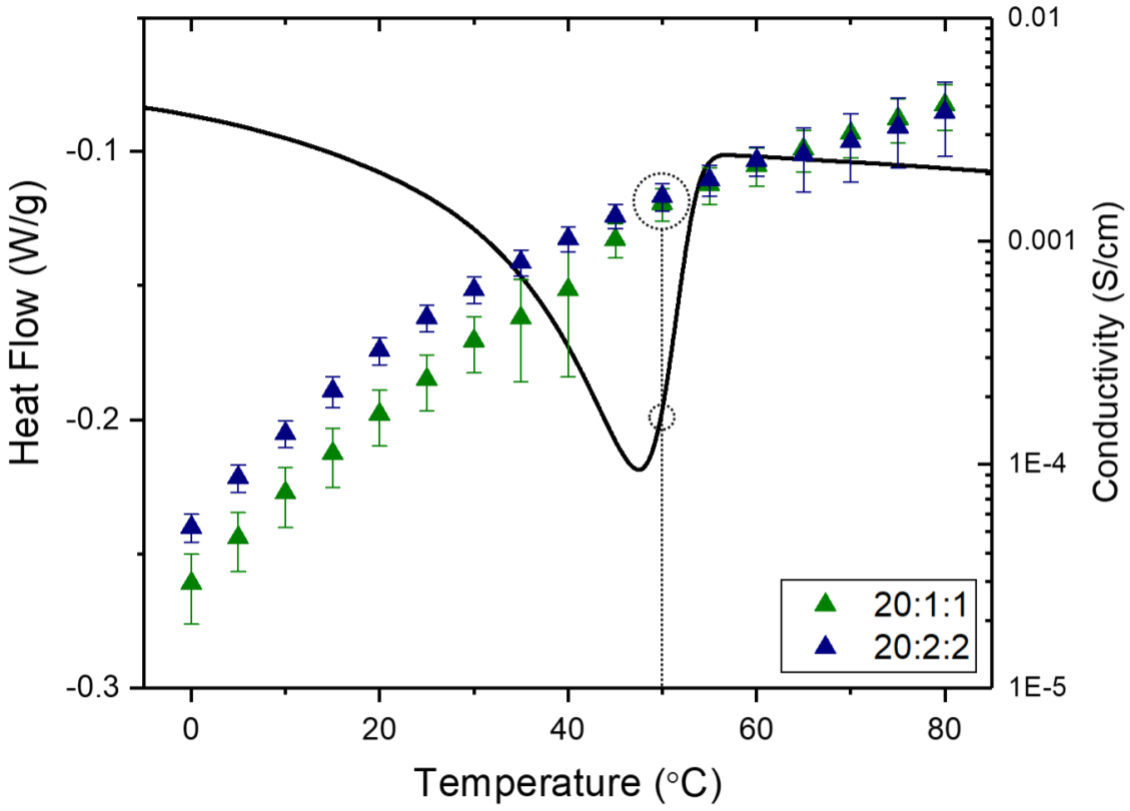

Figure 4.8: Modulated DSC scan, in the heating direction, of 20 (1M):1:1 (black line, left ordinate) overlaid with the conductivity values, obtained from electrochemical impedance spectroscopy, of 20:1:1 (1M) and 20:2:2 (1M) (green and blue triangles respectively, right ordinate) over a range of temperatures from 0°C to 80°C. In the direction of heating, the 20:1:1 (1M) ILSPE has a lower conductivity until 50°C, at which point the ILSPE undergoes a phase transition and the conductivities overlap.

Transference Number

The transference number, which is defined as the fraction of current that is due to Li^+ as a ratio of total charge carriers[133,145], was measured for the different ILSPE electrolytes and is shown in Table 4.2 along with ionic conductivity values at select temperatures and the melting temperature. Of particular importance is the finding that addition of ionic liquid,

which consists of a cation and anion, to plasticize the network does not show an impact on transference number, suggesting that more of the relatively bulky ions do not hamper lithium mobility.

Table 4.2: Thermal and transport properties for different ILSPE electrolytes.

Electrolyte Composition	T_m [°C]	σ at 25°C [mS/cm]	σ at 60°C [mS/cm]	T_{Li^+}
20:1:1 (1M)	47.5	0.24 +/- 0.06	2.2 +/- 0.42	0.35 +/- 0.028
20:1:3 (1M)	37.6	0.01 +/- 0.0062	0.36 +/- 0.047	NA
20:2:2 (1M)	NA	0.45 +/- 0.061	2.3 +/- 0.34	0.25 +/- 0.038
20:4:2 (4M)	NA	0.96 +/- 0.016	4.0 +/- 0.065	0.31 +/- 0.11

CV stability and Li Stripping and Plating

Electrochemical stability against oxidation was measured using CV with a Li reference and titanium working electrode for 20:1:1, 20:2:2, and 20:4:2 and is shown in Figure 4.9. The voltage was swept from 2.5 – 4.5V vs. Li/Li^+ at a rate of 5mV/sec, and Cycle # 1, 2, 10, 100 are shown on the same figure with a vertical offset. This voltage range was chosen as it encompasses the redox potentials for many commercially available high voltage cathodes for LIBs. All compositions show a modest amount of current starting between 3.5 and 4.0V vs Li/Li^+ in the first cycle which is indicative of electrolyte breakdown. During the second cycle the current response of 20:1:1 (1M) and 20:2:2 (1M) has lessened to a significant degree showing strong passivation behavior. For cycle 2 of 20:4:2 (4M) the current has also decreased from cycle 1 displaying passivation behavior, but there remains a higher total current than the other two compositions. This suggests that the 20:4:2 (4M)

composition is less stable against oxidation than its counterparts. By cycle 10 through 100 all compositions show shrinking current response up to 4.5V, with 20:4:2 (4M) showing ~10uA/cm2, 20:2:2 (1M) showing ~1uA/cm2, and 20:1:1 (1M) showing ~0uA/cm2, indicating passivation behavior.

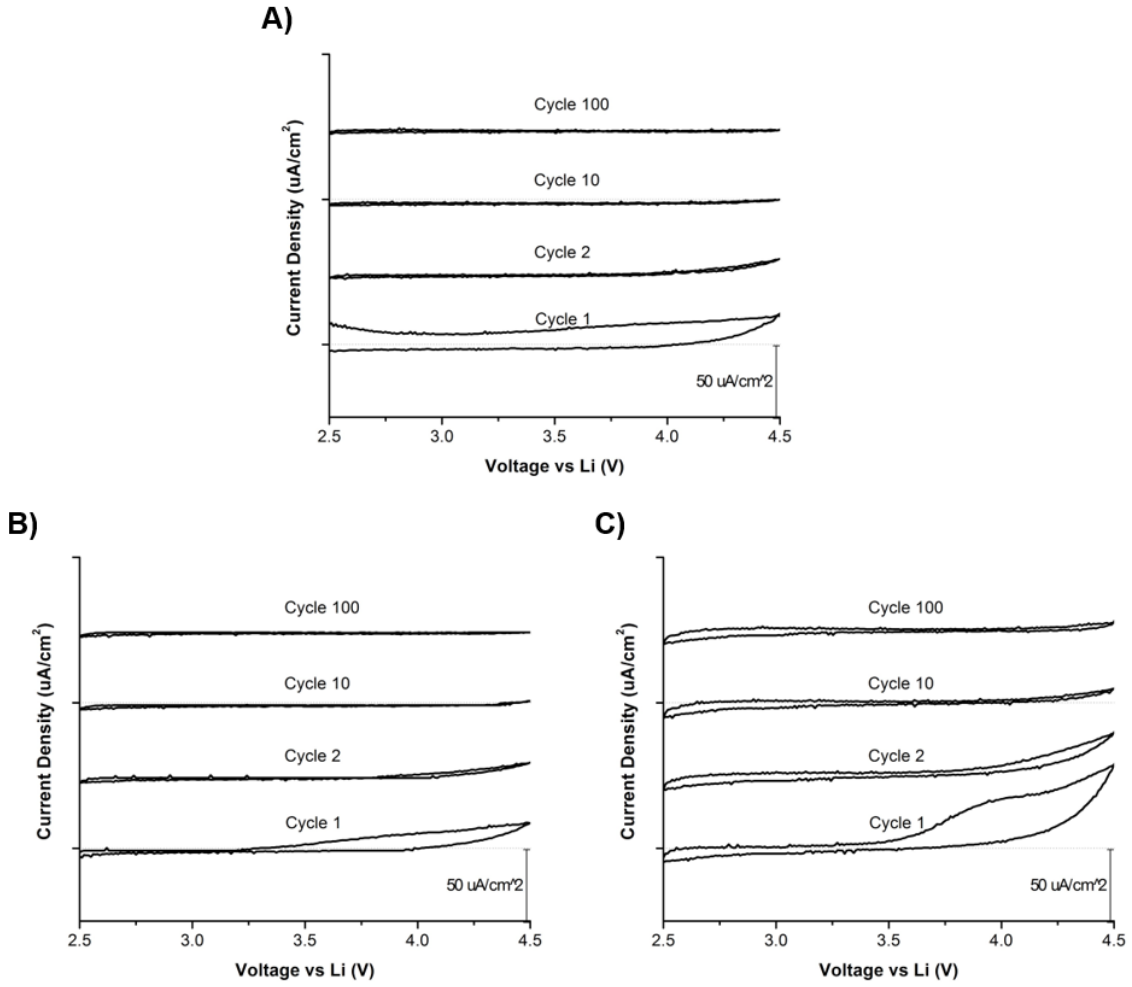

Figure 4.9: CV from 2.5V to 4.5V of A) 20:1:1, B) 20:2:2, and C) 20:4:2. Scans were taken at 60°C at a 5 mV/sec rate for 100 total cycles. Passivation is evident for all compositions by cycle 100.

To measure the interfacial stability of the ILSPE electrolytes with Li metal, Li/ ILSPE/ Li coin cells were constructed for Li stripping and plating experiments. The experiment consists of applying a constant current density of 0.1 mA/cm2 in one direction

for one hour, then reversing the polarity of the current for an hour at 60°C while measuring the overpotential of the cell. The 20:1:1 electrolyte shows the smallest interfacial resistance with an initial overpotential value of 30mV that decreases slightly to 28mV after the first 5 cycles and plateaus through the remainder of the experiment (Figure 10A). The 20:2:2 electrolyte shows the next best interfacial stability with an overpotential value of ~56mV that plateaus at 50mV after 10 cycles (Figure 10B). The 20:4:2 electrolyte has an initial value of ~84mV that decreases and plateaus to ~56mV after 30 cycles. All compositions show an initial higher value of overpotential that decreases and plateaus after a few cycles, demonstrating good stripping/plating behavior and indicating long-term stability with Li.

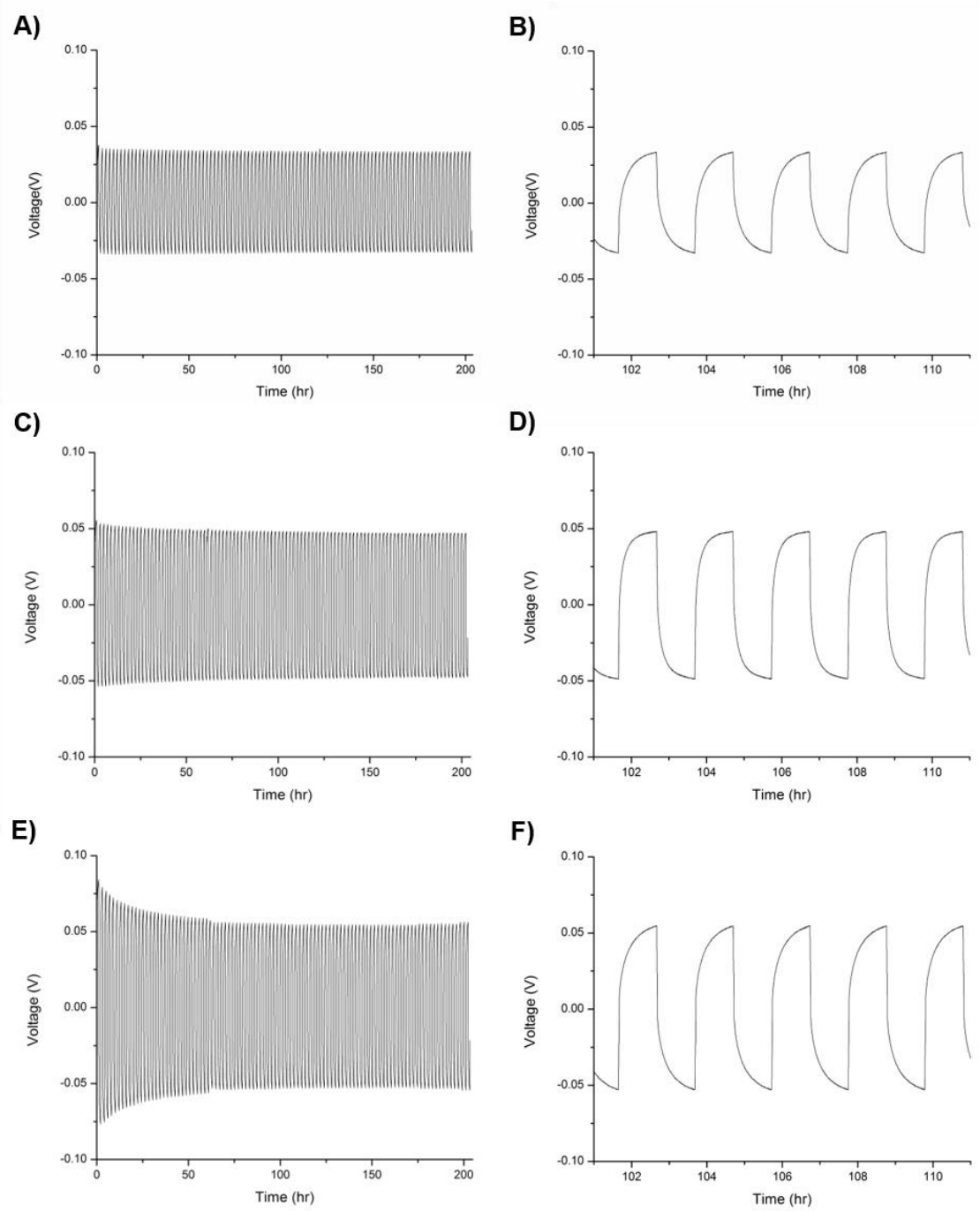

Figure 4.10: Symmetrical Li/ ILSPE/ Li cell stripping and plating at 60°C with a 0.1 mAh/cm2 current density of A) 20:1:1, B) 20:2:2, and C) 20:4:2 for 100 cycles.

Galvanostatic cycling

To ensure good ionic contact between the ILSPE and cathode active material through the bulk of the electrode, a composite electrode incorporating ILSPE components was used (see Figure 4.2). The ILSPE electrolytes were cycled with the composite LFP in a Li/ ILSPE/ LFP coin cell configuration at 60°C with a 1C current rate. Specific capacity and coulombic efficiency vs. cycle number and cell voltage vs. specific capacity are plotted for 20:2:2 (Figure 4.11A, 4.11C) and 20:4:2 (Figure 4.11B, 4.11D). Both compositions cycled with high efficiency (>99%) and capacity retention for 500 cycles, demonstrating practical cyclic stability with a Li metal anode and LFP cathode. For 20:2:2 the initial capacity for the first cycle was 144.9mAh/g. By the 100_{th} cycle, the specific capacity increased to 151.1mAh/g and by the 500_{th} cycle the specific capacity had increased to 153.1mAh/g, or 105.6% of the initial capacity. The origin of this capacity increase with cycle number is likely due to a relaxation effect and increased utilization of the LFP cathode through effective formation of a solid electrolyte interphase. The 20:4:2 composition has a starting capacity of 178.1mAh/g on the first cycle, which decreases slightly to 177.1mAh/g on the 100_{th} cycle. By the 500_{th} cycle the specific capacity delivered was 160.1mAh/g, giving a capacity retention of 89.9%. LFP has a theoretical specific capacity of ~170mAh/g, so it is surprising that 20:4:2 (4M) is reversibly cycling with ~177mAh/g. The best rationalization for this discrepancy is the fact that an average mass loading was used rather than weighing this individual electrode to calculate specific capacity.

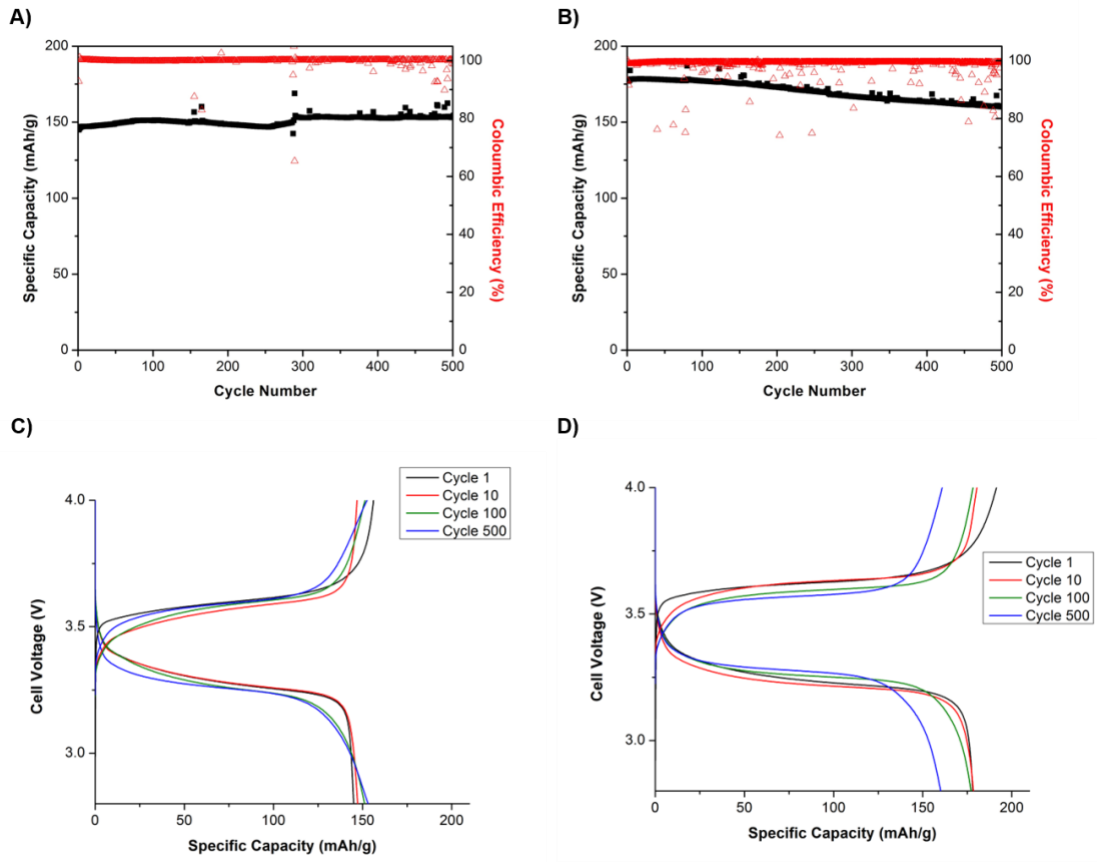

Figure 4.11: Specific capacity vs cycle number of Li/ILSPE/LFP at 60°C with a 1C rate for A) 20:2:2 and B) 20:4:2. Matching voltage vs. specific capacity graphs for C) 20:2:2 and D) 20:4:2.

Given that the 20:2:2 (1M) and 20:4:2 (4M) compositions are amorphous and have ionic conductivity values at room temperature that are exceptionally high for a SPE, , i.e. ~10^{-3} S/cm, these compositions were chosen as good candidates to assess room temperature (22°C) galvanostatic cycling in a Li/ ILSPE/ LFP cell configuration and are shown in Figure 4.12. The 20:2:2 electrolyte has an initial capacity of 139.8mAh/g on the first cycle, which drops to 120.2mAh/g on the 40th cycle for an 85.6% capacity retention with a C/20 rate (Figure 4.12A). The 20:4:2 electrolyte has an initial capacity of 169.0mAh/g on the first cycle, stays steady through the 40th cycle with a capacity of 170.3mAh/g for an 100.7% capacity retention at the same C/20 rate (Figure 4.12C). The accompanying voltage vs.

specific capacity graphs for select cycles are shown in Figures 4.12B and 4.12D for 20:2:2 and 20:4:2 respectively. The full capacity retention of 20:4:2 compared to the 85.6% capacity retention for 20:2:2 after 40 cycles could be attributed to the higher ionic conductivity of the 20:4:2 electrolyte.

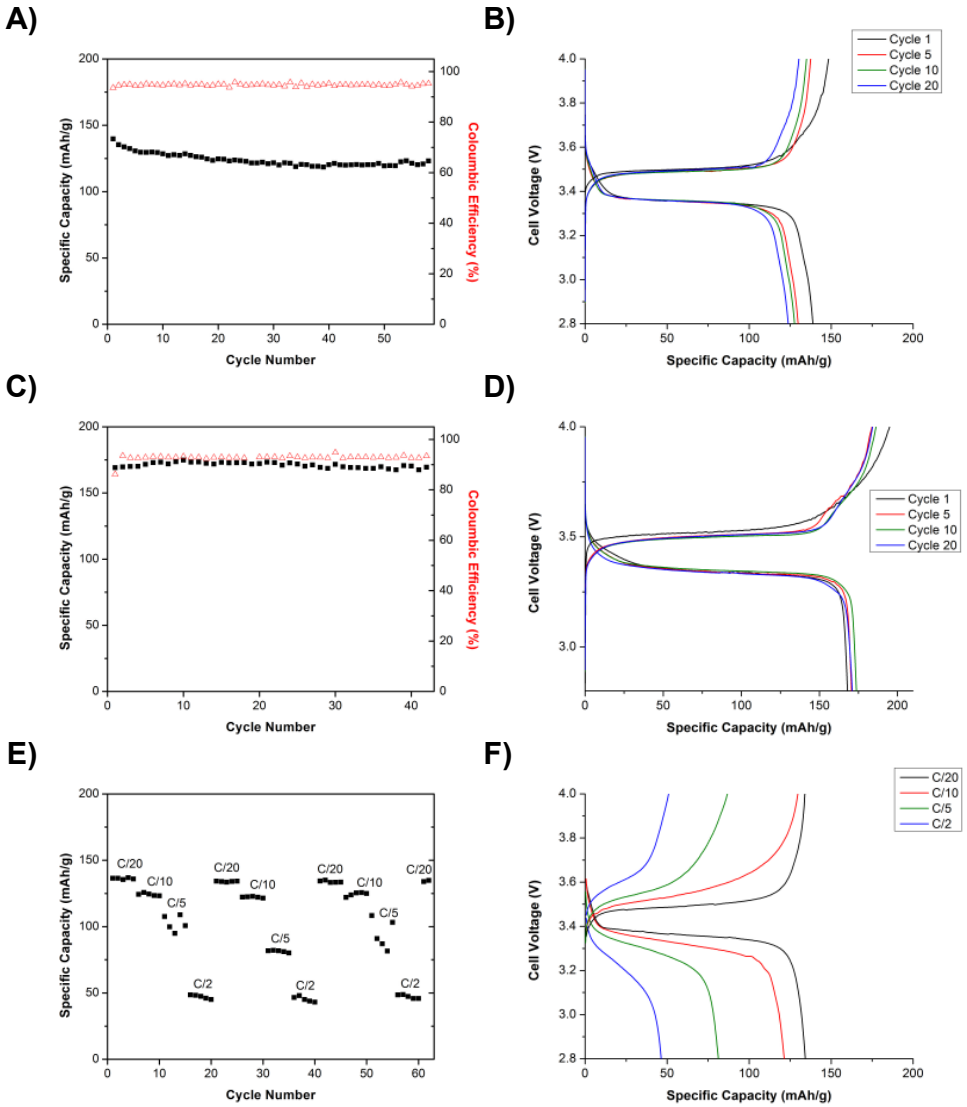

Figure 4.12: Specific capacity vs cycle number of Li/ILSPE/LFP at 22°C with a C/20 rate for A) 20:2:2 and B) 20:4:2 and variable rate for C) 20:2:2. Matching voltage vs. specific capacity graphs for D) 20:2:2, E) 20:4:2, and variable rate F) 20:2:2.

To assess room temperature rate capability of the ILSPE electrolyte, variable rate cycling was performed on 20:2:2 electrolyte at room temperature. The experiment consists of a Li/ ILSPE/ LFP coin cell undergoing 5 cycles at C-rates of C/20, C/10, C/5, and C/2 in succession for a total of 60 cycles (Figure 4.12E). It is typical for a battery system to delivery less capacity at higher C-rates which place a greater demand on the ability of the battery to transport Li^+. However, to demonstrate healthy cycling and good rate capability a battery should be able to demonstrate reversible capacity at any given rate. The corresponding voltage vs. capacity graph for this sample (Figure 4.12F) shows the specific capacity for the middle cycle at each C-rate (i.e. the C/20 curve corresponds to cycle #3, the C/10 curve corresponds to cycle #8, etc.). The percentage of maximal discharge capacity for select cycle rates is displayed in Table 4.3. At a C/20 rate, a specific capacity of 135.5mAh/g is reached on the third cycle. At a C/10 rate the sample exhibits a specific capacity of 91.9% of the C/20 capacity. C/5 rate has a specific capacity of 70.0% of the C/20 capacity, and the C/2 rate shows a specific capacity of 35.1% of the C/20 capacity. Remarkably the next three rounds of C/20 cycling (cycle #21-25, #41-45, #61-65) fully recover the capacity of the initial round of C/20 cycling, demonstrating stability through reversible rate performance. The rate capability could improve with a thinner ILSPE electrolyte, which would decrease the length of migration for Li^+. Given that this system shows full reversible capacity at any given rate is an indication that the electrolyte can handle high current without significant degradation.

Table 4.1: % of C/20 capacity for different C-rates during rate performance testing of 20:2:2 (1M) at room temperature.

Cycling Rate	C/20, cycle #3	C/10, cycle #8	C/5, cycle #13	C/2, cycle #18
% Maximal Discharge Capacity	100%	91.9%	70.0%	35.1%

4.5 Conclusions

SPEs must overcome difficult challenges to be considered viable alternatives to liquid electrolytes, namely their ionic conductivity and interface with electrode materials must be improved. ILSPEs characterized here show a promising step in direction of solving these issues, with ionic conductivity values of 0.45 and 0.96mS/cm for the two most conductive compositions. ILSPEs have also demonstrated the ability to cycle at room temperature with full reversible capacity at different C-rates, a significant improvement to most SPEs that can only cycle at elevated temperatures. This improved capability is due to high ionic conductivity originating from a full plasticized polymer matrix as characterized by DSC, and an improved interface between ILSPE and composite electrode via inclusion of electrolyte components in the electrode.

CHAPTER 5: Aqueous Salt-Based Solid Polymer Electrolytes[2]

5.1 ASPE Justification

Aqueous solid polymer electrolytes (ASPEs) have shown promise as a high performing solid electrolyte with high conductivity and voltage stability. In an ideal world, battery electrolytes would be water-based as water is an abundant, cheap, and environmentally benign resource. The problem with most aqueous electrolytes is their very low energy density due to a confined ESW of at most 2 V for any commercial aqueous battery. The WiSE system has been a huge innovation in the field of aqueous electrolytes and led to a system with a ~3 V ESW. The ASPE system builds on this work in the direction of solid electrolytes. ASPEs are true flexible solids with an aqueous component. The incorporation of an aqueous component inherently makes these SPEs easier to fabricate and process, eliminating the need for an expensive and harmful dry environment. Such batteries would be ideal for applications where high energy density is not needed, such as some implantable medical devices are or personal grooming products requiring batteries.

[2] This work resulting in a manuscript that is in preparation for submission to a peer-review journal: **Matthew D. Widstrom**, Kyle B. Ludwig, Jesse Matthews, Sahana Bhattacharyya, Angelique Jarry, Arthur V. Cresce, Steve Greenbaum, Oleg Borrodin, Peter Kofinas, "Aqueous Solid Polymer Electrolytes for Lithium-Ion Batteries," (*In Prep).*

5.2 Introduction

Current state-of-the-art LIBs rely on liquid organic electrolytes to withstand high voltage battery configurations (>3V) through kinetic passivation via SEI formation. Electrolyte solvents such as EC and DMC are used as chemical substrates to create a passivating interface, however they are inherently flammable and are often coupled with a thermally unstable salt ($LiPF_6$)[14]. The choice of thermally unstable components for the sake of performance makes the battery susceptible to multiple failure modes that would result in thermal runaway and fire, so there is interest in replacing these electrolytes with safer materials[83,113,153–155].

Solid electrolytes are attractive alternatives to liquid organic electrolytes from a safety perspective, as they would address many of the failure modes such as internal short circuits, electrolyte extrusion, high temperatures, and overcharge[14]. SPEs of the PEO + salt variety have shown thermal stabilities well above 200°C, whereas liquid organic electrolytes exhibit an intense exothermic reaction above 200°C[156]. A major limitation SPE adoption for safety enhancement is the poor ionic conductivities these materials exhibit, often below 10^{-3} S/cm[38,149,157–159]. The conductivity limitation of these materials must be addressed before widespread adoption can occur. Attempts to improve the conductivity often focus on plasticizing the polymer matrix with the addition of various materials[30,31,51,53,83,87,140]. Perhaps a more promising route, however, would involve strategies to decouple ion motion with the structural relaxation and segmental motion of the polymer matrix. Ion motion governed by free volume in polymer electrolytes is described by the empirical Vogel-Fulcher-Tammann relationship (7) which is a modification of the Arrhenius equation (8):

$$\sigma = Ae^{\frac{-B}{R(T-T_0)}} \quad (7)$$

$$\sigma = Ae^{\frac{-E_a}{RT}} \quad (8)$$

These equations describe the temperature dependence of ionic conductivity, with constant A, B is a constant related to activation energy, R is gas constant, T is temperature, T_0 is a temperature related to T_g also described as the temperature where conductivity vanishes[160], and E_a is an activation energy. T_g (related to T_0) is an important factor for electrolytes that have ion motion coupled with chain segmental motion, and for such systems it is imperative to lower T_g as much as possible to distance it from the operating temperature of the electrolyte. A SPE that could decouple ion motion from chain segmental motion and follow (8) rather than (7) would be termed "superionic"[161] and would show a large improvement over most systems governed by (7).

A unique approach was taken by Angell et al[115] where instead of studying small amounts of lithium salt in a polymer matrix, he inverted the conventional composition of these materials and studied small amounts of polymer in a large amount of salt called PiSE. The key insight that unlocked appreciable ion transport in these systems was the fact that with increasing salt content the T_g of the electrolyte would exhibit a maximum, which meant that if the salt content was pushed to an extreme (or the PiSE regime) that the T_g of the material would decrease and solid electrolytes with reasonable transport properties could be made. Another interesting observation with PiSE is the decoupling of the cation transport with the structural relaxation of the polymer matrix[161,162]. The suggested mechanism for transport in PiSE materials is cation hopping among a critical network of salt clusters through anion exchange in the first solvation sheath, which follows an Arrhenius relationship (8).

Some researchers observed in their PiSE systems that if residual amounts of solvent were left in the system that the conductivity could jump multiple orders of magnitude[162]. This discovery was taken to its logical conclusion recently, when Suo et al.[113] innovated a highly concentrated 21 m (molal) solution of LiTFSI in water, or "water-in-salt" electrolyte (WiSE). This is analogous to PiSE, with the difference being instead of using a small amount of high molecular weight polymer to plasticize a high concentration of salt a small amount of water is used. However similar to PiSE, WiSE was constructed to solve a fundamentally different problem than decoupling ion motion from chain segmental motion in polymer electrolytes. This system demonstrated for the first time through super-concentration of lithium salts that anion reduction could be an effective route to the formation of a passivating SEI[113,119,121,123,163] in an aqueous electrolyte. Their research showed an expanded electrochemical stability window (ESW) for an aqueous electrolyte to ~3V, with the proof of concept battery pair of a Mo_6S_8 anode and a LMO cathode. This work has sparked interest in highly concentrated electrolytes for aqueous systems as a compositional approach to changing the mechanism for SEI formation, leading to further improvements through the use of bisalt[123,124] and hybrid aqueous/non-aquous[141] systems. Battery systems typically rely on the reduction of electrolyte solvent molecules to form a passivating SEI, such as EC and dimethyl carbonate (DMC) with concentrations of lithium salt ~ 1 M. Anion passivation enabled by a high concentration of lithium salt (> 3 M) constitutes a paradigm shift in interphase formation and opens a range of possibilities for tailoring the SEI that were previously unavailable, enabling higher voltage aqueous battery chemistries.

Extending the aqueous, super-concentration concept to SPEs, an ASPE which consists of incorporating water and a high concentration of lithium salt in a solid polymer system could lead to decoupled ion transport described by (8), while simultaneously ameliorating concerns of crystallization in the polymer leading to exceptional conductivity for a SPE. Additionally, the high salt concentration could aid in SEI formation by providing a chemical substrate other than water to decompose at the electrode/ electrolyte interface. To accomplish this, we report on incorporating water and LiTFSI into a solid PEO polymer matrix to form an aqueous solid polymer electrolyte (ASPE) with a room temperature conductivity of 1.75 mS/cm, and an exceptionally large lithium transference number of ~0.66 for a SPE. The stability of the ASPE system in air eliminates the need for meticulously dry environments and solution processing, which is desirable because manufacturers can settle for moderate humidity control and solid-state processing resulting in substantial savings in production costs.

5.3 Materials and Experimental Methods

LiTFSI ($LiN(SO_2CF_3)_2$) was purchased from BASF and dissolved in deionized water. Poly(ethylene oxide) (PEO, 10^6 M_v) was purchased from Sigma Aldrich. The cathode for cycling tests was received from Argonne National Lab (ANL) and was made of 90wt% LMO, 5wt% Solvay 5130 polyvinylidene fluoride (PVDF) binder, and 5wt% Timcal C45 coated on aluminum foil. The active material loading averaged 18.86 mg/cm^2. Lithium titanate ($Li_4Ti_5O_{12}$, LTO) electrodes were fabricated by mixing a slurry of 80wt% active material, 10wt% carbon additive (Super P), and 10wt% PVdF binder (Kynar 1800). The slurry was then spread using a doctor blade over aluminum foil current collector, and dried

in an oven at 80°C for 18 hours. The electrodes were then stored in a vacuum oven at 100°C for at least 24hr prior to use to remove any remaining impurities. The reference electrode for electrochemical stability tests was lithium iron phosphate and was made of 80wt% $LiFePO_4$ (LFP, Chinese Aviation Corporation), 10wt% PVDF (Kynar 1800), and 10wt% Super P carbon coated on aluminum foil.

Aqueous Solid Polymer Electrolyte (ASPE) Preparation

All ASPEs were fabricated using a solvent-free hot-pressing process. PEO, LiTFSI, and deionized water were mixed with a mortar and pestle. The resulting mixture was sealed in a fluoropolymer-lined aluminum pouch and hot-pressed with a Carver press at 85°C and 1.5 tones to form a thin-film ASPE membrane. Four different compositions were fabricated and characterized, keeping the molar ratio between ethylene oxide (EO) units and LiTFSI the same while changing the amount of water. The compositions of ASPEs #1-4 can be found in Table 1. Electrochemical testing was performed using CR2032 coin cells. All electrolytes were handled in normal lab atmosphere with care taken to minimize the exposure time both during processing and sample making.

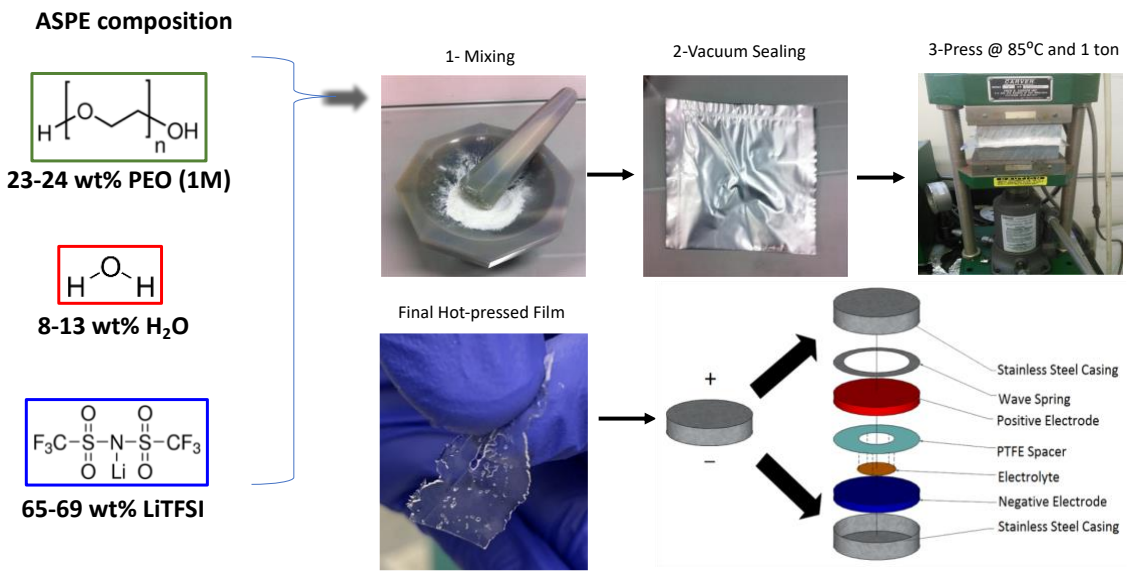

Figure 5.1: High molecular weight poly(ethylene oxide) (1MDa, M = 10_6), water, and lithium salt LiTFSI are combined in varying weight ratios. The components are mixed by mortar and pestle, vacuum sealed in a pouch, and then pressed with heat to produce an ASPE (100-200µm thick).

Electrochemical Impedance Spectroscopy

Electrochemical Impedance Spectroscopy (EIS) for the ASPEs was performed in a stainless-steel (SS)/ASPE/SS coin cell set up, with the inclusion of a Teflon spacer to define the thickness and area of the ASPE at 0.025 cm and 0.126 cm_2 respectively. The amount of electrolyte included in a coin cell for impedance spectroscopy was empirically determined such that the volume of the spacer was completely filled with slight excess. The measurements were taken on a Solartron 1287A/1255B platform with a frequency range from 1 MHz to 1 Hz. Measurements were taken in 5 °C increments from 80 °C to 0 °C. The cells were annealed for 90 min at each temperature before measurements were taken to ensure thermal equilibrium, and impedance spectroscopy was taken on at least three separate cells to provide statistical significance. Data reported are the averages and the error bars are the standard deviation of the set of measurements.

Pulsed-Field Gradient Nuclear Magnetic Resonance

All pulsed-field gradient nuclear magnetic resonance (NMR) samples were packed into 5 mm tubes in ambient atmosphere, and the tubes were then sealed to preserve the same relative humidity value in which they were prepared. NMR experiments were performed by Dr. Steven Greenbaum's group at CUNY at 25 °C with a 300 MHz Varian-S Direct Drive Wide Bore spectrometer equipped with a DOTY Scientific PFG probe (DS-1034, 1400 G/cm maximum gradient). Single peaks were observed for $_{1}$H, $_{19}$F, and $_{7}$Li resonances centered at 302.7, 280.5 and 117.3 MHz, respectively, corresponding to all hydrogen-, lithium-, and fluorine-containing species. A PFG-stimulated echo pulse sequence was used. Gradient pulse durations δ of 2 to 4 ms and diffusion delays Δ of 100 ms were used. The gradient strength g was linearly increased with 32 values steps from 1.7 up to 700 G/cm as needed. From each experiment, the integrated intensities S as a function of applied gradient g (in T/cm) were obtained. Subsequently, diffusion coefficients D were then computed using least-squares fitting of the Stejskal-Tanner Equation[134]

$$S = S_0 e^{-D(g\delta\gamma)^2(\delta - \frac{\Delta}{3})} \quad (3)$$

Differential Scanning Calorimetry

Differential scanning calorimetry (DSC) measurements were conducted on a TA Instruments Q100 DSC. The ASPE samples were sealed in hermetic aluminum pans in ambient atmosphere shortly after being pressed; the pure PEO samples were sealed in sample pans after drying at 60°C for 48h. All samples were measured using a heat/cool/heat

method to erase any thermal history in the temperature range from -40 to 100°C and -100 to 20°C at a 10°C/min heating rate and a 10 °C/min cooling rate.

Linear Sweep Voltammetry

Linear sweep voltammetry (LSV) was performed using the same Solartron set-up as for impedance spectroscopy with half-charged lithium iron phosphate as a counter and reference electrode in a coin cell. Half-charged LFP was prepared by constructing Li/ 3:7 EC:EMC with 1.2 M $LiPF_6$/LFP coin cells. These cells were fully charged and discharge for one cycle, then were half charged and allowed to rest as their open circuit voltage was monitored to determine their equilibrium potential (3.425 V vs. Li/Li^+). These cells were then deconstructed in a dry room and the LFP electrodes were extracted, washed, and then vacuum dried. Half-charged LFP/ASPE/Al cells were constructed and stepped at 1mV/sec from 3.0 V vs. Li/Li^+ (-0.425 V vs. LFP reference) in the anodic and cathodic directions until breakdown of the electrolyte was achieved at room temperature. Breakdown of the electrolyte was determined by surpassing a current density threshold of 0.1 mA/cm^2. The anodic and cathodic scans for different samples were combined to show the electrochemical stability window of the electrolyte.

Cyclic Voltammetry

Cyclic voltammetry (CV) was performed using the Solartron set-up to determine the time/cycle dependence of the electrochemical stability of the electrolyte at room temperature. LFP/ ASPE/ titanium (Ti) cells were cycled 100 times from 3.0 V to 4.5 V vs. Li/Li^+ (-0.425 V to 1.575 V vs. LFP reference) to investigate the anodic stability.

LFP/ASPE/Al cells were cycled 100 times from 3.0 V to 1 V vs. Li/Li^+ (-0.425 V to -2.425 V vs. LFP reference) to investigate the cathodic stability. The scan rate for all CV experiments was 5 mV/sec.

Galvanostatic Cycling

Galvanostatic cycling was performed using an Arbin BT2000 at 23 °C to determine the ASPEs charge/ discharge performance in a full battery. LTO/ ASPE/ LMO cells were constructed for galvanostatic cycling.

Thermogravimetric Analysis

Thermogravimetric Analysis was performed using a TA Instruments TGA 55 to characterize the thermal stability of ASPE electrolytes. A scan rate of 10°C from room temperature to 500°C routine was used.

5.4 Results and Discussion

The ASPE compositions (A1-A4) were selected by fixing the mole ratio of Li^+ : EO (EO being ethylene oxide repeat units in a polymer chain) to 1 : 0.44 and adjusting the molar component of water from 1.36 to 0.76 in 0.2 increments. This was done to study the effect of water concentration on electrolyte properties. ASPE composition information in both weight percentages and relative molar concentrations can be found in Table 5.1. An important note: effort was taken to minimize sample exposure to lab atmosphere, which was necessary to fabricate the electrolytes and to make samples for characterization. It is necessary to minimize ASPE exposure to ambient atmosphere due to PEO being

hygroscopic; the ASPE electrolytes can either gain or lose water depending on the atmosphere they are exposed to and the exposure time. In a dry room the ASPE electrolytes would tend to lose water, while in ambient atmosphere they would tend to gain a small amount of water.

Table 5.1: Compositions of A1-A4 expressed both as a molar ratio and as weight percentages of the three components.

Sample	PEO content [wt%]	LiTFSI content [wt%]	Water content [wt%]	Li:Water Mole ratio	EO:Li:Water Mole ratio
A1	22.7	64.7	12.6	1 : 3.09	1 : 0.44 : 1.36
A2	23.1	66.0	10.9	1 : 2.64	1 : 0.44 : 1.16
A3	23.5	67.3	9.2	1 : 2.18	1 : 0.44 : 0.96
A4	24.0	68.5	7.6	1 : 1.73	1 : 0.44 : 0.76

DSC and TGA

DSC was used to characterize the presence of any reversible phase transitions of ASPE electrolytes and to ensure that the relative concentrations of lithium salt and water were enough to fully plasticize the polymer matrix. Figure 5.2 shows DSC thermograms, measured at a temperature range of -40 to 100 ^{o}C for both the 1M MW PEO matrix (Figure 5.2A) and for the A2 composition that is representative of all ASPE compositions measured in this temperature range (Figure 5.2B). The polymer matrix exhibits a melting peak at ~67°C, which is consistent with literature values of a high molecular weight PEO melting tranisition[151]. The representative ASPE thermogram shows showing no melting or

recrystallization peaks, confirming that the PEO component in the ASPE system is fully amorphous, which is the preferred morphology for ion conduction.

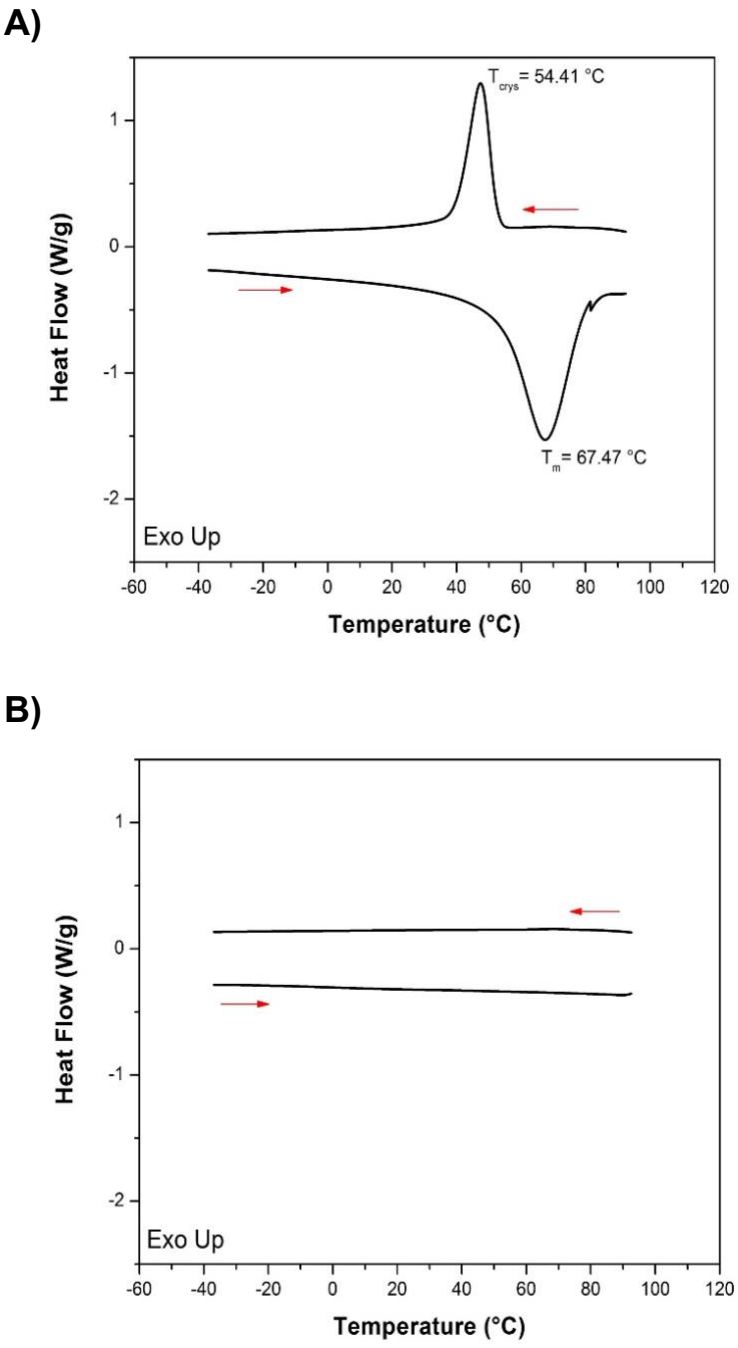

Figure 5.2: Standard DSC thermograms for A) 106 Mv PEO and B) A2 in the temperature range of -40°C to 100°C. Heating rate was 10°c/ min and cooling rate was 10°C /min with a heat/cool/heat program to erase thermal history. A) is the polymer matrix control sample and shows a melting peak at 67°C, and B) is representative of all ASPE compositions, and shows complete plasticization with the absence of any melting peaks. The red arrows show the direction of the scan.

The classic conduction model for ethylene oxide containing polymers is the forming and breaking of coordination bonds between EO and Li^+ in the amorphous fraction of the polymer where chains can be mobile[164]. As bonds are formed and broken (Li^+ will form 4-6 coordination bonds at once[165]), Li^+ will move along and between polymer chains. This Li^+ transport mechanism that involves dynamic bond formation and breaking with EO units relies on the flexibility and segmental motion of the polymer chains to be able to form these bonds. The glass transition temperature (T_g) plays an important role in understanding ion transport in solid polymer electrolytes as it is a strong indicator of segmental dynamics of the polymer chains within the system. Below the glass transition temperature, the amorphous fraction of the electrolyte consists of polymer chains that are glassy and frozen in place. Above T_g, these chain segments start to move and switch from glassy to rubbery behavior[46]. From a design perspective of ion-conducting polymers, the operating temperature of an electrolyte should be as far above T_g as possible (i.e. T_g should be as low as possible) to maximize the segmental mobility of polymer chains and improve ion transport. It is well understood in the ethylene oxide-containing polymer-ion transport literature that there is a maximum in ionic conductivity of the electrolyte as a function of relative salt molar concentration (Li^+:EO)[148,166]. This maximum is a consequence of two competing phenomena that when taken together represent a tradeoff in conductivity. The first effect is that of increasing charge carriers through increasing salt content. From first principles, ionic conductivity improves with a higher density of charge carriers. The opposing effect that leads to a maximum with salt concentration is that increasing salt concentration also increases the T_g (i.e. decreases segmental motion needed for ion transport) of the resulting electrolyte due to associations between the polymer and salt[165–

[167]. This maximum in ionic conductivity is often found to be at lower salt concentrations (Li^+ : EO = 0.08 for LiTFSI in PEO[166]). This is the driving motivation for characterizing the T_g of these ASPE electrolytes, which have a relatively high Li^+ : EO = 0.44. One could expect to see lower T_g values as water, which is a strong plasticizer, is increased. To measure the T_g of ASPE electrolytes, the temperature range was adjusted to scan colder

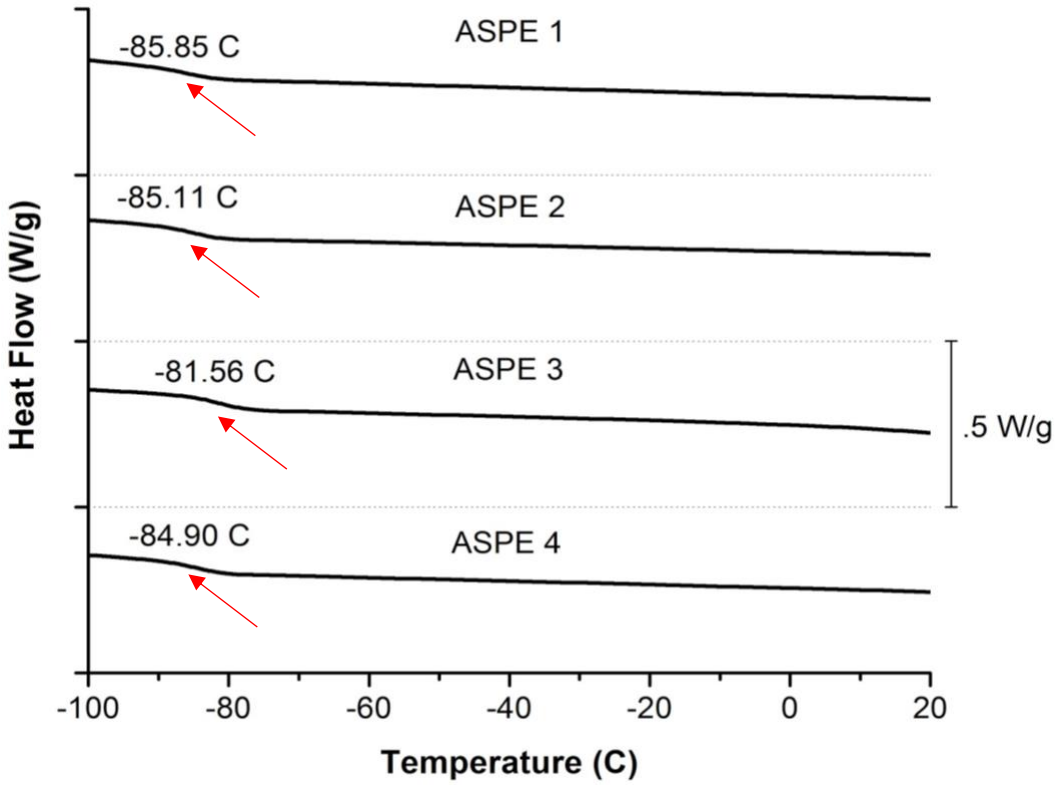

Figure 5.3: DSC thermograms of A1-4 depicted on the same plot with a vertical offset of 0.5 W/g. All ASPE compositions show a T_g in the temperature range of -82 - -86°C. Glass transition temperatures are indicated by each plot with a red arrow and temperature value.

than -40°C, and T_g was taken as the onset temperature at which the slope of the thermogram changes. DSC scans for all ASPE compositions from -100°C to 20°C are shown in Figure 5.3. All ASPE composition show a T_g between -82°C and -86°C, indicated by red arrows in Figure 5.3. The fact that T_g for the ASPE system is ~-85°C shows the tremendous impact

that water has as a plasticizer in this system. The Li : EO mole ratio for A1-A4 is held constant at 0.44. For some context, PEO + LiTFSI salt mixtures with a mole ratio of 0.44 exhibit a T_g of 15°C[167], and high molecular weight PEO with no salt exhibits a T_g of -67°C (See Table 4.1). It is evident that the inclusion of water in the electrolyte suppresses T_g past what is observed for neat PEO, even in the presence of high lithium salt content. It is also unclear how much water is needed to have this plasticization effect, as the T_g for A1-A4 are not appreciably different as the molar component of water changes from 1.36 to 0.76 in 0.2 increments. ASPE compositions with incrementally less water would need to be measured by DSC to determine what threshold of water is necessary to suppress T_g to such a low value.

Thermal stability is a key performance metric for electrolytes that can experience a range of operating temperatures. To measure thermal stability of the ASPE, Thermogravimetric Analysis (TGA) was used. Figure 5.4 shows the results of TGA for the A2 composition. The initial weight loss of 9wt% from room temperature to 250°C can be attributed to water, which constitutes 10.9wt% of A2. The weight loss occurring at ~380°C - 440°C can be attributed to PEO[168] (23.1wt% of the as prepared sample), and the remaining weight loss is due to LiTFSI. Figure 5.4 indicates stability up to ~100°C.

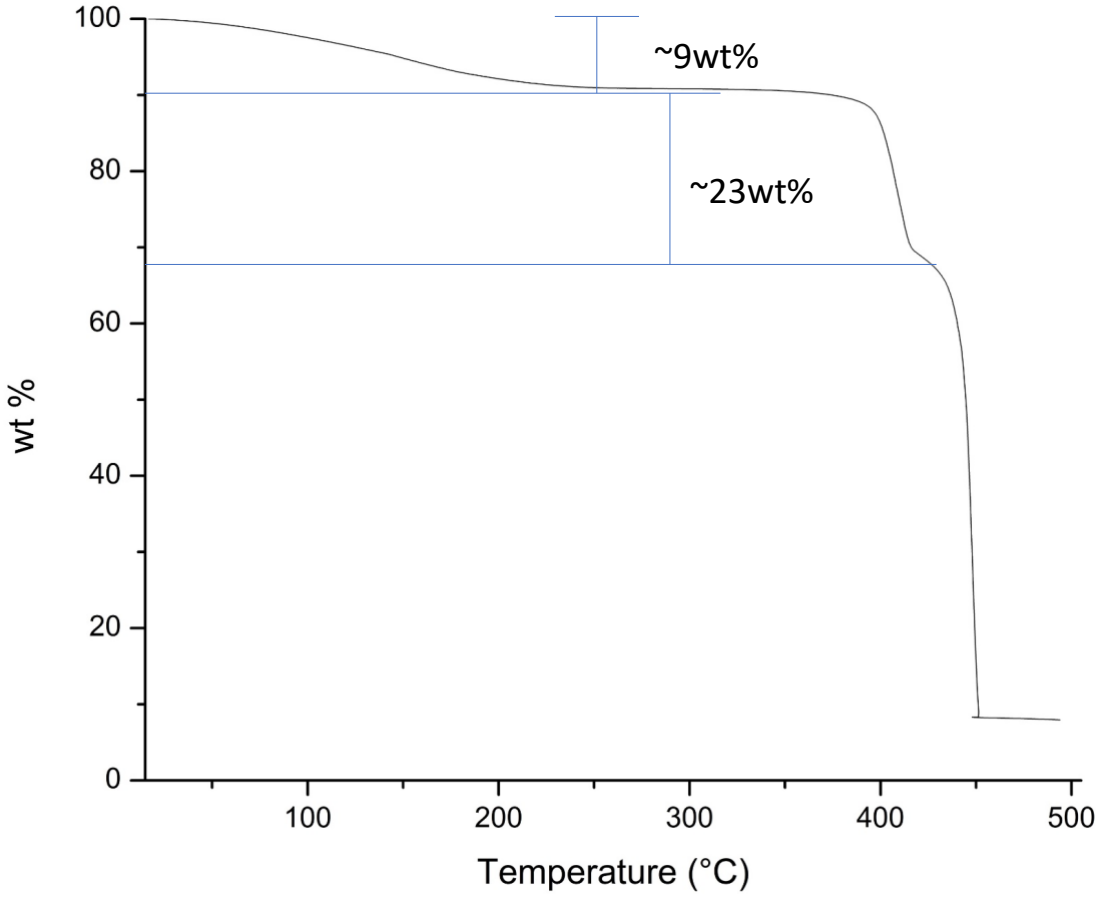

Figure 5.4: TGA of A2 taken from room temperature to 500°C in ambient atmosphere. The initial loss of 9wt% corresponds to water, the second loss of ~23wt% corresponds to PEO, and the final loss of mass corresponds to LiTFSI.

EIS and NMR

EIS was used to measure the ionic conductivity of the ASPE electrolytes. The conductivity values of A1-4 are plotted by convention as a function of inverse temperature, with the temperature values in °C shown on the top x-axis in Figure 5.5. All four compositions are very conductive for SPEs, and they show a clear trend of increasing conductivity with increasing water content. The room temperature conductivity values of the ASPEs investigated here are on the order of 10^{-3} S/cm and can be found in Table 5.2. According to Figure 5.2 which is a representative DSC scan of all ASPE compositions, there are no

thermal transitions present for any ASPE composition which means that the polymer matrix is fully amorphous due to plasticization by the presence of LiTFSI and water in the full compositional range investigated here. The conduction mechanism of PEO transport of Li^+ commonly results in electrolytes with conductivity values on the order of 10^{-6}S/cm in a semi-crystalline system, and values on the order of 10^{-4}S/cm in a fully amorphous system at elevated temperature past the melting point of the polymer matrix. Fast ion transport in SPEs is a characteristic of the amorphous phase and is attributed to the inhibition of crystallization in the polymer matrix. Considering that the conductivity values of the ASPE system are a full order of magnitude higher than those of typical amorphous PEO electrolytes that have been plasticized with ionic additives at higher temperatures, it is likely that a different conduction mechanism besides PEO vehicular transport is dominant. The other two candidate transport mechanisms are informed by PiSE and aqueous salt electrolytes. In the first case, a percolation threshold of salt leads to ions hopping between different salt clusters with a minimum salt content needed to create a network of such clusters. The high salt content is plasticized by a polymer, and anions in the first solvation sheath of Li^+ can exchange as Li^+ moves[29]. This transport mechanism is governed by Arrhenius behavior below and above the T_g of the PiSE electrolyte[162]. In the second case the conduction mechanism consists of liquid-like vehicular transport with both water and $TFSI^-$ in the first solvation sheath of Li^+, also exhibiting Arrhenius behavior. Borodin *et al* showed that for aqueous salt electrolytes there can exist a disproportionation of Li^+ solvation, where Li^+ prefers to be solvated be either mostly water or mostly $TFSI^-$ which leads to nanoscale heterogenous domains for water-assisted fast Li^+ transport[169]. There are likely contributions from all three conduction mechanisms in the case of ASPE,

but given the significant increase in conductivity measured by EIS for incremental increases in water molar concentration between A1 and A4, these water-Li^+ nanoscale domains are likely dominant. The combination of water and salt in this system contribute to a micro liquid-like environment. Within this environment Li^+ can migrate with liquid-like diffusion in heterogenous water domains, while still be contained by the polymer matrix and have the macro properties of a stretchable solid.

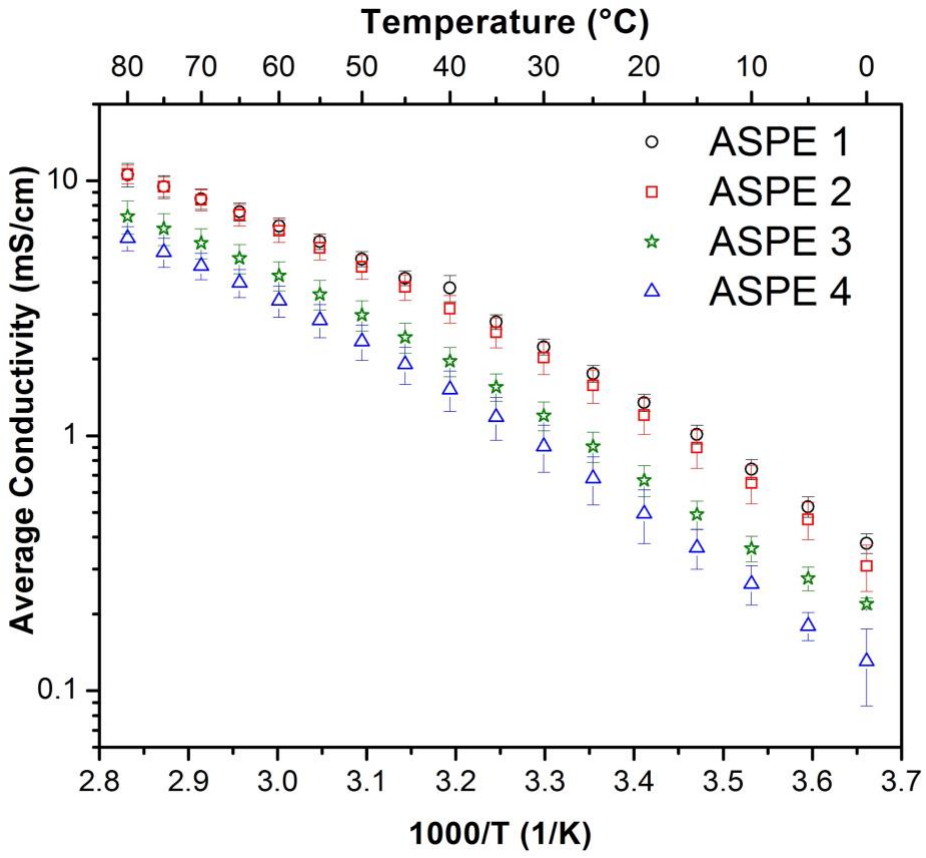

Figure 5.5: Conductivity vs. inverse temperature for A1-4, with temperature in °C shown on the top x-axis. Error bars are standard deviation across three samples.

To further elucidate the transport properties of this ASPE system, two sets of solid-state NMR diffusion measurements were taken each with their own limitations due to the complexity of handling water-containing solids. The first set was taken only at room

temperature, and includes data for fluorine (salt anion), lithium (salt cation), and proton (water) diffusion. This data set was collected with samples that took ~20min to prepare in ambient atmosphere, and likely gained some water during preparation. The second set of samples was prepared with a new method for packing NMR tubes that involved rolling samples in parafilm before packing. This preparation method is illustrated in Figure 5.6

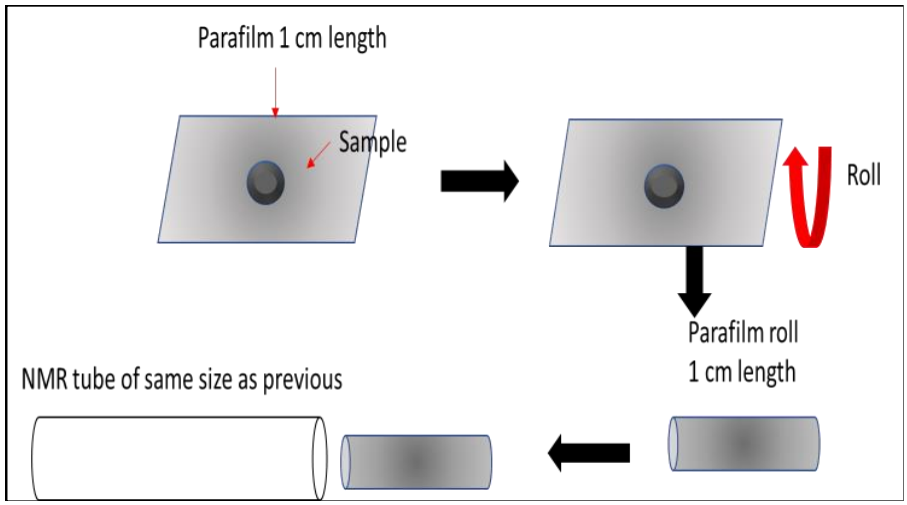

Figure 5.6: NMR sample preparation method that involves rolling sticky electrolyte in parafilm to make packing high aspect ratio NMR tube easier. Sample preparation took less than 5min.

and resulted in preparation times of less than 5min. This second set of samples could not be used to measure proton diffusion (water), as there was too much background signal from parafilm. This difference in sample exposure to ambient atmosphere made a difference in the results collected, as the first set of samples that was exposed to atmosphere for longer time demonstrated higher diffusion coefficients for each species measured due to water absorption. While this is an artificially high set of diffusion coefficients for the first sample set, the values relative to each other can be instructive. The second sample set has the added benefit of diffusion measurements for a range of temperatures, while also being closer to

intended sample compositions with less atmosphere exposure time. The results listed in Table 5.2 and shown as a function of Li:water ratio in Figure 5.7 are for the first sample

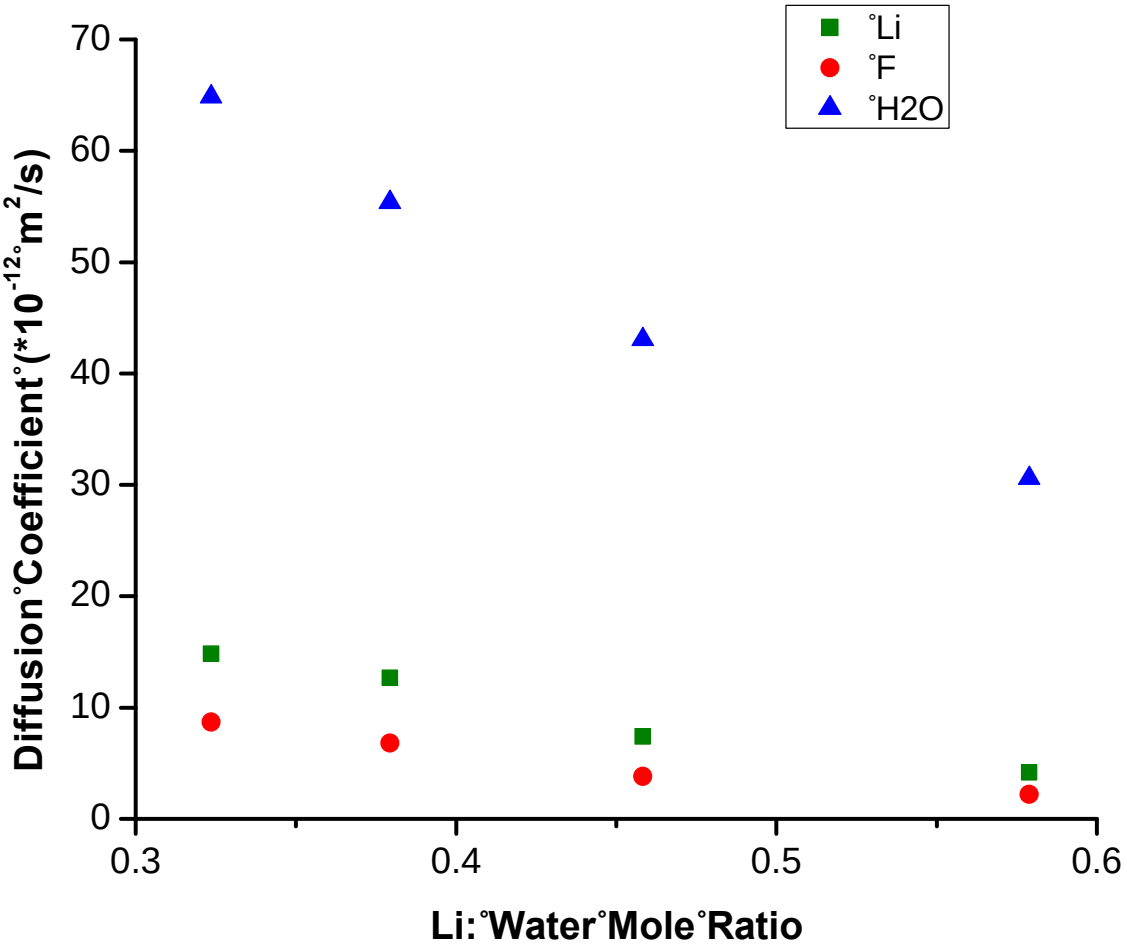

Figure 5.7: Diffusion coefficients for water, cation, and anion in A1-4 expressed as function of Li:water mole ratio measured at room temperature. A1 corresponds to the lowest value of Li:water while A4 corresponds to the highest value. This data is from the first NMR sample set.

set and are remarkable on several counts. First, the room temperature diffusion coefficients are an order of magnitude higher than those typically observed in more dilute (but water-free) PEO-salt complexes at temperatures above the melting point of PEO (~ 60°C)[165]. This is consistent with the high values of ionic conductivity from Figure 5.5, with room temperature values being reported in Table 5.2. Secondly, the cation diffusion coefficient

exceeds that of the anion, which is the opposite situation as that in the "classical" salt-in-polymer PEO complexes. In the latter case, the polyether segments preferentially solvate the cations. This leads to anions be largely unhindered by coordinating species, resulting in higher diffusion coefficients relative to Li^+, and hence cation transference numbers of ~ 0.2-0.3[148]. From the NMR measurements, it is possible to obtain a related quantity, the transport number via (4):

$$t^+ = \frac{D_+}{D_+ + D_-} \quad (4)$$

Those values are also listed in Table 5.2. An important caveat is that the transport number is a less meaningful quantity than the electrochemical transference number in the presence of significant ion pairing. The conductivity can also be calculated using the diffusion coefficients measured by NMR via the Nernst-Einstein equation (NE) (5):

$$\sigma_{\mathrm{NMR}} = \frac{F^2[C]}{RT}(D_+ + D_-) \quad (5)$$

Room temperature conductivity measurements calculated by NE exceed those measured with EIS by up to a factor of two, indicating the presence of ion association. However, even very highly ion-associated electrolyte systems will tend to show approximately equal cation and anion diffusivities[170] and classical PEO salt complexes always exhibit D (Li^+) < D (anion)[148,165]. This suggests that the preferential cation transport exhibited in this system with D (Li^+) > D (anion) is largely due to the presence of water, even for a wide range of Li:water mole ratios. This supports the claim that the ion transport mechanism which is dominant here is the preferential water-assisted vehicular transport where water occupies most of the solvation shell of Li^+[169]. Unfortunately, the presence of water in the

electrolytes does not allow electrochemical transference number measurements with Li electrodes by the Bruce-Vincent method discussed in Chapter 4, but the NMR results clearly indicate preferential cation transport.

Table 5.2: : Compositions of A1-A4 and diffusion coefficients from the first set of NMR experiments for various molecular species in the ASPE electrolytes. Also included is the calculated transport number, the measured by EIS room temperature ionic conductivity, and the conductivity calculated using the Nernst-Einstein equation.

Sample	Li:Water Mole ratio	EO:Li:water Mole ratio	D (Li) 10^{-12} m²/s For nt = 32	D(F) 10^{-12} m²/s	D(H) 10^{-12} m²/s	Li Transport No. [D(Li)/(D(Li+D(F)] (Unitless)	EIS σ @ 25°C [mS/cm]	Nernst Einstein Equation calculated σ @ 23°C [mS/cm]
A1	1 : 3.09	1 : 0.44 : 1.36	14.81	8.69	64.84	0.66	1.75 +/- 0.132	3.67
A2	1 : 2.64	1 : 0.44 : 1.16	12.68	6.8	55.38	0.67	1.58 +/- 0.235	2.54
A3	1 : 2.18	1 : 0.44 : 0.96	7.38	3.8	43.07	0.68	0.909 +/- 0.123	1.76
A4	1 : 1.73	1 : 0.44 : 0.76	4.17	2.21	30.58	0.70	0.681 +/- 0.146	0.998

The second sample set of NMR measurements, which were limited in exposure to atmosphere, were taken in 10°C from 5°C to 55°C. The diffusion coefficients for the cation (Li^+) and anion ($TFSI^-$) are shown in Table 5.3 and 5.4 respectively. Again, the trend of D (Li^+) > D (anion) holds for all compositions at all temperatures except for an anomalous measurement of A2 at 45°C. Interestingly, after measurements were taken ramping up in temperature and maxing out at a temperature of 55°C, a repeat measurement was taken at 25°C and is shown in red. The repeat measurements tend to be less than the initial measurements, indicating that some hysteresis effect may be occurring. One hypothesis is that the NMR tubes were not perfectly sealed, which could allow some water to escape during the higher than ambient temperature measurements.

Table 5.3: Li diffusion coefficients measured from the second set of NMR data for A1-4 as a function of temperature.

Temperature [°C]	A1 D(Li)	A2 D(Li)	A3 D(Li)	A4 D(Li)
5	3.07	2.79	1.1	0.42
15	3.7	2.85	2.14	1.26
25, repeat	10.54, 8.99	9.24, 8.22	3.9, 4.12	2.72, 1.98
35	15.87	12.13	6.78	4.64
45	23.79	10.05	12.07	7.73
55	32.89	31.98	16.21	11.99

Table 5.4: TFSI diffusion coefficients measured from the second set of NMR data for A1-4 as a function of temperature.

Temperature [°C]	A1 D(F)	A2 D(F)	A3 D(F)	A4 D(F)
5	0.52	1.15	0.4	0.18
15	1.32	2.51	1.05	0.57
25, repeat	6.03, 6.22	4.47, 3.90	1.88, 1.01	1.41, 0.98
35	10.57	8.54	3.87	2.61
45	15.51	14.01	7.06	5.04
55	20.34	18.06	9.3	8.37

With multiple measurements at different temperatures, (4) was used to generate a conductivity vs. inverse temperature graph for the NMR data which is plotted along with EIS conductivity data in Figure 5.8. The lines correspond to a linear regression Arrhenius model fit (7) of the data. With this second set of NMR data, the closeness of conductivity as measured by EIS and conductivity calculated from (5) is in much better agreement than the first set of NMR data. Most conductivity values are within 20% of each other for the

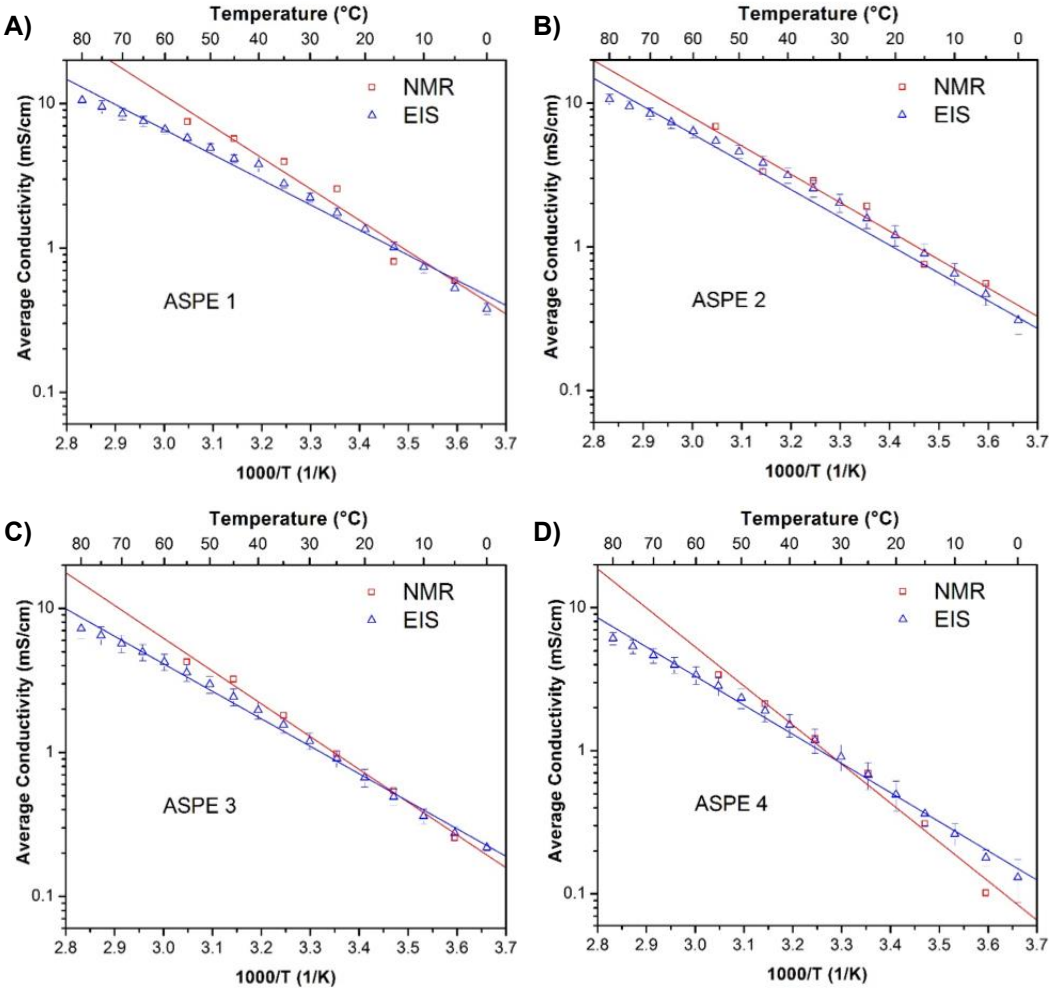

Figure 5.8: Conductivity vs inverse temperature for A1-A4 as measured by EIS and NMR. Temperature in °C is shown on the top x-axis. Diffusion coefficients measured from NMR were used to calculate conductivity using NE equation (4). The second set of NMR data were used. Red and blue lines correspond to Arrhenius fitting.

second set of NMR data with a few exceptions. This validates the faster packing method used (Figure 5.6) in an effort to reduce atmosphere exposure. The activation energies from the Arrhenius fit as well as the goodness of fit parameter, R_2, are included in Table 5.5. The R_2 values for both EIS and NMR data show good agreement with the choice of Arrhenius fit, as R_2 is higher than 0.95 for all samples and mostly higher than 0.99 for samples measured by EIS. This would suggest that the transport mechanism mentioned previously with mostly water-assisted Li^+ transport is correct, as this is described by an Arrhenius fit. The activation energies extracted from Arrhenius fitting in Table 5.3 can be compared to those of the concentrated aqueous salt LiTFSI in water. The activation energy of the LiTFSI-water system is ~0.24eV regardless of concentration[169]. The activation energies resulting from Arrhenius fitting of A1-4 as measured by EIS have values ranging from 0.35 – 0.40eV, which is in good agreement with other PEO-LiTFSI systems[148].

Table 5.5: Linear regression Arrhenius fitting results with activation energies for A1-4 measured by EIS and measured by NMR (second sample set) with conductivities calculated using (5). Goodness of fit R_2 is included.

Sample	Activation Energy (eV)	Arrhenius Fit R_2
A1 - EIS	0.345	.9857
A2 - EIS	0.362	.9904
A3 - EIS	0.379	.9943
A4 - EIS	0.404	.9932
A1 - NMR	0.429	.9576
A2 - NMR	0.393	.9675
A3 - NMR	0.451	.9941
A4 - NMR	0.541	.9851

LSV and CV

While water as a co-solvent imbues the system with exceptional ionic conductivity and lithium transport number, it also has a notoriously small ESW that could hinder its functionality for electrochemical energy storage systems. To investigate the impact water has on the electrochemical stability of this system linear sweep voltammetry (LSV) was performed and is shown in Figure 5.9. This experiment is used to determine the ESW of the electrolyte, and to discover the potentials at which oxidation or reduction reactions of electrolyte components occur. The current at a working electrode is measured while the

potential between the working electrode and a reference electrode is swept linearly in time. Oxidation or reduction of a particular species is registered as a peak or trough in the current signal at the potential at which the species begins to be oxidized or reduced. Figure 1 is a composite graph of eight individual representative LSV experiments to show the ESW of A1-4. Aluminum was used as the working electrode for the cathodic (reductive stability) scans, and titanium was the working electrode for the anodic (oxidative stability) scans. Half charged LFP was chosen as the reference and counter electrode in this two-electrode setup. Unfortunately, lithium metal potential is outside of the ESW of A1-4, such that an ASPE electrolyte in contact with it would turn black. This precludes the use of lithium metal as a reference and counter electrode which would be preferred. The small feature around 3.0 V is an artifact from the LSV routine where the program applied a current to take the sample voltage from its open circuit voltage (OCV) to the procedure start voltage of 3.0 V. There are three distinct regions in both the cathodic and anodic scans for all compositions: a region of little to no current, a region of moderate current, and a region of unmitigated current. The region of little to no current can be assigned as the ESW of the electrolyte. A lower bound of 1.0 V and an upper bound of 3.5 V encompasses all electrolytes studied here, with A1-3 extended their lower bound to ~ 0.5 V. The region between 0.5 to -0.25 V for A1-3 (1 to -0.25 V for A4) and 3.5 to 5 V are moderate current regions. In these regions there are electrochemical reduction (likely water and LiTFSI) and oxidation (all three components) reactions occurring, however the current is small enough that passivation with cycling in these regions may be possible. The regions of unmitigated current, below -0.25 V and above 5.0 V, are due to large-scale electrolyte degradation from redox reactions and are not accessible for a practical energy storage system.

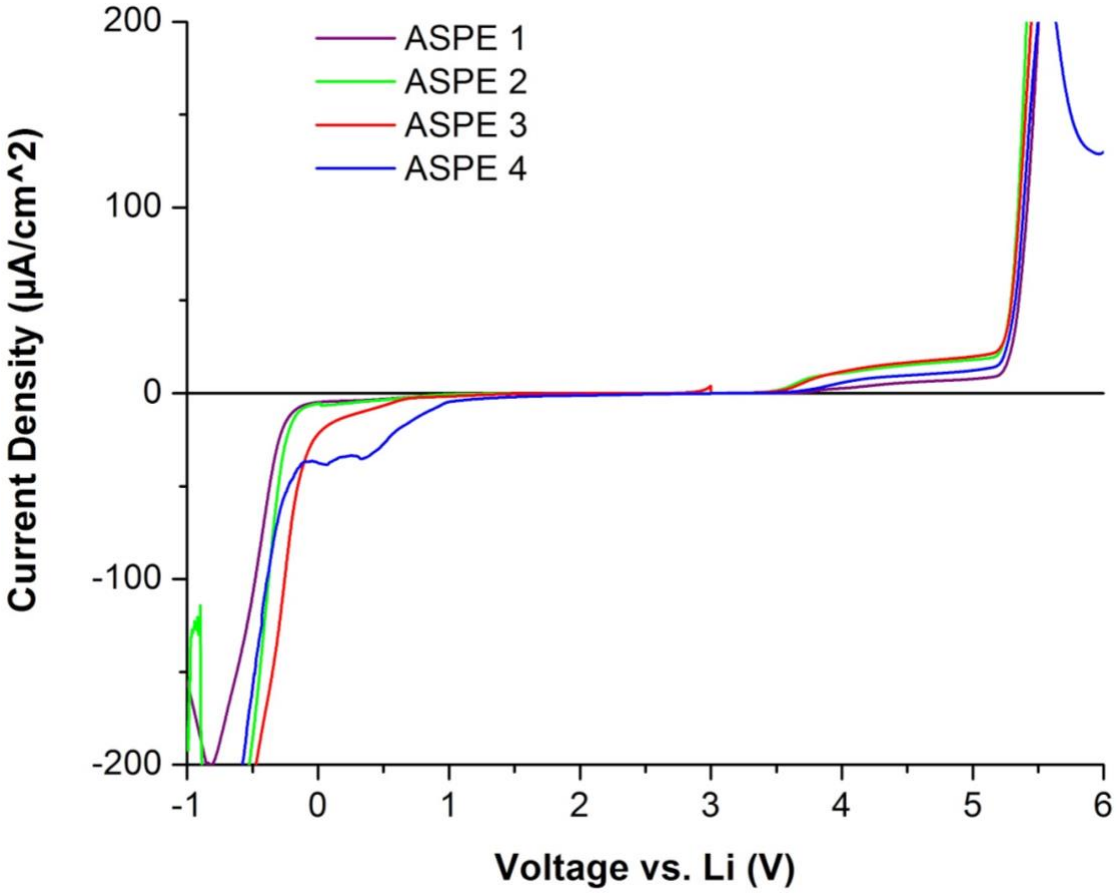

Figure 5.9: Linear sweep voltammetry of LFP/ ASPE/ Al cell for A1-4 shown on the same graph. The voltage was swept from3.425V to -0.5V vs. vs. Li/Li^+ in the cathodic scan and 3.425 to 8.0V in the anodic scan at a rate of 1 mVs^{-1}. Scans were taken at room temperature.

To measure the passivating ability of the ASPE system Cyclic Voltammetry (CV) was performed in both directions for A1-4. CV works in a similar manner as LSV, but instead of trying to identify where breakdown current starts, CV is a method used to determine temporal stability and the ability of the electrode-electrolyte interface to passivate with cycling time. Of particular interest are the regions of moderate current identified by LSV. Anodic CV scans from 3.0 to 4.5 V and cathodic scans from 3.0 to 1.0 V were cycled 100 times and are shown in Figure 5.10. Cycle #1, 2, 50, and 100 are shown with a 10 $\mu A/cm_2$ vertical offset so that the cycles can be easily compared. Cathodic scans

for A1-4 show minimal current on cycle 1 down to 1.0V and excellent passivation behavior with continued cycling. A1-3 show a larger peak on cycle 1 of the anodic scans likely due to oxidation of water. By cycle 2 the current has lessened significantly, and by cycle 50 all four compositions show perfect passivation. All four compositions show good passivation capability by cycle 50 against both reduction and oxidation.

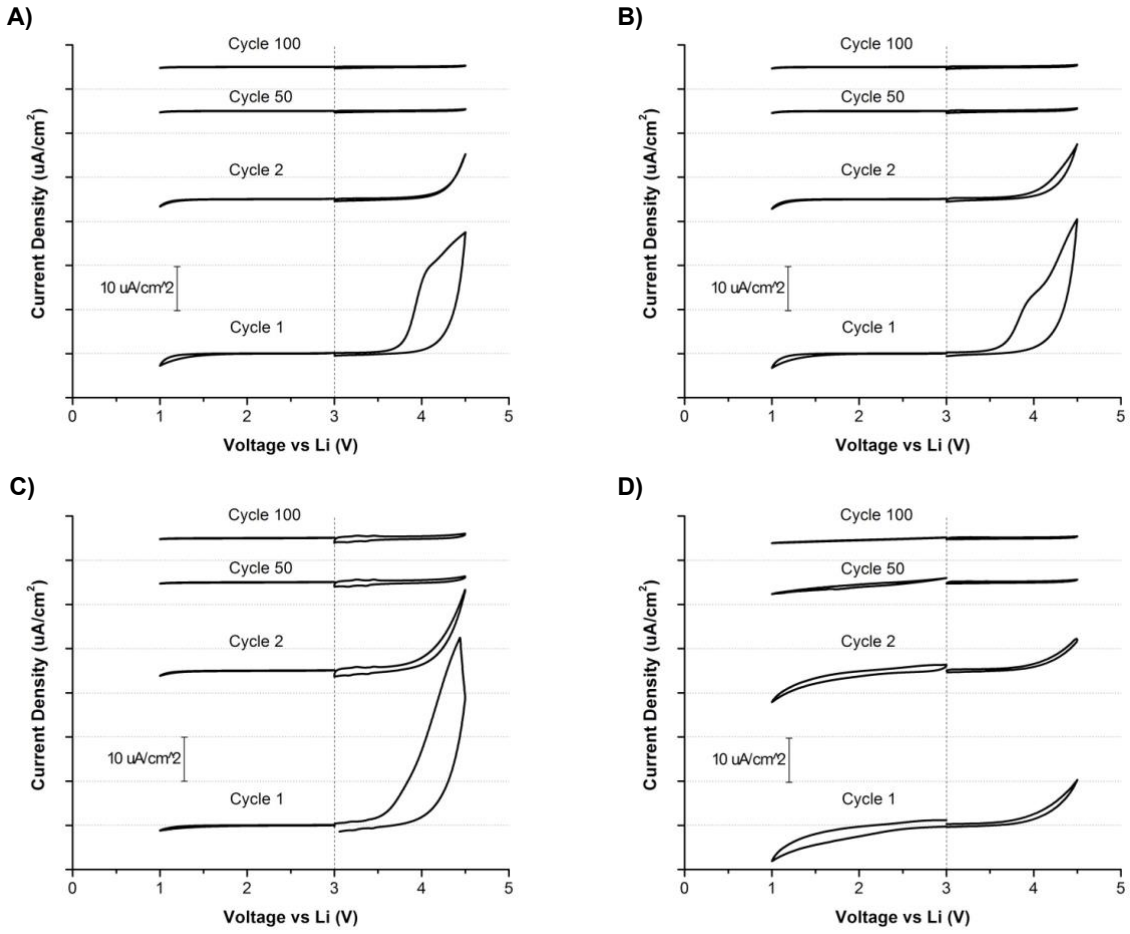

Figure 5.10: CV scans of LFP/ASPE/Al from 3V to 1V, combined with CV scans of LFP/ASPE/Ti from 3.0V to 4.5V all vs. Li/Li. Cycle # 1, 2, 50, and 100 are shown for A) A1, B) A2, C) A3, and D) A4.

Galvanostatic Cycling

While studying the excellent transport properties of the ASPE system was the focus of this chapter, it is still worthwhile to include galvanostatic cycling results which demonstrate the ability of ASPE electrolytes to operate within a battery system. To demonstrate proof-of-concept cycling, a LTO/ A2/ LMO coin cell was constructed and set to cycle at a 1C rate at room temperature. Figure 5.11 shows specific capacity vs cycle number corresponding to black data points, and coulombic efficiency vs cycle number corresponding to red data points. This cell configuration cycled with ~99% coulombic efficiency after 50 cycles. This initial period lower coulombic efficiency is likely due to TiO_2 defects in LTO causing water splitting[171]; LTO is a notoriously challenging anode material for water-containing electrolytes[113,119,120,124,126,141]. Another consideration that would need to be optimized for better performance is the interfacial contact in this system. This is addressed in Chapter 6.

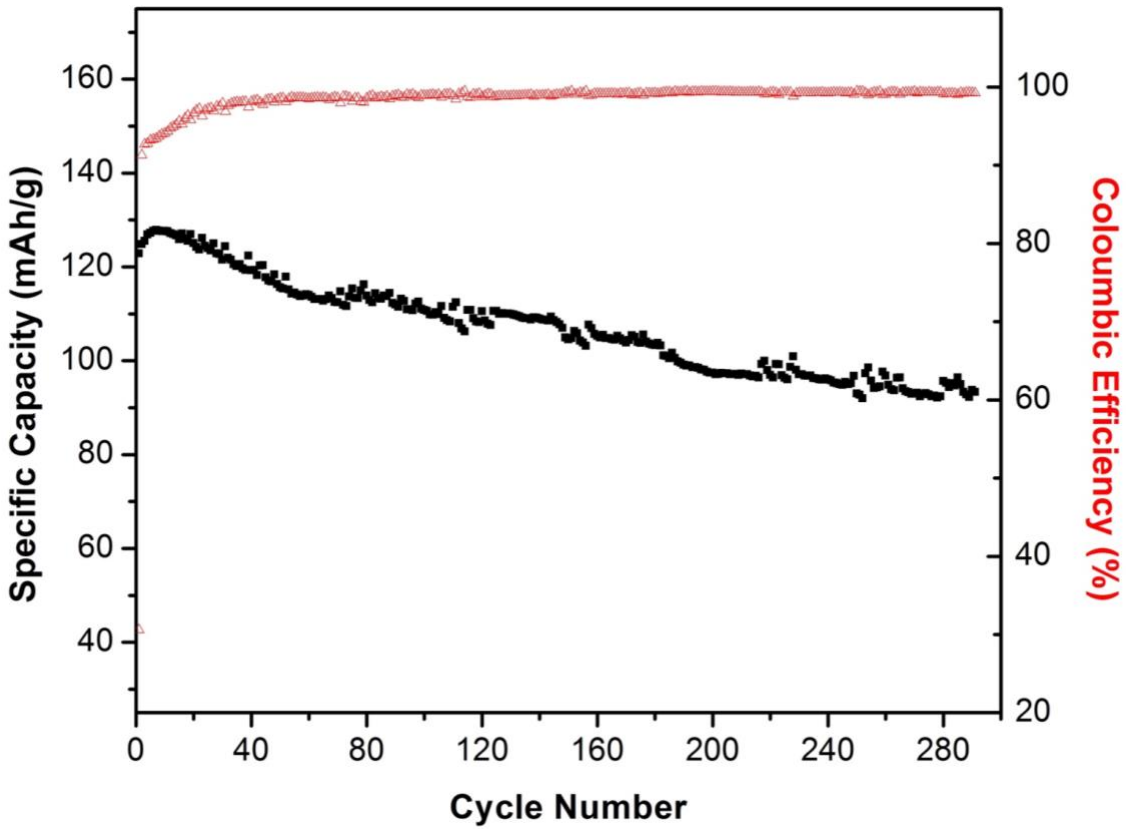

Figure 5.11: Galvanostatic cycling performance of LTO/ ASPE #2/LMO at various 1C rates over 280 cycles. Black data points correspond to specific capacity on the left y-axis, red data points correspond to coulombic efficiency on the right y-axis.

5.5 Conclusions

Lithium-ion batteries (LIBs) have proven to be an effective means for powering devices, however concerns over their safety and environmental impact still exist. These concerns are largely related to the non-aqueous liquid organic electrolytes employed by commercial LIBs. A solid polymer electrolyte (SPE) that incorporates water as a plasticizer results in an electrolyte with high conductivity and the mechanical properties of a flexible solid, while replacing the most dangerous component with water. Here we show an aqueous solid

polymer electrolyte (ASPE) comprised of poly(ethylene oxide) (PEO), water, and lithium salt fabricated via a hot-pressing method with a conductivity of 0.681 - 1.75mS/cm at 25 °C. . The incorporation of a polymer matrix makes this system stable down to the potential of lithium titanate (LTO, 1.55 V vs Li/Li^+), which has only ever been achieved by multi component aqueous salts[123][124,125] and represents a huge boost in energy density for rechargeable aqueous-based batteries as +3 V electrochemical couples can be realized. The transport mechanism of these electrolytes was probed using a combination of EIS, NMR, and data fitting. The suggested dominant conduction mechanism in these electrolytes is water-assisted vehicular transport, which is bolstered by the water concentration dependence of the conductivity results. This ASPE system provides an alternative and addresses many of the issues associated with liquid organic electrolytes.

Chapter 6: Outlook and Future Directions

6.1 ILSPE Future Work

Improving Electrode/ Electrolyte Contact

Chapter 2.3 introduces the interface problem for SPEs, which is the fact that typical electrode processing techniques produce electrodes with significant porosity that is intended to be filled with liquid electrolyte. In the context of a solid analogue, the electrolyte cannot make significant contact with active material through the bulk of the electrode as it cannot effectively fill porosity. An attempt to address this issue was made in Chapter 4 where ILSPE components were mixed with electrode components and slurry cast and vacuum-dried as is typical for electrode processing. The idea here is that electrolyte components mixed throughout the cathode will provide ionic pathways from the electrolyte to all active material particles contained within the electrode. The contrast between an SPE with a normal cathode and a SPE with a composite cathode is illustrated in Figure 6.1. In the first case, large voids as a result of electrode processing are unable to be filled with polymer electrolyte. In the second case, the inclusion of SPE components within the electrode create a conductive network to better distribute ion transport pathways throughout the electrode.

The ILSPE composite cathode resulted in good cycling with high capacity utilization and coulombic efficiency as outlined in Chapter 4, however these electrodes had a loading of ~0.1mAh/cm$_2$ which is an order of magnitude away from commercially relevant electrode loadings of 1-3mAh/cm$_2$. The slurry casting fabrication process also produced a composite cathode with significant porosity which is a staple of solvent

evaporation in this process. A further improvement could come from changing the fabrication of these electrodes from slurry casting and solvent evaporation to a no-solvent hot-pressing approach similar to how SPE electrolytes were fabricated in Chapters 4-5. Mixing all components followed by annealing and hot-pressing in a mold would result in a solvent-free electrode with little to no porosity. The thickness of the electrode could be altered after the pressing process by cold-calendaring to a desired thickness. A demonstration of high capacity utilization and coulombic efficiency with such a cathode would effectively address concerns around SPE/ electrode contact limitations.

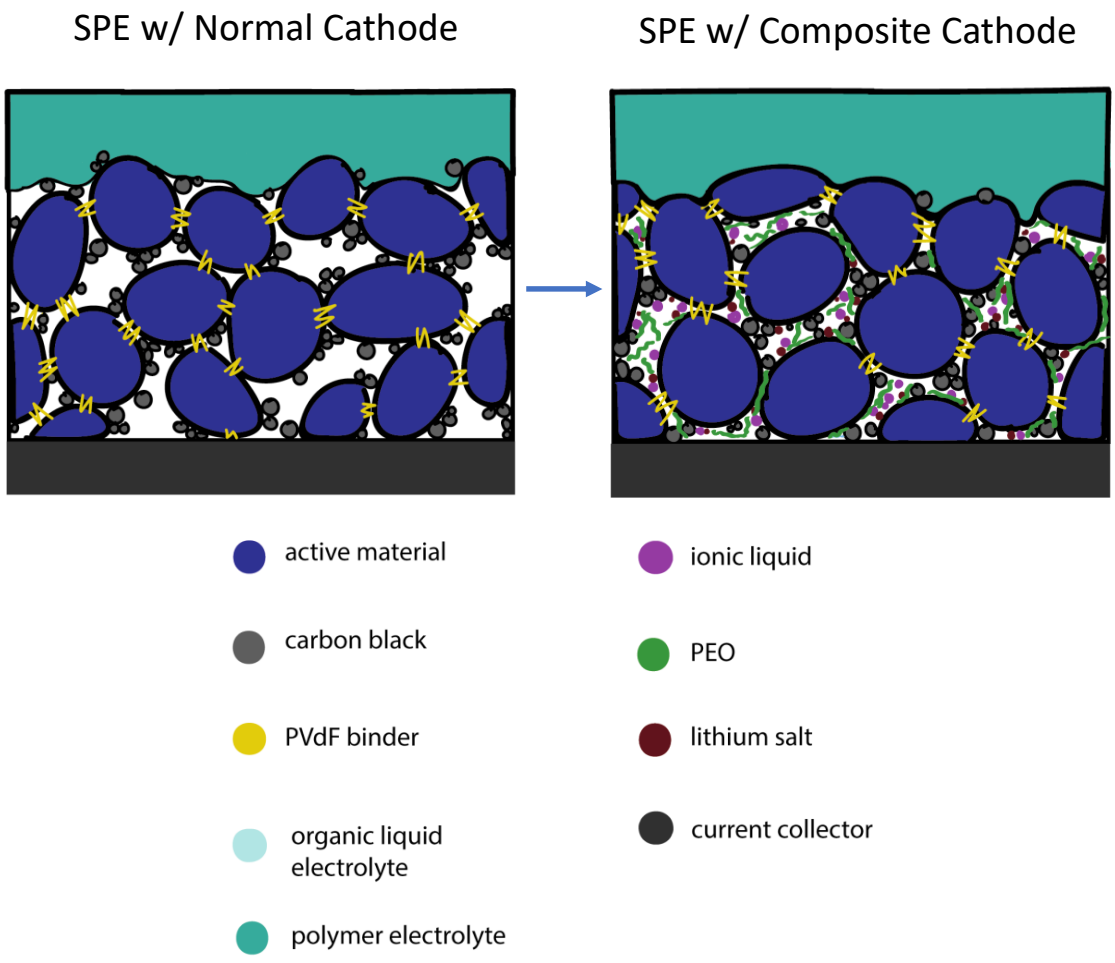

Figure 6.1: Schematic representation of a SPE/ normal electrode interface and a SPE/ composite electrode interface.

Extensive Li Dendrite Studies

Stripping and plating tests were performed on ILSPE electrolytes (see Figure 4.10) to show their temporal stability with lithium electrodeposition. These tests resulted in a total of 200 hours of active stripping and plating with no cells failing due short circuits caused by dendrites. These stripping and plating tests were done at a moderate current density of 0.1mA/cm$_2$, with each cycle totaling 2hr. While this is indeed a demonstration of stability with lithium electrodeposition, this routine could be constructed in such a way were dendrite formation is more likely, acting as a stress test. The next step to rigorously determine the ILSPE long-term stability with a lithium metal anode (no dendrite formation) is to use an aggressive stripping and plating routine until cell failure. An aggressive stripping and plating routine is necessary to ensure that lithium dendrite growth occurs, and the results of such a test could demonstrate which compositions of ILSPE are resilient to dendrite growth and at what current densities do they show resiliency. A routine with prolonged current application, such that each cycle takes 6hr (current polarity changing every 3hr), would be an effective way to stress test the ILSPEs. Additionally, the results of such a test could be compared to benchmarks in literature[172] and would be expressed in terms of total charge passed at the time of dendrite-induced cell failure (C_d, with units C/cm$_2$) and short circuit time (t_{sc}). There are multiple design principles for suppressing lithium dendrite growth, including the use of a mechanically strong separator, having favorable transport properties, and curbing unregulated surface reactions that promote dendrite growth[25]. It is clear that multiple combinations of these principles can lead to the effective suppression of dendrites, and it would be insightful to determine where different

ILSPEs are located on this landscape. These tests would take up significant resources however, using multiple battery test channels for periods of hundreds of hours. Given sufficient time and resources, multiple ILSPE compositions at multiple current densities would be tested.

6.2 ASPE Future Work

Improving Electrode/ Electrolyte Contact

The cycling of the ASPE system in Chapter 5 was not as much about demonstrating good performance as it was about demonstrating Li^+ intercalation in LTO/ LMO electrodes using an aqueous electrolyte, which is notoriously difficult to do[113,119–121,123,124,126,173]. To further improve cycling, a liquid substitute for the solid ASPE called a catholyte/ anolyte (dependent on which electrode is in contact with the solution) can be used to fill porosity and provide ionic contact through the bulk of the electrode. Using low molecular weight polyethylene glycol (PEG, MW = 3,500Da) instead of high molecular weight PEO (MW = 10^6Da), keeping all molar concentration of the components the same, results in liquid ASPE that can serve as a catholyte or anolyte. Electrodes can be soaked in liquid ASPE before a solid ASPE is placed between them to make a battery cell. Figure 6.2 provides an illustration for this proposed system. In this case, the catholyte is able to intimately contact all active material particles due to the porosity of the electrode and the liquid nature of the catholyte, providing an ion conduction pathway through the bulk of the electrode. The electrolyte would still be a high molecular weight solid, such that it can act as the separator in this system.

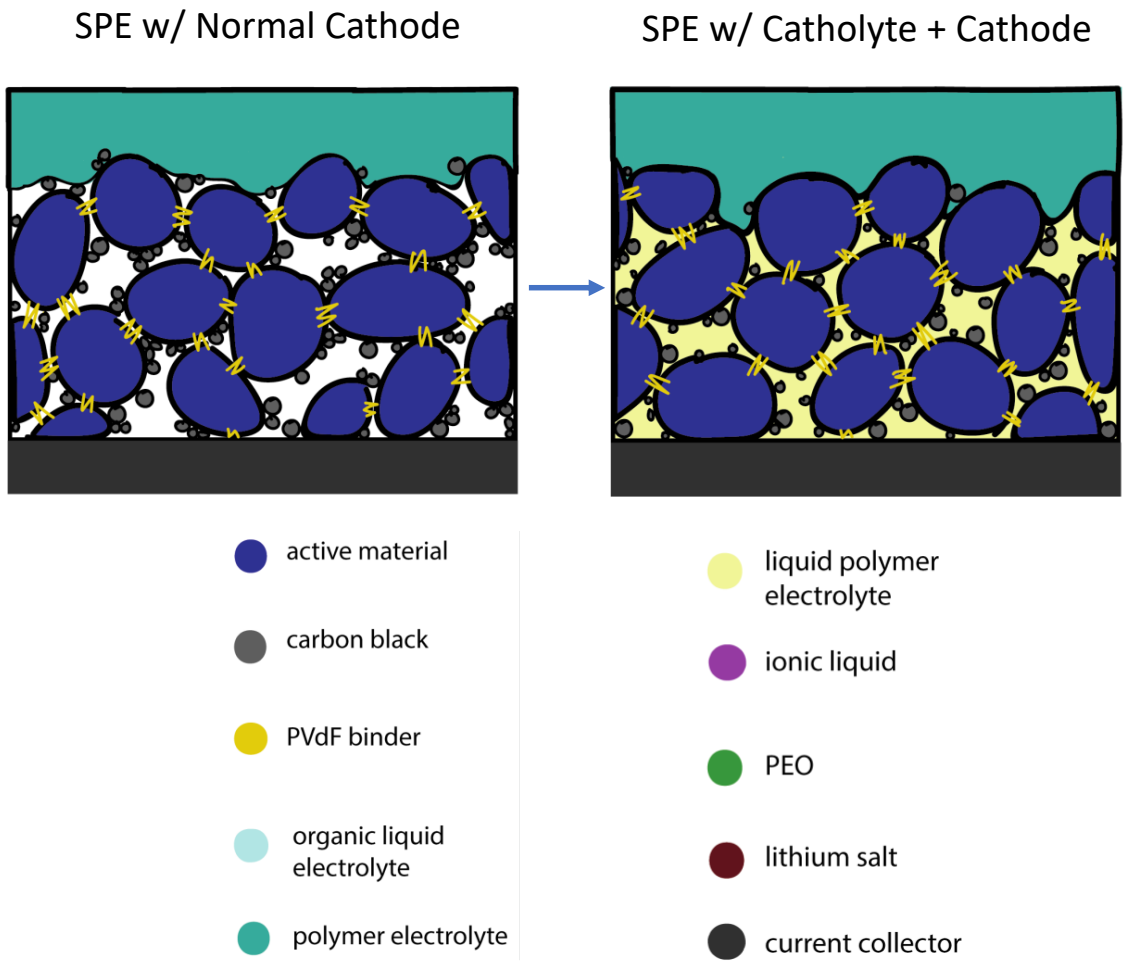

Figure 6.2: Schematic representation of a SPE/ normal electrode interface and a SPE + catholyte/ electrode interface.

Further Stability Studies

One way to verify stability studies done with solid ASPE electrolytes is to substitute them with a liquid counterpart that has the same chemistry. With the recent understanding that low molecular PEG in lieu of high molecular weight PEO will make an ASPE liquid, new electrochemistry characterization techniques become available. Previously, electrochemical stability had to be assessed in a two-electrode coin cell because of the solid nature of the high molecular weight ASPEs. This necessitated the use of half-charged LFP as a counter and reference electrode, which is time consuming to prepare. With liquid

ASPE, CV can be conducted with a three-electrode setup using a Ag/AgCl reference electrode. Additionally, the working electrode no longer has to be inert and active electrodes such as LTO and LMO can be used to demonstrate stability with intercalation/ deintercalation with these materials. Using a liquid proxy to measure the electrochemical stability of our solid system will result in a more robust study and can be easily compared to what was measured in the solid system to validate this approach.

Chemical Characterization of the SEI

Another benefit of using a liquid ASPE with low molecular weight PEG as opposed to high molecular weight PEO is the ease of electrode extraction post-experiment for chemical characterization of the SEI. Previously, the electrode interface could not be exposed without significant damage due to the sticky nature of the high molecular weight solid ASPE. In the case of liquid ASPE, electrodes can be extracted and washed of excess electrolyte easily. The surface chemistry of these electrodes can then be probed using XPS. This now opens up direct observation of interface formation chemistry as a function of electrolyte composition, a characterization mode previously unavailable. With the ability to directly characterize the interface chemistry, intelligent choices can be more easily made with regards to electrolyte design.

New ASPE Formulations

The ASPE formulation in Chapter 5 was informed by the initial 21m LiTFSI in water innovation[113], and since then more aqueous salts have been reported on that improve upon the stability of WISE through the use of multi-salt aqueous salts[123–125]. The inclusion of

polymer has also been shown to provide additional solvation power to raise the effective salt:water ratio as is evidenced by Yang *et al*[126] and by the A3 and A4 formulations in Chapter 5. To create effective new ASPE formulations, the same design principles that are relevant for SPEs must be observed. Namely, the polymer matrix needs to be plasticized and amorphous to facilitate ion transport, and the salt content shouldn't be so high that salt precipitates out. An effective choice of aqueous salt to blend with a polymer matrix will be further informed by CV and XPS characterization mentioned above. Starting with a liquid analogue will make electrochemical characterization easy and more robust, following which the system can be scaled up with a high molecular weight polymer matrix to measure conductivity by EIS.

In addition to tuning the electrochemical stability of the electrolyte through salt selection and concentration, the solvent molecule can be changed to meet the same goal. A mixed aqueous salt + organic solvent molecule system has been investigated with the purpose of the additional organic solvent molecule is that it provides an additional chemical substrate for SEI formation while lowering the concentration of water in the system[141]. Selecting a solvent blend of water + small polar organic solvent molecule such as acetonitrile could be a promising way to lower the water content while keeping salt concentrations high for improved stability.

6.3 Scientific Contributions

My research has resulted in one publication in review and two that are in preparation. The work in this dissertation has been presented 5 times in local, national, and international meetings at the Materials Research Society, Mid-Atlantic Soft Matter Workshop, European Materials Research Society, and the AICHE Annual Student Conference. Additionally, the ASPE work in Chapter 5 has resulted in a U.S. non-provisional patent application (No. 16/241,913).

This work addresses some of the fundamental challenges with SPE implementation in battery systems, namely overcoming poor ionic conductivity and the need for improving interfacial contact between SPEs and electrode materials, with significant headway being made on both accounts. The ILSPE project in Chapter 4 demonstrated through optimized ratios of polymer, salt, and IL a SPE electrolyte with room temperature conductivity of ~1mS/cm. Additionally, these ILSPE electrolytes were coupled with a composite cathode formulation designed to improve ionic contact between the electrode and electrolyte to enable high capacity utilization. Further improvements were suggested for the cathode fabrication process involving a solvent-free die-pressing approach that would eliminate electrode porosity, creating better ionic contact with no dead space.

The ASPE project in Chapter 5 demonstrated that through the addition of water as a plasticizer SPEs could be made that largely decouple ion motion from polymer chains, resulting in what is known as “superionic” behavior. This discovery resulted in ASPEs that exhibit extraordinary transport properties with room temperature conductivities > 1mS/cm and lithium transport numbers of ~0.7. This work lays the foundation for a new area of exploration where high amounts of salt and small amounts of water (or other small solvent

molecules) can be used to create superionic behavior in SPEs. Some suggestions for future ASPE formulations are given in Chapter 6. Additionally, ASPE compositions can be made as both solids or liquids, through the use of high or low molecular weight polymer respectively. This creates the possibility of creating high electrolyte/ electrode interfacial contact with anolyte/ catholyte formulations using the same chemistries as the high molecular weight SPE analog outlined in Chapter 6.

Chapter 7: Appendices

Appendix A: Standard Operating Procedures

Transference Determination

This procedure describes how to measure T_{Li+} of a polymer electrolyte by the Bruce and Vincent potentiostatic polarization method[133,145]. This procedure uses a combination of AC impedance spectroscopy and potentiostatic polarization to determine t_{Li+} through the relationship:

$$T_{Li^+} = \frac{I_{ss} * R_{b,SS}(\Delta V - I_0 * R_{i,0})}{I_0 * R_{b,0}(\Delta V - I_{ss} * R_{i,ss})} \quad (2)$$

where I_0 is the initial current during the potentiostatic polarization, I_{ss} is the current at steady state, $R_{b,0}$ is the initial bulk electrolyte resistance, $R_{b,ss}$ is the bulk electrolyte resistance at steady-state, $R_{i,0}$ is the initial interfacial impedance, $R_{i,ss}$ is the steady-state interfacial impedance, and ΔV is the applied potential. Alternatively, I_Ω can be used in place of I_0, where:

$$I_\Omega = \frac{\Delta V}{R_{b,0} + R_{i,0}} \quad (6)$$

To obtain the necessary values in (2) for a measurement of T_{Li+}, follow this procedure:

1. Construct symmetrical Li / SPE / Li coin cells. Anneal at elevated temperature (>= 60°C) overnight. For this method to work, the SPE needs to have an ability to create a passivating layer with Li electrodes to prevent unmitigated degradation.
2. Run AC impedance spectroscopy to measure the pre-conditioned interfacial resistance.

3. Condition the cells by running 5 charge/discharge (plating/stripping) cycles on the Arbin. Use a small current density of 0.02 mA/cm$_2$ with a 4h charge, 45min rest, 4h discharge, 45min rest for one cycle. This is done to create a stable interface with good contact. Run this test at 60°C.
4. Run AC impedance spectroscopy at 60°C to determine $R_{i,0}$ and $R_{b,0}$, the resistance values before the potentiostatic polarization experiment.
5. Run a potentiostatic polarization experiment on the Solartron choosing a ΔV between 10-80mV, for a period of 4h (or enough time for the current to reach a steady-state value) at 60°C. Take note of I_0 and I_{ss}.
6. Run AC impedance spectroscopy to determine $R_{i,ss}$ and $R_{b,ss}$, the resistance values at steady-state post potentiostatic polarization at 60°C.
7. Take note of all experimental values in a spreadsheet and use (2) to calculate T_{Li+}.
8. Calculate t_{Li+} by using (6) to replace I_0 in (2).

Some notes:

The initial and final bulk electrolyte resistances, $R_{b,ss}$ and $R_{b,0}$, are often the same. They can be found on the Nyquist plot by taking the higher frequency x-intercept (left-most intercept) of the right-most semi-circle.

Chapter 8: References

1. Wetjen, M. *et al.* Thermal and electrochemical properties of PEO-LiTFSI-Pyr 14TFSI-based composite cathodes, incorporating 4 V-class cathode active materials. *J. Power Sources* **246**, 846–857 (2014).
2. Appetecchi, G. B. *et al.* Hot-pressed, solvent-free, nanocomposite, PEO-based electrolyte membranes. *J. Power Sources* **124**, 246–253 (2003).
3. Kim, G. T. *et al.* UV cross-linked, lithium-conducting ternary polymer electrolytes containing ionic liquids. *J. Power Sources* **195**, 6130–6137 (2010).
4. Xu, K. Nonaqueous Liquid Electrolytes for Lithium-Based Rechargeable Batteries. (2004).
5. Mullen, J. & Kwon, K. J. Samsung is recalling the Galaxy Note 7 worldwide over battery problem. *CNN Money* (2016). Available at: http://money.cnn.com/2016/09/02/technology/samsung-galaxy-note-7-recall/.
6. Khurana, R., Schaefer, J. L., Archer, L. A. & Coates, G. W. Suppression of lithium dendrite growth using cross-linked polyethylene/poly(ethylene oxide) electrolytes: a new approach for practical lithium-metal polymer batteries. *J. Am. Chem. Soc.* **136**, 7395–402 (2014).
7. Gerssen-Gondelach, S. J. & Faaij, A. P. C. Performance of batteries for electric vehicles on short and longer term. *J. Power Sources* **212**, 111–129 (2012).
8. Scrosati, B. & Garche, J. Lithium batteries: Status, prospects and future. *J. Power Sources* **195**, 2419–2430 (2010).
9. Dahbi, M., Ghamouss, F., Tran-Van, F., Lemordant, D. & Anouti, M. Comparative

study of EC/DMC LiTFSI and LiPF6 electrolytes for electrochemical storage. *J. Power Sources* **196**, 9743–9750 (2011).

10. Goodenough, J. B. & Kim, Y. Challenges for Rechargeable Li Batteries †. *Chem. Mater.* **22**, 587–603 (2010).
11. Sloop, S. E., Pugh, J. K., Wang, S., Kerr, J. B. & Kinoshita, K. Chemical Reactivity of PF[sub 5] and LiPF[sub 6] in Ethylene Carbonate/Dimethyl Carbonate Solutions. *Electrochem. Solid-State Lett.* **4**, A42 (2001).
12. Dreamliner: Boeing 787 planes grounded on safety fears - BBC News. *BBC News* (2013). Available at: http://www.bbc.com/news/business-21054089. (Accessed: 1st November 2016)
13. Ohnsman, A. & Keane, A. G. Tesla's Third Model S Fire Brings Call for U.S. Inquiry. *Bloomberg* (2013). Available at: http://www.bloomberg.com/news/articles/2013-11-07/tesla-s-third-model-s-fire-brings-call-for-u-s-inquiry. (Accessed: 1st November 2016)
14. Wang, Q., Jiang, L., Yu, Y. & Sun, J. Progress of enhancing the safety of lithium ion battery from the electrolyte aspect. *Nano Energy* **55**, 93–114 (2019).
15. Meyer, W. H. Polymer Electrolytes for Lithium-Ion Batteries. *Adv. Mater.* **10**, 439–448 (1998).
16. Xue, Z., He, D. & Xie, X. Poly(ethylene oxide)-based electrolytes for lithium-ion batteries. *J. Mater. Chem. A* **3**, 19218–19253 (2015).
17. Abruña, H. D., Kiya, Y. & Henderson, J. C. Batteries and electrochemical capacitors. *Phys. Today* (2008). doi:10.1063/1.3047681
18. Aurbach, D., Zinigrad, E., Cohen, Y. & Teller, H. A short review of failure

mechanisms of lithium metal and lithiated graphite anodes in liquid electrolyte solutions. *Solid State Ionics* **148**, 405–416 (2002).

19. Jansen, A. N., Amine, K., Newman, A. E., Vissers, D. R. & Henriksen, G. L. Low-cost, flexible battery packaging materials. *JOM* **54**, 29–32 (2002).
20. Tarascon, J. M. & Armand, M. Issues and challenges facing rechargeable lithium batteries. *Nature* **414**, 359–67 (2001).
21. Zhang, S. S. A review on the separators of liquid electrolyte Li-ion batteries. *J. Power Sources* **164**, 351–364 (2007).
22. Agrawal, R. C. & Pandey, G. P. Solid polymer electrolytes: materials designing and all-solid-state battery applications: an overview. *J. Phys. D. Appl. Phys.* **41**, 223001 (2008).
23. Diederichsen, K. M., McShane, E. J. & McCloskey, B. D. Promising Routes to a High Li + Transference Number Electrolyte for Lithium Ion Batteries. *ACS Energy Lett.* **2**, 2563–2575 (2017).
24. Tikekar, M. D., Archer, L. A. & Koch, D. L. Stabilizing electrodeposition in elastic solid electrolytes containing immobilized anions. *Sci. Adv.* **2**, e1600320 (2016).
25. Tikekar, M. D., Choudhury, S., Tu, Z. & Archer, L. A. Design principles for electrolytes and interfaces for stable lithium-metal batteries. *Nat. Energy* **1**, 16114 (2016).
26. Song, J. Y., Wang, Y. Y. & Wan, C. C. Review of gel-type polymer electrolytes for lithium-ion batteries. *J. Power Sources* **77**, 183–197 (1999).
27. Cheng, X., Pan, J., Zhao, Y., Liao, M. & Peng, H. Gel Polymer Electrolytes for Electrochemical Energy Storage. *Adv. Energy Mater.* **8**, 1702184 (2018).

28. Manuel Stephan, A. Review on gel polymer electrolytes for lithium batteries. *Eur. Polym. J.* **42**, 21–42 (2006).

29. Mindemark, J., Lacey, M. J., Bowden, T. & Brandell, D. Beyond PEO—Alternative host materials for Li+-conducting solid polymer electrolytes. *Prog. Polym. Sci.* **81**, 114–143 (2018).

30. Fisher, A. S., Khalid, M. B., Widstrom, M. & Kofinas, P. Anion Effects on Solid Polymer Electrolytes Containing Sulfur Based Ionic Liquid for Lithium Batteries. *Journal of The Electrochemical Society* **159**, A592 (2012).

31. Fisher, A. S., Khalid, M. B., Widstrom, M. & Kofinas, P. Solid polymer electrolytes with sulfur based ionic liquid for lithium batteries. *J. Power Sources* **196**, 9767–9773 (2011).

32. Kim, G.-T., Appetecchi, G. B., Alessandrini, F. & Passerini, S. Solvent-free, PYR1ATFSI ionic liquid-based ternary polymer electrolyte systems. *J. Power Sources* **171**, 861–869 (2007).

33. Appetecchi, G. . *et al.* Hot-pressed, dry, composite, PEO-based electrolyte membranes. *J. Power Sources* **114**, 105–112 (2003).

34. Marks, T., Trussler, S., Smith, a. J., Xiong, D. & Dahn, J. R. A Guide to Li-Ion Coin-Cell Electrode Making for Academic Researchers. *J. Electrochem. Soc.* **158**, A51 (2011).

35. S. Besner, A. Vallée, G. Bouchard, J. P. Effect of anion polarization on conductivity behavior of poly (ethylene oxide) complexed with alkali salts. *Macromolecules* **25**, 6480–6488 (1992).

36. Papke, B. L., Ratner, M. A. & Shriver, D. F. Conformation and Ion-Transport

Models for the Structure and Ionic Conductivity in Complexes of Polyethers with Alkali Metal Salts. *J. Electrochem. Soc.* **129**, 1694 (1982).

37. Fenton, D. E., Parker, J. M. & Wright, P. V. Complexes of alkali metal ions with poly(ethylene oxide). *Polymer (Guildf).* **14**, 589 (1973).

38. Murata, K., Izuchi, S. & Yoshihisa, Y. An overview of the research and development of solid polymer electrolyte batteries. *Electrochim. Acta* **45**, 1501–1508 (2000).

39. Varzi, A., Raccichini, R., Passerini, S. & Scrosati, B. Challenges and prospects of the role of solid electrolytes in the revitalization of lithium metal batteries. *J. Mater. Chem. A* **4**, 17251–17259 (2016).

40. Cheng, X.-B., Zhang, R., Zhao, C.-Z. & Zhang, Q. Toward Safe Lithium Metal Anode in Rechargeable Batteries: A Review. *Chem. Rev.* **117**, 10403–10473 (2017).

41. Liu, B., Zhang, J. G. & Xu, W. Advancing Lithium Metal Batteries. *Joule* **2**, (2018).

42. Zhang, K., Lee, G.-H., Park, M., Li, W. & Kang, Y.-M. Recent Developments of the Lithium Metal Anode for Rechargeable Non-Aqueous Batteries. *Adv. Energy Mater.* **6**, 1600811 (2016).

43. Arya, A. & Sharma, A. L. Insights into the use of polyethylene oxide in energy storage/conversion devices: a critical review. *J. Phys. D. Appl. Phys.* **50**, 443002 (2017).

44. Xue, Z., He, D. & Xie, X. Poly(ethylene oxide)-based electrolytes for lithium-ion batteries. *J. Mater. Chem. A* **3**, 19218–19253 (2015).

45. Osada, I., de Vries, H., Scrosati, B. & Passerini, S. Ionic-Liquid-Based Polymer Electrolytes for Battery Applications. *Angew. Chemie Int. Ed.* n/a-n/a (2015). doi:10.1002/anie.201504971

46. Ratner, M. A. & Shriver, D. F. Ion transport in solvent-free polymers. *Chem. Rev.* **88**, 109–124 (1988).

47. Hallinan, D. T. & Balsara, N. P. Polymer Electrolytes. *Annu. Rev. Mater. Res.* **43**, 503–525 (2013).

48. Xu, K. Electrolytes and Interphases in Li-Ion Batteries and Beyond. *Chem. Rev.* **114**, 141029061722005 (2014).

49. Shin, J.-H., Henderson, W. A. & Passerini, S. An Elegant Fix for Polymer Electrolytes. *Electrochem. Solid-State Lett.* **8**, A125 (2005).

50. Scrosati, B., Croce, F., Appetecchi, G. B. & Persi, L. Nanocomposite polymer electrolytes for lithium batteries. *Nature* **394**, 456–458 (1998).

51. Capiglia, C., Mustarelli, P., Quartarone, E., Tomasi, C. & Magistris, A. Effects of nanoscale SiO2 on the thermal and transport properties of solvent-free, poly(ethylene oxide) (PEO)-based polymer electrolytes. *Solid State Ionics* **118**, 73–79 (1999).

52. Leo, C. J., Subba Rao, G. V. & Chowdari, B. V. R. Studies on plasticized PEO–lithium triflate–ceramic filler composite electrolyte system. *Solid State Ionics* **148**, 159–171 (2002).

53. Croce, F. *et al.* Role of the ceramic fillers in enhancing the transport properties of composite polymer electrolytes. *Electrochim. Acta* **46**, 2457–2461 (2001).

54. Xiong, H. M., Zhao, X. & Chen, J. S. New polymer-inorganic nanocomposites: PEO-ZnO and PEO-ZnO-LiClO4 films. *J. Phys. Chem. B* **105**, 10169–10174 (2001).

55. Liu, W. *et al.* Ionic Conductivity Enhancement of Polymer Electrolytes with

Ceramic Nanowire Fillers. *Nano Lett.* **15**, 2740–2745 (2015).

56. Leo, C. J., Subba Rao, G. V. & Chowdari, B. V. R. Studies on plasticized PEO-lithium triflate-ceramic filler composite electrolyte system. *Solid State Ionics* **148**, 159–171 (2002).

57. Wang, W., Yi, E., Fici, A. J., Laine, R. M. & Kieffer, J. Lithium Ion Conducting Poly(ethylene oxide)-Based Solid Electrolytes Containing Active or Passive Ceramic Nanoparticles. *J. Phys. Chem. C* **121**, 2563–2573 (2017).

58. Appetecchi, G. B. *et al.* Composite polymer electrolytes with improved lithium metal electrode interfacial properties: I. Electrochemical properties of dry PEO-LiX systems. *J. Electrochem. Soc.* **145**, 4126–4132 (1998).

59. Keller, M., Varzi, A. & Passerini, S. Hybrid electrolytes for lithium metal batteries. *J. Power Sources* **392**, 206–225 (2018).

60. Srivastava, S., Schaefer, J. L., Yang, Z., Tu, Z. & Archer, L. A. 25th Anniversary Article: Polymer-Particle Composites: Phase Stability and Applications in Electrochemical Energy Storage. *Adv. Mater.* **26**, 201–234 (2014).

61. Wang, W., Alexandridis, P., Wang, W. & Alexandridis, P. Composite Polymer Electrolytes: Nanoparticles Affect Structure and Properties. *Polymers (Basel).* **8**, 387 (2016).

62. Zhao, Y. *et al.* A promising PEO/LAGP hybrid electrolyte prepared by a simple method for all-solid-state lithium batteries. *Solid State Ionics* **295**, 65–71 (2016).

63. F. Croce *et al.* Physical and Chemical Properties of Nanocomposite Polymer Electrolytes. (1999). doi:10.1021/JP992307U

64. Bouchet, R. *et al.* Charge Transport in Nanostructured PS–PEO–PS Triblock

Copolymer Electrolytes. *Macromolecules* **47**, 2659–2665 (2014).

65. Phan, T. N., Issa, S. & Gigmes, D. Poly(ethylene oxide)-based block copolymer electrolytes for lithium metal batteries. *Polym. Int.* **68**, 7–13 (2019).

66. Young, W.-S., Kuan, W.-F. & Epps, T. H. Block copolymer electrolytes for rechargeable lithium batteries. *J. Polym. Sci. Part B Polym. Phys.* **52**, 1–16 (2014).

67. Gomez, E. D. *et al.* Effect of Ion Distribution on Conductivity of Block Copolymer Electrolytes. *Nano Lett.* **9**, 1212–1216 (2009).

68. Chintapalli, M. *et al.* Structure and Ionic Conductivity of Polystyrene- block -poly(ethylene oxide) Electrolytes in the High Salt Concentration Limit. *Macromolecules* **49**, 1770–1780 (2016).

69. Thelen, J. L. *et al.* Correlations between Salt-Induced Crystallization, Morphology, Segmental Dynamics, and Conductivity in Amorphous Block Copolymer Electrolytes. *Macromolecules* **51**, 1733–1740 (2018).

70. Jo, G., Ahn, H. & Park, M. J. Simple Route for Tuning the Morphology and Conductivity of Polymer Electrolytes: One End Functional Group is Enough. *ACS Macro Lett.* **2**, 990–995 (2013).

71. Bouchet, R. *et al.* Single-ion BAB triblock copolymers as highly efficient electrolytes for lithium-metal batteries. *Nat. Mater.* **12**, 452–457 (2013).

72. Galiński, M., Lewandowski, A. & Stępniak, I. Ionic liquids as electrolytes. *Electrochim. Acta* **51**, 5567–5580 (2006).

73. Le Bideau, J., Viau, L. & Vioux, A. Ionogels, ionic liquid based hybrid materials. *Chem. Soc. Rev.* **40**, 907–25 (2011).

74. Matsumoto, H., Matsuda, T. & Miyazaki, Y. Room Temperature Molten Salts Based

on Trialkylsulfonium Cations and Bis(trifluoromethylsulfonyl)imide. *Chem. Lett.* **29**, 1430–1431 (2000).

75. Zhang, Q. *et al.* Novel Cyclic Sulfonium-Based Ionic Liquids: Synthesis, Characterization, and Physicochemical Properties. *Chem. - A Eur. J.* **15**, 765–778 (2009).

76. Li, M., Yang, L., Fang, S. & Dong, S. Novel polymeric ionic liquid membranes as solid polymer electrolytes with high ionic conductivity at moderate temperature. *J. Memb. Sci.* **366**, 245–250 (2011).

77. Fernicola, A. *et al.* Lithium-Ion-Conducting Electrolytes: From an Ionic Liquid to the Polymer Membrane. *J. Electrochem. Soc.* **156**, A514 (2009).

78. Zhang, S., Lee, K. H., Sun, J., Frisbie, C. D. & Lodge, T. P. Viscoelastic Properties, Ionic Conductivity, and Materials Design Considerations for Poly(styrene- b -ethylene oxide- b -styrene)-Based Ion Gel Electrolytes. *Macromolecules* **44**, 8981–8989 (2011).

79. Seki, S. *et al.* Quaternary Ammonium Room-Temperature Ionic Liquid/Lithium Salt Binary Electrolytes: Electrochemical Study. *J. Electrochem. Soc.* **155**, A421 (2008).

80. Kitazawa, Y. *et al.* Gelation of Solvate Ionic Liquid by Self-Assembly of Block Copolymer and Characterization as Polymer Electrolyte. *Macromolecules* **47**, 6009–6016 (2014).

81. Susan, M. A. B. H., Kaneko, T., Noda, A. & Watanabe, M. Ion gels prepared by in situ radical polymerization of vinyl monomers in an ionic liquid and their characterization as polymer electrolytes. *J. Am. Chem. Soc.* **127**, 4976–83 (2005).

82. Li, M., Wang, L. & Du, T. Preparation of polymer electrolytes based on the

polymerized imidazolium ionic liquid and their applications in lithium batteries. *J. Appl. Polym. Sci.* **131**, n/a-n/a (2014).

83. Shin, J.-H., Henderson, W. A. & Passerini, S. *Ionic liquids to the rescue? Overcoming the ionic conductivity limitations of polymer electrolytes*. *Electrochemistry Communications* **5**, (2003).

84. Yongxin, A., Xinqun, C., Pengjian, Z., Lixia, L. & Geping, Y. Improved properties of polymer electrolyte by ionic liquid PP1.3TFSI for secondary lithium ion battery. *J. Solid State Electrochem.* **16**, 383–389 (2011).

85. Shin, J.-H., Henderson, W. A., Scaccia, S., Prosini, P. P. & Passerini, S. Solid-state Li/LiFePO4 polymer electrolyte batteries incorporating an ionic liquid cycled at 40°C. *J. Power Sources* **156**, 560–566 (2006).

86. Zhu, C., Cheng, H. & Yang, Y. Electrochemical Characterization of Two Types of PEO-Based Polymer Electrolytes with Room-Temperature Ionic Liquids. *J. Electrochem. Soc.* **155**, A569 (2008).

87. Fisher, A. S., Khalid, M. B. & Kofinas, P. Block Copolymer Electrolyte with Sulfur Based Ionic Liquid for Lithium Batteries. *J. Electrochem. Soc.* **159**, A2124–A2129 (2012).

88. Zhou, D. *et al.* Non-Volatile Polymer Electrolyte Based on Poly(propylene carbonate), Ionic Liquid, and Lithium Perchlorate for Electrochromic Devices. *J. Phys. Chem. B* **117**, 7783–7789 (2013).

89. Shin, J.-H., Henderson, W. A. & Passerini, S. PEO-Based Polymer Electrolytes with Ionic Liquids and Their Use in Lithium Metal-Polymer Electrolyte Batteries. *J. Electrochem. Soc.* **152**, A978 (2005).

90. Ye, Y.-S., Rick, J. & Hwang, B.-J. Ionic liquid polymer electrolytes. *J. Mater. Chem. A* **1**, 2719–2743 (2013).

91. Nakagawa, H., Izuchi, S., Kuwana, K., Nukuda, T. & Aihara, Y. Liquid and Polymer Gel Electrolytes for Lithium Batteries Composed of Room-Temperature Molten Salt Doped by Lithium Salt. *J. Electrochem. Soc.* **150**, A695 (2003).

92. Green, O., Grubjesic, S., Lee, S. & Firestone, M. A. The Design of Polymeric Ionic Liquids for the Preparation of Functional Materials. *Polym. Rev.* **49**, 339–360 (2009).

93. Yuan, J., Mecerreyes, D. & Antonietti, M. Poly(ionic liquid)s: An update. *Prog. Polym. Sci.* **38**, 1009–1036 (2013).

94. Meek, K. M. & Elabd, Y. A. Polymerized ionic liquid block copolymers for electrochemical energy. *Journal of Materials Chemistry A* **3**, 24187–24194 (2015).

95. Yongxin, A., Xinqun, C., Pengjian, Z., Lixia, L. & Geping, Y. Improved properties of polymer electrolyte by ionic liquid PP1.3TFSI for secondary lithium ion battery. *J. Solid State Electrochem.* **16**, 383–389 (2012).

96. Zhu, C., Cheng, H. & Yang, Y. Electrochemical Characterization of Two Types of PEO-Based Polymer Electrolytes with Room-Temperature Ionic Liquids. *J. Electrochem. Soc.* **155**, A569 (2008).

97. Shaplov, A. S., Marcilla, R. & Mecerreyes, D. Recent Advances in Innovative Polymer Electrolytes based on Poly(ionic liquid)s. *Electrochim. Acta* **175**, 18–34 (2015).

98. Eftekhari, A. & Saito, T. Synthesis and properties of polymerized ionic liquids. *Eur. Polym. J.* **90**, 245–272 (2017).

99. Tiyapiboonchaiya, C., MacFarlane, D. R., Sun, J. & Forsyth, M. Polymer-in-ionic-liquid electrolytes. *Macromol. Chem. Phys.* **203**, 1906–1911 (2002).

100. MacFarlane, D. R. *et al.* Ionic liquids and their solid-state analogues as materials for energy generation and storage. *Nat. Rev. Mater.* **1**, 15005 (2016).

101. Dautzenberg, G., Croce, F., Passerini, S. & Scrosati, B. Characterization of PAN-Based Gel Electrolytes. Electrochemical Stability and Lithium Cyclability. *Chem. Mater.* **6**, 538–542 (1994).

102. Manthiram, A., Yu, X. & Wang, S. Lithium battery chemistries enabled by solid-state electrolytes. *Nature Reviews Materials* **2**, (2017).

103. Suzuki, N., Inaba, T. & Shiga, T. Electrochemical properties of LiPON films made from a mixed powder target of Li 3PO 4 and Li 2O. *Thin Solid Films* **520**, 1821–1825 (2012).

104. Tikekar, M. D., Choudhury, S., Tu, Z. & Archer, L. A. Design principles for electrolytes and interfaces for stable lithium-metal batteries. *Nature Energy* **1**, (2016).

105. Kim, J. G. *et al.* A review of lithium and non-lithium based solid state batteries. *J. Power Sources* **282**, 299–322 (2015).

106. Catti, M. First-Principles Modeling of Lithium Ordering in the LLTO (Li $_x$ La $_{2/3-x/3}$ TiO $_3$) Superionic Conductor. *Chem. Mater.* **19**, 3963–3972 (2007).

107. Kanno, R. & Murayama, M. Lithium Ionic Conductor Thio-LISICON: The Li 2S-GeS 2-P 2S 5 System. *J. Electrochem. Soc.* **148**, (2001).

108. Thangadurai, V. & Weppner, W. Li6ALa2Ta2O12 (A = Sr, Ba): Novel Garnet-Like Oxides for Fast Lithium Ion Conduction. *Adv. Funct. Mater.* **15**, 107–112 (2005).

109. Kamaya, N. *et al.* A lithium superionic conductor. *Nat. Mater.* **10**, 682–686 (2011).

110. Hummel, R. E. *Electronic Properties of Materials*. (Springer New York, 2011). doi:10.1007/978-1-4419-8164-6

111. Beck, F. & Rüetschi, P. Rechargeable batteries with aqueous electrolytes. *Electrochim. Acta* **45**, 2467–2482 (2000).

112. Abraham, K. M. Prospects and Limits of Energy Storage in Batteries. *J. Phys. Chem. Lett.* **6**, 830–844 (2015).

113. Suo, L. *et al.* 'Water-in-salt' electrolyte enables high-voltage aqueous lithium-ion chemistries. *Science* **350**, 938–43 (2015).

114. Alias, N. & Mohamad, A. A. Advances of aqueous rechargeable lithium-ion battery: A review. *J. Power Sources* **274**, 237–251 (2015).

115. Angell, C. A., Liu, C. & Sanchez, E. Rubbery solid electrolytes with dominant cationic transport and high ambient conductivity. *Nature* **362**, 137–139 (1993).

116. Wang, H. *et al.* Polymer-in-salt like conduction behavior of small-molecule electrolytes. *Chem. Commun.* **10**, 2186–2187 (2004).

117. Bushkova, O. V., Popov, S. E., Yaroslavtseva, T. V., Zhukovsky, V. M. & Nikiforov, A. E. Ion-molecular and ion-ion interactions in solvent-free polymer electrolytes based on amorphous butadiene - acrylontrile copolymer and LiAsF6. *Solid State Ionics* **178**, 1817–1830 (2008).

118. Ferry, A., Edman, L., Forsyth, M., MacFarlane, D. R. & Sun, J. Connectivity, ionic interactions, and migration in a fast-ion-conducting polymer-in-salt electrolyte based on poly(acrylonitrile) and LiCF3SO3. *J. Appl. Phys.* **86**, 2346–2348 (1999).

119. Suo, L. *et al.* How Solid-Electrolyte Interphase Forms in Aqueous Electrolytes. *J.*

Am. Chem. Soc. **139**, 18670–18680 (2017).

120. Yamada, Y. & Yamada, A. Superconcentrated Electrolytes to Create New Interfacial Chemistry in Non-aqueous and Aqueous Rechargeable Batteries. *Chem. Lett.* **46**, 1056–1064 (2017).

121. Vatamanu, J. & Borodin, O. Ramifications of Water-in-Salt Interfacial Structure at Charged Electrodes for Electrolyte Electrochemical Stability. *J. Phys. Chem. Lett.* **8**, 4362–4367 (2017).

122. Borodin, O. *et al.* Liquid Structure with Nano-Heterogeneity Promotes Cationic Transport in Concentrated Electrolytes. *ACS Nano* **11**, 10462–10471 (2017).

123. Suo, L. *et al.* Advanced High-Voltage Aqueous Lithium-Ion Battery Enabled by "Water-in-Bisalt" Electrolyte. *Angew. Chemie* **128**, 7252–7257 (2016).

124. Yamada, Y. *et al.* Hydrate-melt electrolytes for high-energy-density aqueous batteries. *Nat. Energy* **1**, 16129 (2016).

125. Ko, S. *et al.* Lithium-salt monohydrate melt: A stable electrolyte for aqueous lithium-ion batteries. *Electrochem. commun.* **104**, 106488 (2019).

126. Yang, C. *et al.* Flexible Aqueous Li-Ion Battery with High Energy and Power Densities. *Adv. Mater.* 1701972 (2017). doi:10.1002/adma.201701972

127. Zhang, J. *et al.* Safety-Reinforced Poly(Propylene Carbonate)-Based All-Solid-State Polymer Electrolyte for Ambient-Temperature Solid Polymer Lithium Batteries. *Adv. Energy Mater.* **5**, 1501082 (2015).

128. Ghosh, A. & Kofinas, P. Nanostructured Block Copolymer Dry Electrolyte. *J. Electrochem. Soc.* **155**, A428 (2008).

129. Uno, T., Kawaguchi, S., Kubo, M. & Itoh, T. Ionic conductivity and thermal

property of solid hybrid polymer electrolyte composed of oligo(ethylene oxide) unit and butyrolactone unit. *J. Power Sources* **178**, 716–722 (2008).

130. Krause, L. J. *et al.* Corrosion of aluminum at high voltages in non-aqueous electrolytes containing perfluoroalkylsulfonyl imides; new lithium salts for lithium-ion cells. *J. Power Sources* **68**, 320–325 (1997).
131. Nairn, K. M., Best, A. S., Newman, P. J., MacFarlane, D. R. & Forsyth, M. Ceramic-polymer interface in composite electrolytes of lithium aluminum titanium phosphate and polyetherurethane polymer electrolyte. *Solid State Ionics* **121**, 115–119 (1999).
132. olsen, I., Koksbang, R. & Skou, E. Transference number measurements on a hybrid polymer electrolyte. *Electrochim. Acta* **40**, 1701–1706 (1995).
133. Evans, J., Vincent, C. A. & Bruce, P. G. Electrochemical measurement of transference numbers in polymer electrolytes. *Polymer (Guildf).* **28**, 2324–2328 (1987).
134. Stejskal, E. O. & Tanner, J. E. Spin Diffusion Measurements: Spin Echoes in the Presence of a Time-Dependent Field Gradient. *J. Chem. Phys.* **42**, 288–292 (1965).
135. Matsumoto, H., Matsuda, T. & Miyazaki, Y. Room Temperature Molten Salts Based on Trialkylsulfonium Cations and Bis(trifluoromethylsulfonyl)imide. *Chem. Lett.* **29**, 1430–1431 (2000).
136. Dunn, B., Kamath, H. & Tarascon, J.-M. Electrical energy storage for the grid: a battery of choices. *Science* **334**, 928–35 (2011).
137. Williard, N., He, W., Hendricks, C. & Pecht, M. Lessons Learned from the 787 Dreamliner Issue on Lithium-Ion Battery Reliability. *Energies* **6**, 4682–4695 (2013).
138. Wang, Q. *et al.* Thermal runaway caused fire and explosion of lithium ion battery.

J. Power Sources **208**, 210–224 (2012).

139. ARMAND, M. The history of polymer electrolytes. *Solid State Ionics* **69**, 309–319 (1994).

140. Croce, F., Appetecchi, G., Persi, L. & Scrosati, B. Nanocomposite polymer electrolytes for lithium batteries. *Nature* **394**, 456–458 (1998).

141. Wang, F. *et al.* Hybrid Aqueous/Non-aqueous Electrolyte for Safe and High-Energy Li-Ion Batteries. *Joule* (2018). doi:10.1016/J.JOULE.2018.02.011

142. Meyer, W. H. Polymer Electrolytes for Lithium-Ion Batteries. *Adv. Mater.* **10**, 439–448 (1998).

143. Lu, L., Han, X., Li, J., Hua, J. & Ouyang, M. A review on the key issues for lithium-ion battery management in electric vehicles. *J. Power Sources* **226**, 272–288 (2013).

144. Hallinan, D. T., Villaluenga, I. & Balsara, N. P. Polymer and composite electrolytes. *MRS Bull.* **43**, 759–767 (2018).

145. Bruce, P. G., Evans, J. & Vincent, C. A. Conductivity and transference number measurements on polymer electrolytes. *Solid State Ionics* **28**, 918–922 (1988).

146. Teran, A. A., Tang, M. H., Mullin, S. A. & Balsara, N. P. Effect of molecular weight on conductivity of polymer electrolytes. *Solid State Ionics* **203**, 18–21 (2011).

147. Vallée, A., Besner, S. & Prud'Homme, J. Comparative study of poly(ethylene oxide) electrolytes made with LiN(CF3SO2)2, LiCF3SO3 and LiClO4: Thermal properties and conductivity behaviour. *Electrochim. Acta* **37**, 1579–1583 (1992).

148. Gorecki, W., Jeannin, M., Belorizky, E., Roux, C. & Armand, M. Physical properties of solid polymer electrolyte PEO(LiTFSI) complexes. *J. Phys. Condens. Matter* **7**, 6823–6832 (1995).

149. Rey, I., Lassègues, J. C., Grondin, J. & Servant, L. Infrared and Raman study of the PEO-LiTFSI polymer electrolyte. *Electrochim. Acta* **43**, 1505–1510 (1998).

150. Cui, Y. *et al.* Improved performance using a plasticized polymer electrolyte for quasi-solid state dye-sensitized solar cells. *Electrochim. Acta* **74**, 194–200 (2012).

151. Aziz, S. B., Woo, T. J., Kadir, M. F. Z. & Ahmed, H. M. A conceptual review on polymer electrolytes and ion transport models. *J. Sci. Adv. Mater. Devices* **3**, 1–17 (2018).

152. Diederichsen, K. M., Buss, H. G. & McCloskey, B. D. The Compensation Effect in the Vogel–Tammann–Fulcher (VTF) Equation for Polymer-Based Electrolytes. *Macromolecules* **50**, 3831–3840 (2017).

153. Eftekhari, A. High-Energy Aqueous Lithium Batteries. *Adv. Energy Mater.* **8**, 1801156 (2018).

154. Forsyth, M., Porcarelli, L., Wang, X., Goujon, N. & Mecerreyes, D. Innovative Electrolytes Based on Ionic Liquids and Polymers for Next-Generation Solid-State Batteries. *Acc. Chem. Res.* **52**, 686–694 (2019).

155. Porcarelli, L., Gerbaldi, C., Bella, F. & Nair, J. R. Super Soft All-Ethylene Oxide Polymer Electrolyte for Safe All-Solid Lithium Batteries. *Sci. Rep.* **6**, 19892 (2016).

156. Wang, Q., Sun, J., Yao, X. & Chen, C. Micro calorimeter study on the thermal stability of lithium-ion battery electrolytes. *J. Loss Prev. Process Ind.* **19**, 561–569 (2006).

157. Edman, L., Doeff, M. M., Ferry, A., Kerr, J. & De Jonghe, L. C. Transport Properties of the Solid Polymer Electrolyte System P(EO) $_n$ LiTFSI. *J. Phys. Chem. B* **104**, 3476–3480 (2000).

158. Judez, X. *et al.* Lithium Bis(fluorosulfonyl)imide/Poly(ethylene oxide) Polymer Electrolyte for All Solid-State Li–S Cell. *J. Phys. Chem. Lett.* 1956–1960 (2017). doi:10.1021/acs.jpclett.7b00593

159. Jiang, Y. *et al.* Development of the PEO Based Solid Polymer Electrolytes for All-Solid State Lithium Ion Batteries. *Polym. 2018, Vol. 10, Page 1237* **10**, 1237 (2018).

160. Xu, K. Nonaqueous Liquid Electrolytes for Lithium-Based Rechargeable Batteries. *Chem. Rev.* **104**, 4303–4418 (2004).

161. Forsyth, M., MacFarlane, D. . & Hill, A. . Glass transition and free volume behaviour of poly(acrylonitrile)/LiCF3SO3 polymer-in-salt electrolytes compared to poly(ether urethane)/LiClO4 solid polymer electrolytes. *Electrochim. Acta* **45**, 1243–1247 (2000).

162. Forsyth, M., Sun, J., Macfarlane, D. R. & Hill, A. J. Compositional dependence of free volume in PAN/LiCF3SO3 polymer-in-salt electrolytes and the effect on ionic conductivity. *J. Polym. Sci. Part B Polym. Phys.* **38**, 341–350 (2000).

163. Xu, K. & Wang, C. Batteries: Widening voltage windows. *Nat. Energy* **1**, 16161 (2016).

164. Xu, G. The effects of chain segment motion on ionic diffusion in solid polymer electrolytes. *Solid State Ionics* **50**, 345–347 (1992).

165. Borodin, O. & Smith, G. D. Mechanism of ion transport in amorphous poly(ethylene oxide)/ LiTFSI from molecular dynamics simulations. *Macromolecules* **39**, 1620–1629 (2006).

166. Mongcopa, K. I. S. *et al.* Relationship between Segmental Dynamics Measured by Quasi-Elastic Neutron Scattering and Conductivity in Polymer Electrolytes. *ACS*

Macro Lett. **7**, 504–508 (2018).

167. Lascaud, S. *et al.* Phase Diagrams and Conductivity Behavior of Poly(ethylene oxide)-Molten Salt Rubbery Electrolytes. *Macromolecules* **27**, 7469–7477 (1994).

168. Polu, A. R., Kim, D. K. & Rhee, H.-W. Poly(ethylene oxide)-lithium difluoro(oxalato)borate new solid polymer electrolytes: ion–polymer interaction, structural, thermal, and ionic conductivity studies. *Ionics (Kiel).* **21**, 2771–2780 (2015).

169. Borodin, O. *et al.* Liquid Structure with Nano-Heterogeneity Promotes Cationic Transport in Concentrated Electrolytes. *ACS Nano* **11**, 10462–10471 (2017).

170. Carbone, L. *et al.* Polyethylene glycol dimethyl ether (PEGDME)-based electrolyte for lithium metal battery. *J. Power Sources* **299**, 460–464 (2015).

171. Li, Z., Chen, Y., Shen, J. & Cui, X. Facile synthesis of a heterogeneous Li2TiO3/TiO2nanocomposite with enhanced photoelectrochemical water splitting. *New J. Chem.* **41**, 6305–6314 (2017).

172. Khurana, R., Schaefer, J. L., Archer, L. A. & Coates, G. W. Suppression of Lithium Dendrite Growth Using Cross-Linked Polyethylene/Poly(ethylene oxide) Electrolytes: A New Approach for Practical Lithium-Metal Polymer Batteries. *J. Am. Chem. Soc.* **136**, 7395–7402 (2014).

173. Kitta, M., Taguchi, N., Fukada, C. & Kohyama, M. Study of the Hydrate-Melt/Li 4 Ti 5 O 12 Interphase by Scanning Electron Microscopy-Based Spectroscopy. *Langmuir* **33**, 13923–13928 (2017).